Department of Electrical and Computer Engineering

Primary and Secondary Control of Parallel Operating Converter-Interfaced Distributed Energy Resources in Microgrids

Ruwan P. S. Chandrasena

This thesis is presented for the Degree of

Doctor of Philosophy

of

Curtin University

November 2014

Declaration

To the best of my knowledge and belief this thesis contains no material previously published by any other person except where due acknowledgment has been made.

This thesis contains no material which has been accepted for the award of any other degree or diploma in any university.

Signature: R.P.S. Chandrasena

Date: 19/11/2014

Acknowledgements

I am deeply grateful to my supervisors, Dr. Farhad Shahnia and Dr. Sumedha Rajakaruna for their incomparable guidance, continuous patience and encouragement throughout my doctoral study. Without your endless support, this thesis could have been a nightmare.

Then, I wish to express my warmest gratitude to Prof. Arindam Ghosh for his insightful guidance and support during the course of my study.

I am much obliged to the staff members of the Department of Electrical and Computer Engineering, Curtin University, especially Zibby Cielma, Russel Wilkinson, Nicholas King and Mark Fowler for their support rendered in various ways during this work.

I wish to acknowledge the Faculty of Engineering, University of Ruhuna, Sri Lanka for granting me the required leave and financial support to pursue my higher studies.

Finally, I need to acknowledge the financial support received from Curtin University through Curtin International Postgraduate Research Scholarship (CPIRS) to complete my studies with peace of mind.

Dedication

To my beloved wife Shiromi and my kids Omaya and Onali, for their unconditional love, understanding, commitment and moral support to make this work a success.

Abstract

The necessity of utilizing sustainable energy resources as well as reducing the energy generation costs and electricity transmission losses are driving the modern power systems towards embedding renewable energy based dispersed generation units in the low voltage and medium voltage distribution networks. Nowadays, photovoltaic cells, wind turbines and fuel cells are among the most popular distributed energy resources (DER) for generation of electric power. These DERs are usually converter-interfaced and need to be controlled properly.

The microgrid concept was introduced in 2002 as a better way of harnessing energy from the renewable energy based DERs. Microgrid is a cluster of DERs and loads which appears as a single controllable unit that promptly responds to the demand changes. Microgrid can operate either in grid-connected mode or in off-grid mode. In grid-connected mode, the grid dictates the voltage and frequency and DERs can operate at the rated or maximum generation capacities. In off-grid mode, if the DERs generation capacity is higher than local load demand, they can share the loads while maintaining the voltage and frequency within acceptable limits.

In this thesis, a hierarchical control system is proposed for the proper operation and control of the DERs in a microgrid. The proposed primary controller has a robust and optimal feedback control system which ensures the DERs are generating and tracking the desired references at their output. The proposed secondary controller adjusts the set points of the primary controllers of the DERs to ensure the voltage and frequency are kept within the acceptable limits. It also dynamically adjusts the power sharing ratio among the DERs in the microgrid and sheds the loads to prevent voltage and frequency collapse in the system. The developed control system ensures the DERs can successfully supply all different types of loads in the microgrid such as balanced, unbalanced and harmonic loads. The in this thesis, both single-phase and three-phase DERs are considered. In case of single-phase DERs with different ratings arbitrarily distributed among the three phases in the microgrid, two alternative methods are proposed to circulate the power from the phase with excess generation to the other phase(s) which need more power due to lack of generation. In addition, the possibility of interconnecting two or more neighboring off-grid microgrids is proposed to reduce the load shedding requirement in a microgrid with deficiency of power, if the neighboring microgrids have sufficient generation

capacity to supply the generation deficiency in the considered microgrid. Finally, a dc microgrid system is also proposed and its interconnection with an ac microgrid through an interlinking converter is discussed. Proper control and management methods are proposed to ensure the effective operation of the interlinked ac-dc hybrid microgrid at all different modes of operation. Several scenarios and case studies are considered and the proposed concepts are validated by extensive computer-based simulation studies in PSCAD/EMTDC.

Table of Contents

List of Figures

List of Tables

List of Abbreviations

ac	Alternating Current
CB	Circuit Breaker
dc	Direct Current
dq	Direct Quadrature
DER	Distributed Energy Resource
DSTATCOM	Distribution Static Compensator
IGBT	Insulated Gate Bipolar Transistors
KCL	Kirchhoff's Circuit Laws
LQR	Linear Quadratic Regulator
LV	Low Voltage
MG	Microgrid
MPPT	Maximum Power Point Tracking
MV	Medium Voltage
pcc	Point of Common Coupling
PLL	Phase-Locked Loop
pu	Per Unit
PV	Photovoltaic Cells
TC	Tie-Converter
VSC	Voltage Source Converter

Chapter 1 Introduction

1.1 Literature review

The ever increasing energy demand along with the necessity of cost reduction and higher reliability requirements are driving the modern power systems towards distributed energy resources (DER) as an alternative to the expansion of the current energy distribution systems [1]. In particular, small DERs, typically with power levels ranging from few kilowatts to megawatts, located near the loads are gaining popularity due to their higher operating efficiencies. Nowadays, photovoltaic cells (PV), wind turbines, fuel cells, batteries and micro turbines are among the most popular DERs for generation of electric power mostly during peak times or in rural areas [2]. However, the stochastic nature of the renewable energy sources creates technical challenges in integrating such energy sources to the distribution grid.

The concept of microgrid (MG) was introduced in 2002 [3] and it has been identified as a better way of harnessing the energy from the renewable energy based DERs. Microgrids are clusters of DERs, loads and energy storages. To deliver high quality and reliable power, the microgrid should appear as a single controllable unit that promptly responds to the changes in the system [3]. Microgrid can operate either in grid-connected mode or in off-grid mode due to planned (e.g. network maintenance) or unplanned (e.g. network fault) network operating conditions [4].

In grid-connected mode, the grid dictates voltage and frequency of the network and DERs can operate at their nominal (rated) capacities. In this mode of operation, the desired reference for DERs output can be derived using a constant power control strategy [5]. Alternatively, in off-grid mode, if the DERs generation capacity is higher than the local load demand, they will be sharing the loads. In this regard, voltage and frequency droop control strategy is proposed in [6] for deriving the references for the DER converters, in order to share the power among parallel

converter-interfaced DERs similar to the droop control technique used for power sharing among generators in a conventional power system. Later, voltage and angle droop was proposed in [7] to be used instead of the voltage and frequency droop for converter-interfaced DER applications. For improving the system response, a modified droop control has been proposed in [8]. For improving the small signal stability, an arctan power frequency droop has been proposed in [9] instead of the conventional droop method. Recently, intelligent power sharing algorithms such as adaptive droop control [10] and intelligent droop control [11] are proposed to remove the dependency of droop control on line parameters. In addition, in [12], a potential function based method has been utilized instead of the droop control to adjust common set points required for power sharing among the DERs in a microgrid. Stability of the microgrid system with different power sharing algorithms is also investigated in [13]-[15]. Once the references for the DERs are assigned, the DER converters can be controlled using either voltage-controlled [16]-[17] or current-controlled [18]-[19] strategies to track the desired references.

In grid-connected mode, the grid defines the network voltage; however, in off-grid mode, the network voltage can be indirectly regulated by the DERs based on the droop control. Although in both modes, the voltage along the low voltage network is maintained within acceptable limits, it is desired to hold the voltage to the nominal value of 1 per unit (pu). This can be achieved if one of the DERs in microgrid regulates the network voltage to 1 pu, referred to as Master DER in [20]. If DERs generation capacity in an off-grid microgrid is less than the local load demand, load shedding has to be carried out in order to maintain the voltage and frequency in the microgrid [21]-[22]. However, the DERs in residential low voltage networks are owned by customers and are not responsible for network voltage support. This is because utilizing the converter of a DER to generate reactive power, for supporting the network voltage profile, will reduce the active power generation capacity of the converter which is not desired by the owners point of view. Alternatively, a distribution static compensator (DSTATCOM) can be used in each microgrid to regulate the voltage at its point of common coupling (pcc) [23].

Another important issue in microgrids is islanding detection and resynchronization. Islanding is referred to the isolating the microgrid from the main grid. Different islanding detection methods are presented in [24]. In [24], it is

indicated that a communication based method can be utilized to send the circuit breaker status from the circuit breaker to the DER converters. This method is preferred among other islanding detection methods since it is free from none detection zones. Resynchronization is referred to the reconnection process of a DER to the microgrid or reconnection of a microgrid to grid [25]. If a DER operates in current-controlled strategy, no resynchronization is required when the DERs are connecting to the microgrid. However, if a DER operates in voltage-controlled strategy, proper resynchronization is required. Reconnection should only take place once the voltage magnitude difference and voltage phase difference across the respective circuit breaker is zero or lower than a small specified value [25]. Inappropriate reconnection may cause fluctuations in current which can damage the network assets or result in system instability. Different resynchronisation methods are proposed in [26]-[28].

General introduction on microgrid basics, including the architecture, protection and power management is given in [29]-[30]. A review of ongoing research projects on microgrid in US, Canada, Europe and Japan is presented in [30]-[31]. Different power management strategies and controlling algorithms for a microgrid are proposed in [32]-[33].

1.1.1 Hierarchical control of microgrids

A three-level hierarchical control architecture can be identified for microgrid control as presented in [31]. The distribution network tertiary controller analyses the data such as load and weather forecast, electricity market and economic dispatch results to define the references for the output power of each DER within the microgrid. These references are communicated to the microgrid secondary (central) controller which passes this information to the primary level controllers. The primary controllers are within each DER and are responsible for controlling the DER outputs based on the references received from the central controller. Hence, the required output of a DER can vary from zero to its maximum capacity based on the commands of the tertiary controller.

To realize a power ratio among the DERs in the microgrid, droop controller coefficients need to be designed properly [34]. Many researches propose to design the coupling inductances of the DERs such that their ratio is inversely proportional to

the desired ratio of the output powers of the DERs. However, it is not practical to adjust the coupling inductances dynamically for varying output power ratios. A virtual impedance-based technique is introduced and utilized in [35] to overcome this problem. However, in general, dynamic power sharing ratios can be achieved by adjusting the droop control coefficients with the help of the central controller for any ratios of the coupling inductances. However, the secondary control level should also monitor and adjust the references for the voltage and frequency within the microgrid if they are fallen outside acceptable ranges.

1.1.2 Microgrids with balanced, unbalanced and harmonic loads

One of the main issues yet to be investigated in microgrids is the effect of single-phase, unbalanced and harmonic loads on the control, operation and power sharing among parallel converter interfaced DERs. In the presence of balanced, unbalanced and linear loads, the converters can be operated in voltage control mode [7]-[8],[36]-[37] or current control mode [38]-[41]. Majority of the literature on DER converter control in microgrids utilise current control mode [38]-[41]. For this, the output current reference for each converter should be calculated properly based on the load demand and the desired power sharing ratio among existing DERs. Later, the DER can supply the desired reference current to the microgrid by employing a proper switching mechanism in the converter. This can be relatively complex when the microgrid is supplying single-phase, unbalanced or harmonic loads. In this case, the DERs not only should share the active and reactive power but also should share harmonic, negative and zero sequence currents. This needs a fast and accurate negative and zero sequence and harmonic current extraction mechanism as discussed in [39][42]. If the extracted sequence and harmonic currents mismatch the actual load requirement, the operation and power sharing of DERs can be significantly affected. However, by using a voltage control mode, there is no requirement to measure and analyse the load current and to extract the sequence and harmonic current components.

1.1.3 Interconnected microgrids

Smart Grid is a term referred to the improved condition of existing electric networks into more reliable, efficient, sustainable and customer interactive system by

properly adding advanced metering, protection and communication infrastructures [43]-[44]. A general summary of the available smart grid definitions, standards, protection and management plans and the required information technology, energy and communication infrastructures are given in [43]. Among various anticipated smart features, self-healing is a key attribute in smart grid concept. It is mainly driven by the requirement to improve system reliability [44]-[46]. In a self-healing network, it is expected that the network can continuously detect, analyze and respond to faults and restore the feeders with minimum human intervention. Therefore, in case of a fault in the network, the normal operation can be restored in different feeder sections by properly isolating only the faulted subsections such that the amount of the affected loads is minimized. The feasibility study carried out in [47] concludes that integration of self-healing capabilities to the future smart grids will bring high financial benefits for both utilities and the customers by reducing the number of affected customers as well as the amount of unsupplied energy.

For a self-healing network, the intelligent agents are required to adapt the system operation conditions. These agents are then utilized for analyzing and maintaining the system reliability in real-time. A framework, required to implement off-grid agents throughout an interconnected system, was proposed in [48]. Such a framework can be utilized to support a self-healing smart grid through the system monitoring and controlling. Some self-healing reconfiguration techniques were proposed in [49]-[50] to divide the network into isolated grids while minimizing the number of effected loads. Some utilities in US have already started implementing self-healing projects [51].

It is expected that in the near future, there will be several microgrids in each distribution network. They will be located in a neighborhood and the networks will be facilitated with self-healing capabilities. In such a scenario, an off-grid operation of a microgrid is not anymore desired due to load shedding possibility. However, in such systems, the concept of microgrids supporting each other becomes more viable. The topic of “interconnected microgrids” or “clusters of microgrids” is the next stage of future research in distribution networks. In [52]-[53] based on the microgrid and power market concepts and availability of control and communication infrastructures, a model of distributed off-grid microgrids was proposed. In such a model, if the DERs generation capacity in an off-grid microgrid is less than the local

load demand but there is surplus generation capacity in DERs of neighboring off-grid microgrids, interconnecting these two microgrids can reduce the load shedding in the microgird with deficiency of generation. In this model, the DERs in interconnected microgrids should be properly controlled to share the total load demand in the interconnected system. With the increased interest in smart grid and self-healing networks, there will be a possibility of interconnecting off-grid microgrids in the near future. The following assumptions are required when interconnecting two off-grid microgrids:

- Availability of communication infrastructure among DERs, protection devices and circuit breakers,
- Self-healing capability in the network,
- Surplus generation capacity of the DERs in one of the microgrids,
- Possibility of bypassing some of the current technical requirements for DER interconnection.

1.1.4 Single-phase DERs in microgrids

In near future, it is expected that majority of the houses will have single-phase grid-connected DERs. Hence, a group of neighboring houses can form a low voltage network which probably is capable of operating in off-grid mode, referred as a low voltage microgrid. Single-phase DERs in the microgrid will deliver the required active and reactive power demand while regulating the network voltage magnitude and frequency within the acceptable limits [32]-[34],[54]-[55].

The microgrid concept is well-established and ample of literature is available on power management and control in three-phase microgrids. So far, not much research is carried out on single-phase DERs operation in three-phase microgrids. In [56], the grid-connected operation of single-phase DERs is discussed. In [57], the off-grid operation of single-phase DERs is discussed; however, it is assumed that the three-phase network falls into three separate single-phase networks and the loads in each phase are only supplied by the DERs in the same phase. Therefore, the off-grid operation of the single-phase DERs, with different generation capacities, distributed unequally in a three-phase microgrid is yet to be explored.

1.1.5 AC-DC microgrids

It can be envisaged that the majority of houses connected to the future distribution network will have some form of DERs. Hence, it is realistic to expect forming a self-controlled small-scale power system named as microgrid [58] by aggregating the resources in the neighboring houses which are supplied by the same utility feeder. These houses, referred to as 'community houses' in this thesis, can therefore share the power generated by DERs such as PVs and energy storages units (e.g. battery banks) during off-grid or grid-connected operation.

Nowadays, most of the domestic loads are designed to work on ac voltage; hence, proper conversion systems are required to convert the dc voltage, generated by some DERs, to the ac voltage. Recently, some residential loads have been designed to operate on dc supply [59]. In [60], an efficiency comparison is carried out for different types of residential loads supplied by ac and dc supplies. It is shown that the efficiency of supplying the loads by dc voltage generated by dc DERs, is higher than that of supplying the loads from the converted ac supply. In [61], a new efficient dc power distribution system is proposed for future residential premises, which increases the total conversions efficiency from 80% to 94%. A novel low voltage bipolar dc distribution system is proposed and verified experimentally in [62]-[63] for residential applications. In addition, some experiments are already conducted on deploying smart control over ac and dc DERs within residential premises [64]-[65].

AC microgrids have been a significant research area since the microgrid concept was introduced [16],[18],[31]-[34],[66]-[69]. In recent years, the dc microgrids have also gained attention of the researchers, due to efficiency and flexibility in their control. In this regard, a hierarchical control system and an adaptive droop control are introduced for a dc microgrid system in [70]-[71]. The control and operation of DERs in a dc microgrid in grid-connected and off-grid statuses are studied in [72]-[73].

In this thesis, a small-scale, low voltage microgrid is considered as the power supply unit for future community houses. The discussed microgrid integrates both ac and dc types of loads and DERs, which are connected to the respective ac and dc buses. These two buses are interconnected through a power converter, referred to as Tie-Converter (TC). The ac-dc microgrid is a relatively new concept, with its

operation not been explored extensively. Therefore, proper primary and secondary control levels for the dynamic operation of the DERs within a hybrid ac-dc microgrid, in different modes of operation needs to be studied.

1.2 Aims and objectives of the thesis

The main objective of this thesis is to propose, develop and verify new strategies for operation and control of the microgrids with different types of loads, single-phase and three-phase DERs, with ac and dc buses and the possibility of being interconnected to neighboring microgrids. To achieve this goal, the aims of the research project are identified as:

- developing a primary control level for each DER in the microgrid,
- developing a secondary control level for the DERs in the microgrid,
- developing a power circulation mechanism among the phases in the presence of single-phase DERs in the microgrid,
- developing a power sharing mechanism among the DERs when two or more neighboring microgrids are interconnected,
- developing a power transfer control between the ac bus and dc bus of ac-dc microgrids.

1.3 Significance of research

It is expected that the future distribution networks will be in the form of interconnected microgrids. This research will help to improve the operation and control of the parallel connected DERs in an interconnected microgrids.

1.4 Original contributions of the research

The main objective of this research was to develop new strategies for dynamic operation and control of the parallel DERs in the microgrids. The main contributions of this research can be listed as follows:

- Proposing a hierarchical control system for the parallel converter-interfaced DERs in microgrids to achieve a desired power sharing ratio among them,
- Proposing the operation and control strategy for the DERs of a microgrid to support its neighboring microgrid.

- Proposing a mechanism of utilizing single-phase DERs with unequally distributed among the three phases of a microgrid,
- Proposing a mechanism of power circulation among the phases of a microgrid with single phase DERs with different capacities distributed unequally among the three phases in microgrid,
- Proposing a mechanism for power flow control between the ac bus and the dc bus of ac-dc microgrids.

1.5 Structure of the thesis

This thesis is organized in seven chapters. The research aims and objectives along with the need and the justification through a literature review for the research topic are outlined in **Chapter 1**. The microgrid structure and the developed low level control of the DERs in grid-connected and off-grid modes of operation are presented in **Chapter 2**. A hierarchical control system for the microgird is also discussed in this chapter and the proposed primary and secondary control levels for the DERs are presented to achieve a desired power sharing ratio among the DERs as well as proper voltage and frequency regulation within the microgrid. The simulation results for the proposed primary and secondary control levels are represented in **Chapter 3**. In **Chapter 4**, the dynamic operation and control of DERs in a system of interconnected microgrids is presented. The proposed operation strategy for single-phase DERs in a microgrid is presented in **Chapter 5** and a new power circulation strategy is presented to facilitate the extra power transfer from one phase to another. **Chapter 6** discusses the ac-dc hybrid microgrids and hierarchical control of the dc DERs in a dc microgrid. Power flow control among the ac bus and the dc bus through the interlinking converter of the hybrid microgrid while maintaining the voltage in both buses and the frequency in the ac bus is also discussed. Conclusions drawn from this research and recommendations for future research are given in **Chapter 7**.

Chapter 2 Microgrid Modeling and Hierarchical Control

In this chapter, the microgrid structure and its hierarchical control system are presented. The microgrid is a low voltage network composed of only converter-interfaced DERs. The hierarchical control system is composed of the primary and secondary control levels. The secondary control level constitutes several modules that maintain the voltage and frequency of the microgrid within acceptable limits in addition to providing a desired power sharing ratio among the DERs. The primary control level is responsible for ensuring the converters switchings lead to generation of the derived voltage references by the secondary control system at the converter output.

2.1 Microgrid structure

Let us consider a medium voltage feeder connected to a low voltage microgrid, namely microgrid, through distribution transformer T_1, as shown in Fig. 2.1. The microgrid is connected to the grid through a static type circuit breaker, CB_M, which is referred to as the main circuit breaker of the microgrid in the rest of the thesis. The microgrid has 3 DERs (i.e. DER_1 to DER_3) and 5 loads. A DSTATCOM is installed at the secondary side of the distribution transformer in the microgrid to regulate the voltage at its pcc. The loads are assumed to be residential loads and all DERs are assumed to be converter-interfaced DERs.

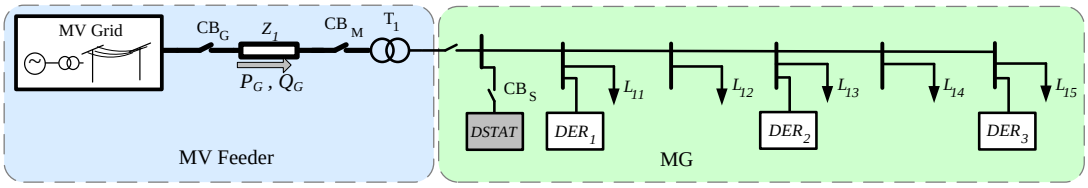

Fig. 2.1 Structure of the microgrid under consideration.

During grid-connected mode, all DERs will be operating at their rated capacities or the capacities determined by the economic analyses. During planned maintenance or unplanned fault condition on the medium voltage feeder, the microgrid main circuit breaker CB_M is open and the microgrid operates in off-grid mode while the DERs are sharing its loads. If the load demand in the microgrid is higher than the power generation capacity of the DERs in the microgrid, non-critical load shedding must be applied in order to maintain the voltage and frequency of the microgrid.

2.1.1 DER and converter structure and modeling

The DERs considered in this research are PV, fuel cells and batteries, connected to the microgrid through voltage source converters (VSC). Detailed dynamic models of these DERs are utilized in this research. These models are presented below and their technical data are given in the Appendix.

2.1.1.1 Fuel cell

Fuel cells are gaining popularity in electric networks as a DER because of their cleanness, high efficiency, and high reliability. A review on their technology, characteristics and ongoing research are reported in [74]. In this study, a typical PEM type fuel cell with simplified model shown in Fig. 2.2 is used. Its output V-I characteristic given in (2.1) is being verified experimentally in [75].

$$V(i) = 371.3 - 12.38\log(i) - 0.2195i - 0.2242e^{0.025i} \quad (2.1)$$

Similar characteristic is given for all fuel cells in [76]-[78] where their numerical values differ according to their rating, output voltage and application. A boost chopper is used at output of the fuel cell for regulating the necessary dc voltage v_c across the capacitor as shown in Fig. 2.2.

Fuel cells also have several shortcomings, too such as slow dynamic response, output voltage fluctuation with load and difficult cold start, etc.[78]. Therefore, an electric storage such as battery or ultracapacitor must be accompanied with the fuel cell to improve its dynamic characteristics. If the storage is in parallel directly with the dc bus, its charge and discharge cannot be controlled [78]; therefore, a bidirectional converter is needed between the dc bus and the electric storage to

control its state of charge. The basics and detailed control algorithm for the bidirectional converter of the storage is verified and presented in [79]. The studies carried out in the thesis, show that the fuel cell has a good and acceptable dynamic response for power quality improvement and power sharing objectives and no storage unit on fuel cell is used in the thesis.

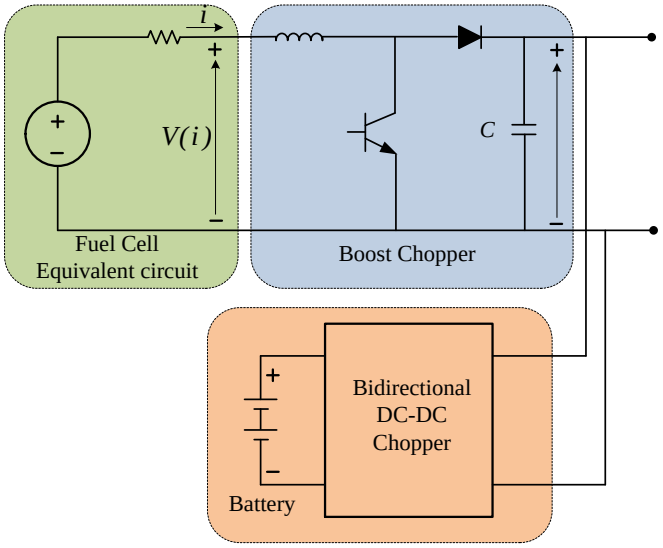

Fig. 2.2 Fuel cell and storage model equivalent circuit.

2.1.1.2 PV

A series and parallel combination of PV cells constitute a PV array. Fig. 2.3 shows the simplified equivalent circuit where output voltage is a function of the output current while the current is a function of load current, ambient temperature and radiation level [80]. The voltage equation of the PV is calculated by

$$V_{PV} = \frac{AkT_c}{e} Ln\left(\frac{I_{ph} + I_o - I_c}{I_o}\right) - R_s I_c \tag{2.2}$$

where

A: constant value for curve fitting

e: electron charge (1.602×10^{-19} C)

k: Boltzmann constant (1.38×10^{-23} J/^{o}k)

I_c: output current of PV cell

I_{ph}: photocurrent (1 A)

I_o: diode reverse saturation current (0.2 mA)

R_s: series resistance of PV cell (1 mΩ)

V_{PV}: output voltage of PV cell

T_c: PV cell reference temperature (25°C)

The output chopper controls the voltage v_c across the capacitor. A maximum power point tracking (MPPT) method is used to set the reference voltage of the chopper to achieve maximum power from the PV based on the load or ambient condition changes. The MPPT algorithm used in this thesis is given in [80]. A Proportional-Integral (PI) regulator is used in the chopper in order to achieve the desired reference voltage set by the MPPT. A battery storage system is connected in parallel with the dc bus of the chopper output through a bidirectional converter which is used to control the charging and discharging the battery. Depending on the terminal voltage of the PV, the battery gets charged or discharged. A more detailed explanation on bidirectional converter control of PV storage system is given in [81].

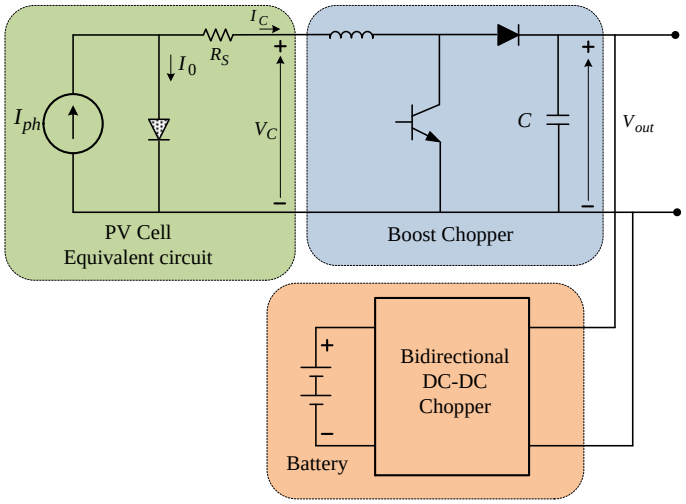

Fig. 2.3 Equivalent circuit of PV, boost chopper based on MPPT and storage.

2.1.1.3 Battery

The battery is assumed to be a constant voltage source with fixed amount of energy and modeled as a constant dc voltage source with series internal resistance where the VSC is connected to its output. The battery has a limitation on the duration of its generated power and depends on the amount of current supplied by it. It is assumed that the battery is charged at the off-peak load periods of the network and is

discharged at peak load times through the converter. In this thesis, for the dynamic study of the network, the battery is assumed to be with full state of charge and no restriction on rate of discharging.

2.1.1.4 DER converter

The considered DERs have a VSC consisting of three single-phase H-bridges, as shown in Fig. 2.4. This VSC structure has better controllability and dynamic performance under unbalanced conditions in the network compared to VSCs with three-phase three-leg configurations; since in this configuration, each phase is controlled individually. Alternatively, a three-phase four-leg configuration can be utilized.

Each H-bridge of VSCs is composed of insulated gate bipolar transistors (IGBT) with proper parallel reverse diode and snubber circuits. The outputs of each H-bridge are connected to a single-phase transformer, with 1 : a ratio, and the three transformers are wye-connected. The transformers provide galvanic isolation as well as voltage boosting. In this Fig 2.4, the resistance R_f represents the switching and transformer losses, while the inductance L_f represents the leakage reactance of the transformers. The filter capacitor C_f is connected to the output of the transformers to bypass the switching harmonics.

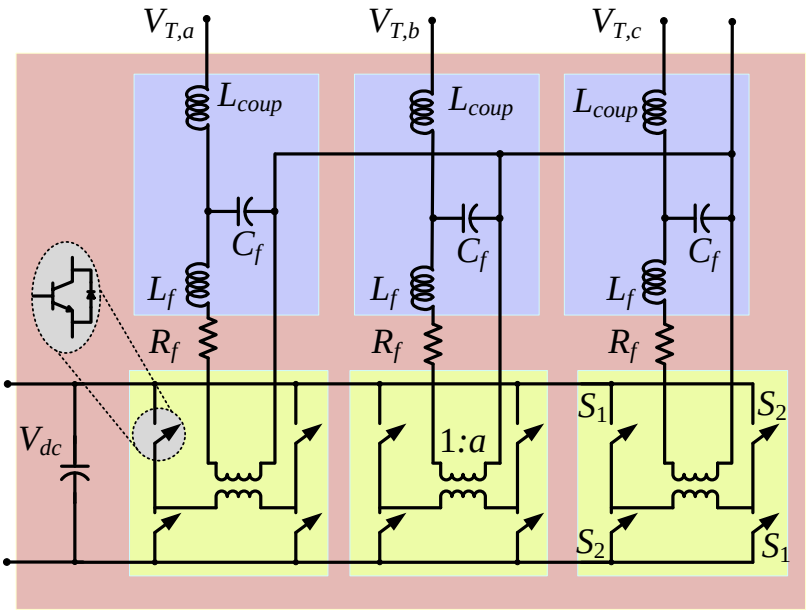

Fig. 2.4 Structure of the DER converter

2.1.1.5 Network Voltage Regulation

As mentioned in Chapter 1, in grid-connected mode, the grid dictates the network voltage and in off-grid mode, the DERs indirectly regulate the network voltage based on the droop control. Although in both modes, the voltage along the low voltage network will be within acceptable limits, it is desired to hold the network voltage to its nominal value of 1 pu. For this, in this research, voltage regulation in the microgrid is achieved by a DSTATCOM installed at the secondary side of the distribution transformer of the microgrid, which regulates its pcc voltage to a desired value, by exchanging reactive power with the network. The implemented DSTATCOM has the same converter structure as those of the DERs and its control is discussed in section 2.2.5.

2.1.1.6 Microgrid resynchronization

As mentioned in Chapter 1, in this research, resynchronization of a DER to the microgrid and a microgrid to the grid is required as DERs are operating in voltage-controlled strategy. For resynchronisation, the voltage magnitude and angle are measured on both sides of the circuit breaker. A phase-locked loop (PLL) is utilised for measuring the voltage angle [25]. The circuit breaker closes once the voltage angles and magnitudes are the same on both sides of the circuit breaker. However, based on network and load parameters, resynchronization can be slow and may take from several milliseconds to minutes [27].

It is to be noted that resynchronisation can be a complicated process depending on the network configuration, existence of systems of interconnected microgrids and their location along the medium voltage feeder [82]. Therefore, a general resynchronisation, self-healing and automatic supply restoration algorithm is required for this purpose. This controller will utilise communications between the network circuit breakers.

2.2 Microgrid hierarchical control

For proper operation of a microgrid within a network, a three-level hierarchical control system [12],[83]-[84], shown in Fig. 2.5 is required as discussed below:

- The primary (lowest) control level consists of inner-loop and outer-loop controls. Inner-loop control is responsible for appropriate switching of the converter

switches such that a proper tracking of the desired reference of DER converter output is achieved. This control is based on the references determined by outer-loop control and the local current and voltage measurements in DER converter output. Outer-loop control is responsible for proper output power control of DERs in the microgrid. This control generates the proper references for the inner-loop control and is different for grid-connected and off-grid modes. The dynamic performance of DER converters in the system of interconnected microgrids depends on the primary control level.

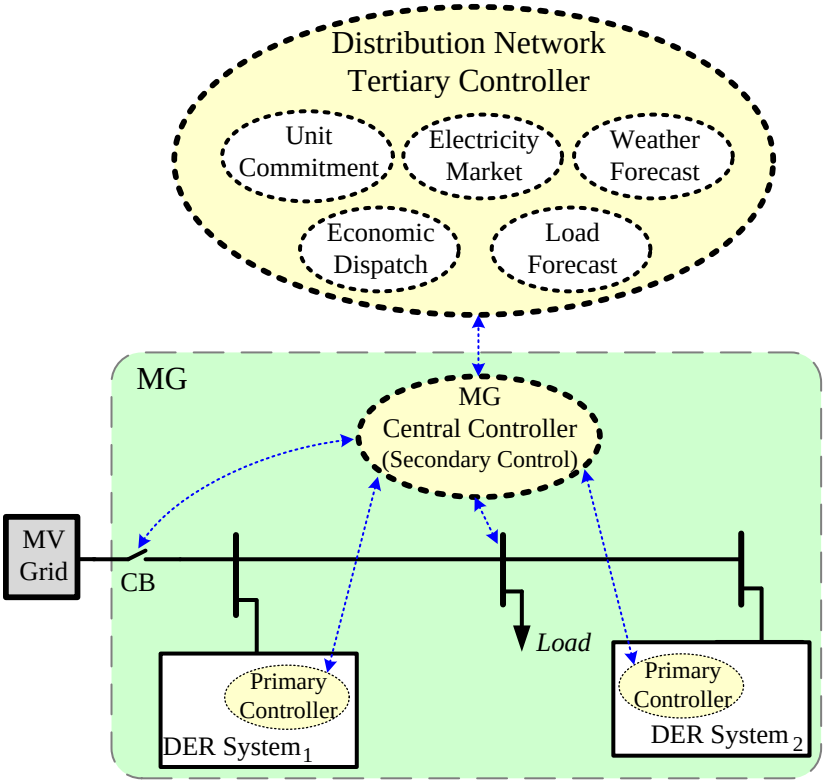

Fig. 2.5 Hierarchical microgrid control structure

- The secondary control is the central controller of the microgrid. This controller sends the desired (reference) output power of each DER converter to their primary controller. In grid-connected mode, the desired output power of each DER converter is received from the tertiary controller. However, in off-grid mode, this controller sends reference signals to DER converters in the form of voltage magnitude and angle, based on monitoring the network voltage and frequency, whenever required. This controller runs in a slower time frame

compared to that of the primary control [12]. It is to be noted that in the proposed system, the DSTATCOMs are operating individually based on their pre-default set points and are not controlled by the secondary controller.

- The tertiary (highest) control communicates with the central controllers in each microgrid and the protection devices and circuit breakers of the network. In general, this controller can utilize load forecasting, electricity market and demand response information for optimal power flow of the network and microgrids [85].

2.2.1 Outer-loop control of the primary controller during grid-connected mode

Let us consider Fig. 2.6, which shows one phase of the DER VSC and filter structure shown in Fig. 2.4 (Fig. 2,6a), its equivalent circuit (Fig. 2.6b) and its thevenin equivalent circuit (Fig. 2.6c). The thevenin equivalent parameters (i.e. V_{Th} and Z_{Th}) are shown in Fig. 2.6c.

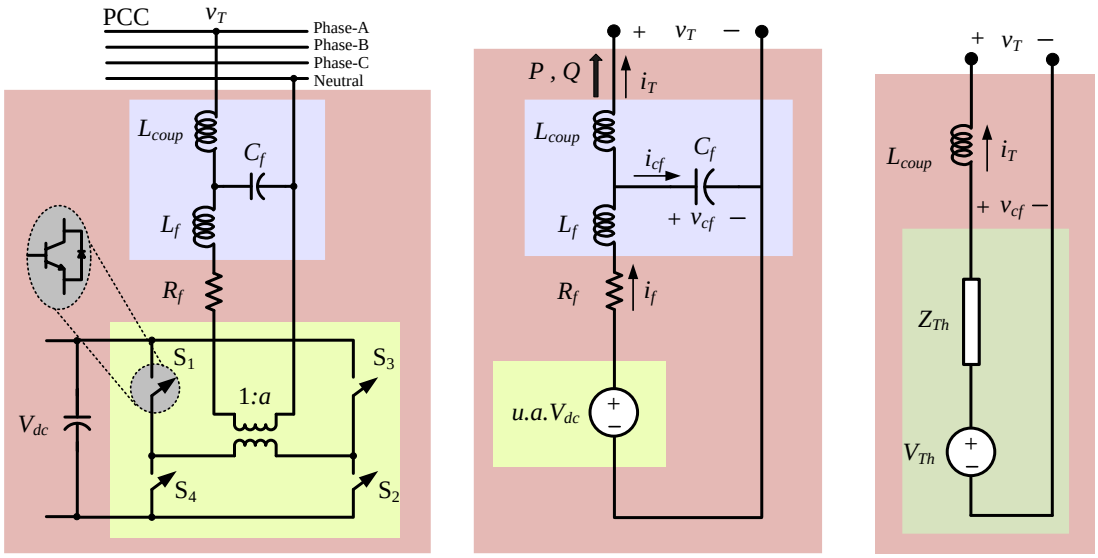

(a) (b) (c)

Fig. 2.6 (a) Single phase representation of the DER converter, (b) Simplified equivalent circuit of the DER single-phase converter, (c) Thevenin equivalent circuit.

From Fig 2.6c, it can be shown that the instantaneous active power (p) and reactive power (q) supplied from DER-i to its pcc can be expressed as [86]

$$
\begin{aligned}
p_i &= \frac{\left(\left|V_{T,i}\right|\left|V_{Th,i}\right|\cos\phi_i - \left|V_{Th,i}\right|^2\right)\cos\theta_i + \left|V_{T,i}\right|\left|V_{Th,i}\right|\sin\phi_i \sin\theta_i}{\left|Z_{Th,i} + Z_{coup,i}\right|} \\
q_i &= \frac{\left(\left|V_{T,i}\right|\left|V_{Th,i}\right|\cos\phi_i - \left|V_{Th,i}\right|^2\right)\sin\theta_i - \left|V_{T,i}\right|\left|V_{Th,i}\right|\sin\phi_i \cos\theta_i}{\left|Z_{Th,i} + Z_{coup,i}\right|} \\
\phi_i &= \delta_{Th,i} - \delta_{T,i} \\
\theta_i &= \angle\left(Z_{Th,i} + Z_{coup,i}\right)
\end{aligned}
\tag{2.3}
$$

where V_T is the pcc voltage, Z_{coup} is the coupling impedance and $V = |V| \angle\delta$ represents the phasor notation of $v(t)$. It is to be noted that the coupling impedance is dominantly inductive (i.e. $Z_{coup} \approx j\omega L_{coup}$). In section 2.2.3, it will be shown that after applying the proposed converter control, Z_{Th} is dominantly inductive in 50 Hz (i.e. $Z_{Th} \approx j\omega L_{conv}$) and has a very small magnitude. Therefore, it is expected that $V_{Th} \approx V_{cf}$ where V_{cf} is the voltage across the capacitor C_f. Based on these assumptions, (2.3) can be simplified as

$$
\begin{aligned}
p_i &= \frac{\left|V_{T,i}\right|\left|V_{cf,i}\right|\sin\left(\delta_{cf,i} - \delta_{T,i}\right)}{\omega L_{conv,i} + \omega L_{coup,i}} \\
q_i &= \frac{\left|V_{T,i}\right|\left|V_{cf,i}\right|\cos\left(\delta_{cf,i} - \delta_{T,i}\right) - \left|V_{T,i}\right|^2}{\omega L_{conv,i} + \omega L_{coup,i}}
\end{aligned}
\tag{2.4}
$$

The average active power (P) and reactive power (Q) supplied by each DER can then be calculated from p and q using a low pass filter.

In grid-connected mode, the grid dictates voltage and frequency of the network and the DERs operate at their nominal (rated) capacities. This can be achieved using a constant power control mode of operation [5]. In this research, a voltage-controlled technique is utilized which will monitor the pcc voltage (V_T) to regulate DER converter output voltage (V_{cf}) such that the desired nominal active and reactive power are injected into the network. For this, the pcc voltage magnitude and angles should be measured instantaneously and used in (2.4) to calculate the converter output reference voltage ($V_{cf,ref}$) for the desired powers and the known coupling inductance. This reference voltage will later be used in the inner-loop control to generate the switching signals for the converter. The schematic diagram of the system with the

discussed control is shown in Fig. 2.7 whereas the detailed block diagram of the controller is shown in Fig. 2.8.

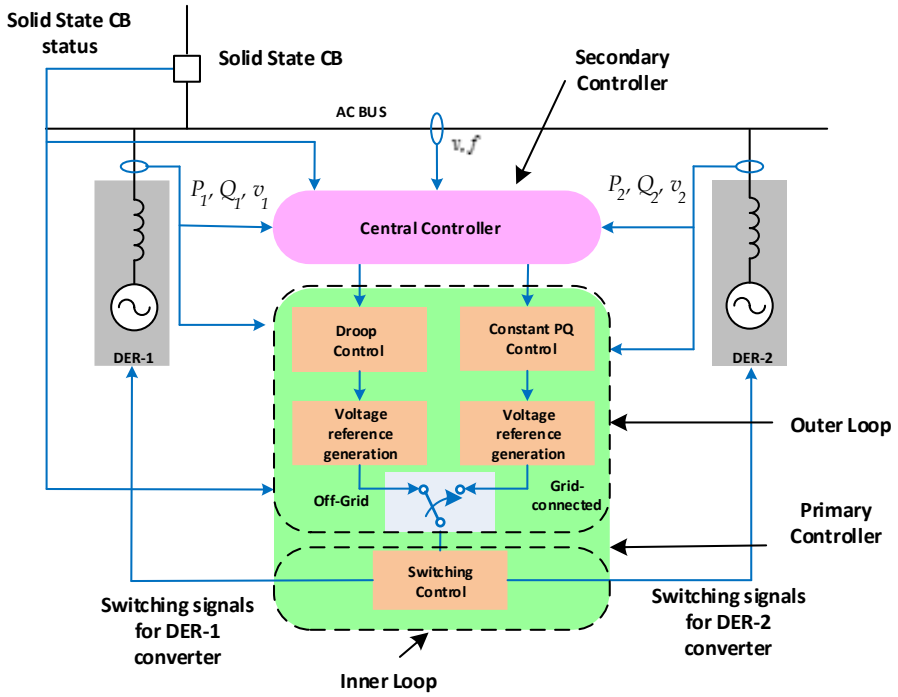

Fig. 2.7 Primary and secondary control levels of the microgrid system.

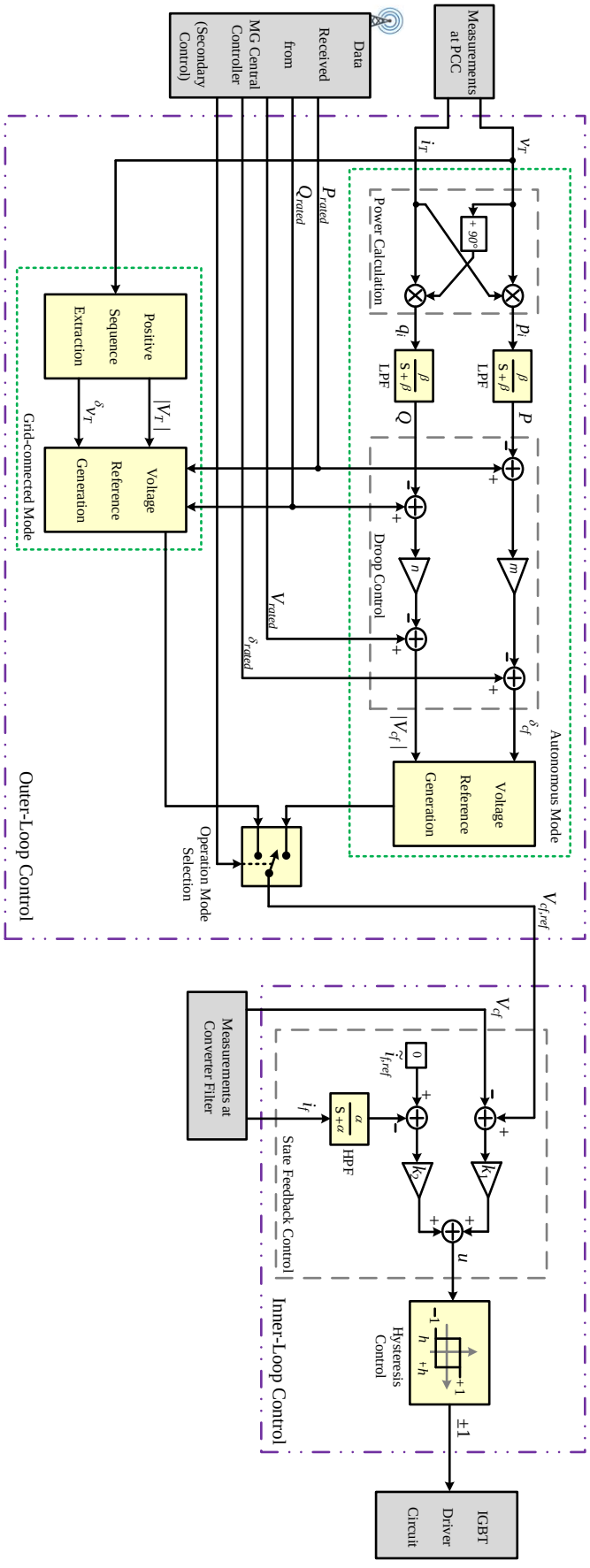

Fig. 2.8 Detailed block diagram of the primary control level of the DER converter control.

2.2.2 Outer-loop control of the primary controller during off-grid mode

During off-grid mode, network voltage and frequency should be regulated by the DERs. In addition, a proper power sharing among the DERs is desired. Below, a detailed description of the designed and implemented power sharing algorithm based on droop control is given.

Let us consider the microgrid shown in Fig. 2.1 with 2 DERs (i.e. DER-1 and DER-2) supplying a common load. DER-1 is connected to the load through a feeder impedance of $Z_{line,1}$ where DER-2 is connected to the load through a feeder impedance of $Z_{line,2}$. Let us also assume the feeder is highly inductive (i.e. $Z_{line} \approx j\omega L_{line}$). Assuming the voltage at load pcc is V_{load}, the active and reactive power supplied from each DER can be expressed as

$$\begin{aligned} p_i &= \frac{|V_{load,i}||V_{cf,i}|\sin(\delta_{cf,i} - \delta_{load,i})}{\omega L_{conv,i} + \omega L_{coup,i} + \omega L_{line,i}} \\ q_i &= \frac{|V_{load,i}||V_{cf,i}|\cos(\delta_{cf,i} - \delta_{load,i}) - |V_{load,i}|^2}{\omega L_{conv,i} + \omega L_{coup,i} + \omega L_{line,i}} \end{aligned} \tag{2.5}$$

As the feeder is assumed to be highly inductive, the active and reactive powers are decoupled and a decoupled load flow analysis can be applied. In addition, the angle difference between V_{cf} and V_{load} is small. Based on decoupled load flow, the average active power supplied from each DER to the load is

$$P_i = \frac{|V_{load,i}||V_{cf,i}|(\delta_{cf,i} - \delta_{load})}{\omega L_{conv,i} + \omega L_{coup,i} + \omega L_{line,i}} \tag{2.6}$$

To supply the load with an average active power of P_i , from (2.6), the angle of the voltage across the filter capacitor of DER-*i* will be

$$\delta_{cf,i} = P_i(\Gamma_{conv,i} + \Gamma_{coup,i} + \Gamma_{line,i}) + \delta_{load} \tag{2.7}$$

where $\Gamma_i = \dfrac{\omega L_i}{|V_{cf,i}||V_{load}|}$

Decentralized power sharing among several DERs in a microgrid can be achieved by changing the voltage magnitude and angle of DERs using the droop control as [11]

$$\begin{aligned}\delta_{cf,i} &= \delta_{rated,i} - m_i\left[\frac{X_{line}}{Z_{line}}\left(P_{rated,i}-P_i\right)-\frac{R_{line}}{Z_{line}}\left(Q_{rated,i}-Q_i\right)\right]\\ \left|V_{cf,i}\right| &= V_{rated,i} - n_i\left[\frac{R_{line}}{Z_{line}}\left(P_{rated,i}-P_i\right)+\frac{X_{line}}{Z_{line}}\left(Q_{rated,i}-Q_i\right)\right]\end{aligned} \tag{2.8}$$

where V_{rated} and δ_{rated} are respectively the rated voltage magnitude and angle of the DER when supplying rated active power (P_{rated}) and reactive power (Q_{rated}). Reactive power-voltage and active power-angle droop coefficients are represented by n and m, respectively. By designing the coupling inductance of the DER converter to be ten times larger than the line impedance, (2.8) can be further simplified as

$$\begin{aligned}\delta_{cf,i} &= \delta_{rated,i} - m_i\left(P_{rated,i}-P_i\right)\\ \left|V_{cf,i}\right| &= V_{rated,i} - n_i\left(Q_{rated,i}-Q_i\right)\end{aligned} \tag{2.9}$$

Hence, the active and reactive power outputs of the DERs are monitored and the microgrid voltage and frequency are controlled, accordingly by the outer-loop control. Therefore, it is expected that the outer-loop control determines the desired V_{cf} for each DER in microgrid. The block diagram of outer-loop control is shown in Fig. 2.8.

Let us assume when each DER changes its output active power from zero to its nominal (rated) capacity, the DER frequency reduces by $\Delta\omega$. Based on this assumption, the active power-angle droop coefficient for each DER [87] is derived from

$$m_i = \frac{\Delta\omega}{P_{rated,i}} \tag{2.10}$$

Assuming $\Delta\omega$ to be constant for DERs i and j with different nominal capacities, we have

$$\frac{m_i}{m_j} = \frac{P_{rated,j}}{P_{rated,i}} \tag{2.11}$$

Now, let us assume that all DERs in the microgrid have the same power factor and when each DER changes its output reactive power from zero to its nominal

(rated) capacity, the DER voltage reduces by ΔV. Based on this assumption, the reactive power-voltage droop coefficient for each DER [87] is derived from

$$n_i = \frac{\Delta V}{Q_{rated,i}} \tag{2.12}$$

Assuming ΔV to be constant for DERs i and j with different nominal capacities, we have

$$\frac{n_i}{n_j} = \frac{Q_{rated,j}}{Q_{rated,i}} \tag{2.13}$$

Now, for the microgrid in steady state condition, let us assume DER-i and DER-j have the same δ_{rated}. Therefore, from (2.9) and (2.11) we have

$$\begin{aligned} &\delta_{cf,i} - \delta_{cf,j} \\ &\quad = \left(\delta_{rated,i} - \delta_{rated,j}\right) - m_i\left(P_{rated,i} - P_i\right) + m_j\left(P_{rated,j} - P_j\right) \\ &\quad = m_i P_i - m_j P_j \end{aligned} \tag{2.14}$$

Replacing $\delta_{cf,i}$ and $\delta_{cf,j}$ from (2.7) in (2.14), we have

$$\begin{aligned} &P_i\left(\Gamma_{conv,i} + \Gamma_{coup,i} + \Gamma_{line,i}\right) - P_j\left(\Gamma_{conv,j} + \Gamma_{coup,j} + \Gamma_{line,j}\right) \\ &= m_i P_i - m_j P_j \end{aligned} \tag{2.15}$$

Therefore, the ratio of the active power supplied by the DERs is equal to

$$\frac{P_j}{P_i} = \frac{-m_i + \Gamma_{conv,i} + \Gamma_{coup,i} + \Gamma_{line,i}}{-m_j + \Gamma_{conv,j} + \Gamma_{coup,j} + \Gamma_{line,j}} \tag{2.16}$$

Eq. (2.16) shows that output active power of each DER is inversely proportional to the sum of Γ in its output. The three components of Γ_{conv}, Γ_{coup} and Γ_{line} are dependent on three inductances between the DER and the load. Since Γ has a parameter of voltage square in its denominator, it is expected that

$$\Gamma_{conv,i} << \Gamma_{line,i} << \Gamma_{coup,i} << m_i \tag{2.17}$$

Therefore, (2.16) can be simplified further as

$$\frac{P_j}{P_i} \approx \frac{m_i}{m_j} \tag{2.18}$$

In a similar way, it can be shown that the ratio of the reactive power supplied by the DERs in the microgrid will be

$$\frac{Q_j}{Q_i} \approx \frac{n_i}{n_j} \tag{2.19}$$

Hence, based on the above assumption, from (2.11), (2.18) and (2.13), (2.19), it is expected that the output active and reactive power ratio among two DERs in the microgrid will be same as the ratio of their nominal active and reactive power capacities.

On the other hand, in parallel operation of converter-interfaced DERs in a microgrid, for all the DERs, it is desired that the voltage angle difference across their coupling inductances (i.e. $\delta_{cf} - \delta_T$) in (2.4) to be constant. This voltage angle difference is preferred to be small [87] so that it is on the linear section of sinusoidal P-δ characteristic of (2.4). Similarly, it is desired the voltage drop across the coupling inductances (i.e. $|V_{cf}| - |V_T|$) in (2.4) to be constant, for all the DERs. This voltage drop is preferred to be small and in the range of 1-2 % [88]. For achieving these assumptions, the coupling inductances are designed inversely proportional to the nominal power ratio of DERs as

$$\frac{L_{coup,i}}{L_{coup,j}} = \frac{P_{rated,j}}{P_{rated,i}} = \frac{Q_{rated,j}}{Q_{rated,i}} \tag{2.20}$$

From (2.3)-(2.20), it is concluded that for an accurate power sharing among DERs in microgrid, it is required that

$$\begin{aligned} \frac{P_j}{P_i} &\approx \frac{m_i}{m_j} = \frac{L_{coup,i}}{L_{coup,j}} = \frac{P_{rated,j}}{P_{rated,i}} \\ \frac{Q_j}{Q_i} &\approx \frac{n_i}{n_j} = \frac{L_{coup,i}}{L_{coup,j}} = \frac{Q_{rated,j}}{Q_{rated,i}} \end{aligned} \tag{2.21}$$

2.2.3 Inner-loop control

As mentioned before, the outer-loop control regulates the output power of the DERs by adjusting the proper references for the each DER from (2.4) or (2.9). The inner-loop control will calculate and apply proper switching signals for the IGBTs in the DER converter such that the desired voltage ($V_{cf,ref}$) is perfectly generated across the ac filter capacitor (C_f).

It is desired to develop a per-phase based control technique (i.e. *abc*) instead of the conventional Direct-Quadrature (*dq*) transformation based techniques. For this, let us consider the equivalent single-phase circuit of VSC as shown in Fig. 2.6b. In this figure, $u \cdot a \cdot V_{dc}$ represents the converter output voltage, where u is the switching function. For a 2-level (bipolar) switching, u can take ±1, which will be used subsequently to turn ON/OFF the IGBTs.

Let us consider the DER converter and its output filter as a single system for which a controller is to be developed. By referring to Fig. 2.6c, the differential equations that describe the dynamic behavior of this system are given by

$$\begin{aligned} u_i.a.Vdc &= R_f i_{f,i} + L_f \frac{di_{f,i}}{dt} + v_{cf,i} \\ i_{f,i} &= C_f \frac{dv_{cf,i}}{dt} + i_{T,i} \end{aligned} \tag{2.22}$$

A closed-loop optimal linear robust controller based on state feedback is utilized to generate u. Let us assume the state vector $x(t)$ for each phase of the system is defined as

$$x_i(t) = [v_{cf,i}(t) \quad i_{f,i}(t)]^T \tag{2.23}$$

where $v_{cf}(t)$ represent the instantaneous voltage across ac filter capacitor, $i_f(t)$ is the current passing through filter inductor L_f and T is the transpose operator. Then, the equivalent circuit of this system can be represented with state space equation of

$$\dot{x}_i(t) = A x_i(t) + B_1 u_{c,i}(t) + B_2 i_{T,i}(t) \tag{2.24}$$

where

$$A=\begin{bmatrix} 0 & \frac{1}{C_f} \\ -\frac{1}{L_f} & -\frac{R_f}{L_f} \end{bmatrix} \quad B_1=\begin{bmatrix} 0 \\ \frac{a.Vdc}{L_f} \end{bmatrix} \quad B_2=\begin{bmatrix} -\frac{1}{C_f} \\ 0 \end{bmatrix} \tag{2.25}$$

In (2.24), $u_c(t)$ is the continuous time version of switching function u and i_T represents the network load change effects on this system; hence it is assumed as a disturbance for the controller.

In the control systems, the desired values for each control parameter in steady state condition must be known. However, it is rather hard to determine the reference for i_f in (2.23). Nevertheless, it is desired i_f does not have high frequency components. Therefore, instead of using i_f as a control parameter, its high frequency components ($\tilde{i}_f$) can be used in the control system. Based on this assumption, $\tilde{i}_f$ can be described and expanded in Laplace domain as [89]

$$\tilde{i}_f(s)=\frac{s}{s+\alpha}i_f(s)=\left(1-\frac{\alpha}{s+\alpha}\right)i_f(s)=i_f(s)-\hat{i}_f(s) \tag{2.26}$$

where α is the cut-off frequency of this high-pass filter and $\hat{i}_f$ is the low frequency components of i_f which is given by

$$\hat{i}_f(s)=\frac{\alpha}{s+\alpha}i_f(s) \tag{2.27}$$

Eq. (2.27) can be expressed in differential equation form as

$$\frac{d\hat{i}_f(t)}{dt}=\alpha\left(i_f(t)-\hat{i}_f(t)\right) \tag{2.28}$$

Now, let us define a new state vector for the system, which includes $\hat{i}_f$ as a state vector, as in [89]

$$x_i'(t)=[v_{cf,i}(t) \quad i_{f,i}(t) \quad \hat{i}_{f,i}(t)]^T \tag{2.29}$$

In this case, the system can be represented with new state space equation of

$$\dot{x}_i'(t)=A'x_i(t)+B_1'u_{c,i}(t)+B_2'i_{T,i}(t) \tag{2.30}$$

where

$$A' = \begin{bmatrix} 0 & \frac{1}{C_f} & 0 \\ -\frac{1}{L_f} & -\frac{R_f}{L_f} & 0 \\ 0 & \alpha & -\alpha \end{bmatrix} \quad B_1' = \begin{bmatrix} B_1 \\ 0 \end{bmatrix} \quad B_2' = \begin{bmatrix} B_2 \\ 0 \end{bmatrix} \tag{2.31}$$

Eq. (2.30) can be represented in discrete-time domain as [90]

$$x_i'(k+1) = Fx_i'(k) + G_1 u_{c,i}(k) + G_2 i_{T,i}(k) \tag{2.32}$$

where

$$F = e^{A'.T_s} \quad , \quad G_1 = \int_0^{T_s} e^{A't} B_1' \, dt \quad , \quad G_2 = \int_0^{T_s} e^{A't} B_2' \, dt \tag{2.33}$$

where T_s is the sampling time. From (2.32), $u_c(k)$ can be computed, using a suitable state feedback control law, as

$$u_{c,i}(k) = -K[x_i'(k) - x_{ref,i}'(k)] \tag{2.34}$$

where K is a gain matrix and $x'_{ref}(k)$ is the desired state vector for (2.29), in discrete-time domain. Fig. 2.9 shows the closed-loop block diagram of an linear quadratic regulator (LQR)-based control system for the DERs.

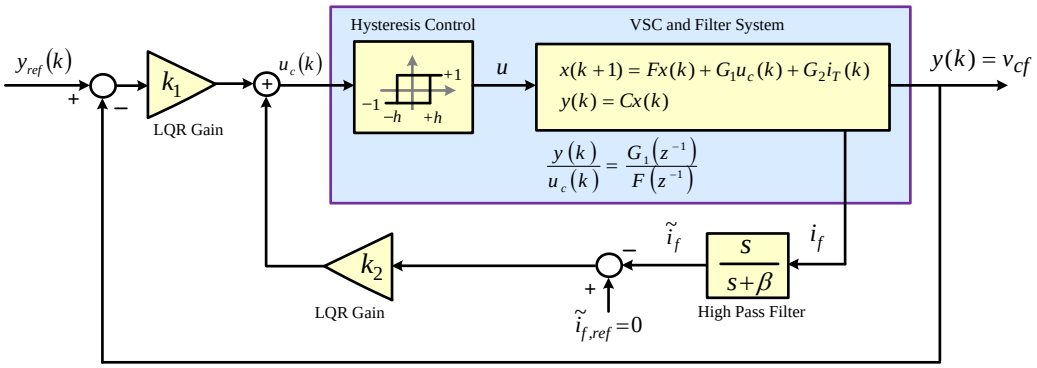

Fig. 2.9 Closed-loop switching control block diagram for voltage control strategy based on LQR.

It is to be noted that the desired reference value for $v_{cf}(t)$ for each DER will be determined by the outer-loop control. This value is calculated from (2.4) when microgrid operates in grid-connected mode and from (2.9) when microgrid operates

in off-grid mode. As mentioned before, the desired reference value for $\tilde{i}_f(t)$ for all DERs is always set to zero to minimize the high frequency components of the current flowing through L_f. Therefore, $i_f(t)$ must only contain low frequency components (i.e. $i_f(t) = \hat{i}_f(t)$). Now, the reference vector, X'_{ref} can be defined for each DER as

$$X'_{ref,i} = [V_{cf,ref,i} \quad \hat{I}_f \quad \hat{I}_f]^T = [V_{cf,i} \angle \delta_{cf,i} \quad \hat{I}_f \quad \hat{I}_f]^T \tag{2.35}$$

As the system behavior in steady-state is interested and assuming a full control over $u_c(k)$, an infinite time LQR [90] based design technique can be utilized to define K. This controller is more stable than proportional-integrator-derivative (PID) based controls and prevents the instability among parallel connected DERs when two off-grid microgrids are interconnected together. In addition, PID based controllers are not very effective when utilized in per-phase based controls.

In a discrete LQR problem, an objective function J is chosen as

$$J_i(k) = \sum_{k=0}^{\infty} \begin{bmatrix} \left(x'_i(k) - x'_{ref,i}(k)\right)^T Q_i(k) \left(x'_i(k) - x'_{ref,i}(k)\right) \\ + u_i(k)^T R_i(k) u_i(k) \end{bmatrix} \tag{2.36}$$

where R is the control cost matrix, Q is the state weighting matrix which reflects the importance of each controlling parameter in x while $J(\infty)$ represents the objective function at infinite time (steady-state condition) for the system. Eq. (2.36) is then minimized to obtain the optimal control law $u(k)$ through solution of steady state Riccati equations [90] while satisfying system constraints in (2.32). The LQR method ensures the desired results for the system while the variations of system load and source parameters are within acceptable limits of reality.

Eq. (2.34) shows the total tracking error of each DER converter. The tracking error can be minimized by limiting this error within a very small bandwidth (e.g. $h = 10^{-4}$). Now, from (2.34), for each DER, the switching function u (i.e. which pairs of IGBTs to turn ON/OFF) is generated using a hysteresis control based on the error level as

$$\begin{aligned} &\textit{If} \quad u_{c,i}(k) > +h \quad \textit{then} \quad u_i = +1 \\ &\textit{If} \quad -h \le u_{c,i}(k) \le +h \quad \textit{then} \quad u_i = \textit{previous } u_i \\ &\textit{If} \quad u_{c,i}(k) < -h \quad \textit{then} \quad u_i = -1 \end{aligned} \tag{2.37}$$

More detail on the discussed converter control is given in [23].

To achieve a good tracking of the output voltage, a state feedback control was utilized for each DER. Therefore, the controller expression can be presented as

$$\begin{aligned} u_i.a.Vdc &= v_{cf,ref,i} - K(X_i' - X'_{ref,i}) \\ &= v_{cf,ref,i} - k_1\left(v_{cf,i} - v_{cf,ref,i}\right) - k_2\left(\tilde{i}_{f,i} - 0\right) \end{aligned} \tag{2.38}$$

where $K = [k_1 \;\; k_2 \;\; k_2]$ is the gain matrix in (2.34).
Replacing (2.38) in (2.22) and representing that in Laplace domain, we have

$$\begin{aligned} &V_{cf,i}(s)\left[L_f C_f s^2 + R_f C_f s + 1\right] + I_{T,i}(s)\left[L_f s + R_f\right] \\ &\quad = V_{cf,ref,i}(s)\left[k_1 + 1\right] - k_1 V_{cf,i}(s) - \frac{k_2 s}{s+\alpha} I_{f,i}(s) \end{aligned} \tag{2.39}$$

From (2.39), the parameters of the thevenin equivalent circuit of the DER converter and filter including the developed state feedback control are given by

$$V_{cf,i}(s) = G_1(s) V_{cf,ref,i}(s) + G_2(s) I_{T,i}(s) \tag{2.40}$$

where $G_1(s)$ and $G_2(s)$ are defined as

$$\begin{aligned} G_1(s) &= \frac{(k_1+1)s + \alpha(k_1+1)}{L_f C_f s^3 + C_f\left(R_f + k_2 + \alpha L_f\right)s^2 + \left(k_1 + 1 + \alpha R_f C_f\right)s + \alpha(k_1+1)} \\ G_2(s) &= \frac{L_f S^2 + \left(R_f + \alpha L_f - k_2\right)S + \alpha R_f}{L_f C_f s^3 + C_f\left(R_f + k_2 + \alpha L_f\right)s^2 + \left(k_1 + 1 + \alpha R_f C_f\right)s + \alpha(k_1+1)} \end{aligned} \tag{2.41}$$

and $G_1(s)\, V_{cf,ref}(s) = V_{Th}$ and $G_2(s) = -Z_{Th}$.

The performance of the state feedback control versus the open loop transfer function of the DER converter and filter system can be studied from frequency domain analysis. For this, the Bode diagram of $G_1(s)$ and $G_2(s)$ are obtained and shown in Fig. 2.10a and Fig. 2.10b, respectively. In Fig. 2.10a, it can be seen that at frequency range of interest (i.e. 50 Hz), $G_1(s)$ has the property of a unity gain with zero angle (i.e. $V_{Th} \approx V_{cf}$). This helped us to simplify (2.3) into (2.4) in section 2.2.1. On the other hand, in Fig. 2.10b, it can be seen that at frequency range of interest, $G_2(s)$ magnitude is relatively high in open loop condition. The high value takes the network load and i_T change effects into the DER converter control. This magnitude is reduced effectively by properly designing the state feedback gains. It is to be noted

that $G_2(s)$ is relatively inductive around 50 Hz. This is the reason for assuming Z_{Th} to be pure inductive in (2.3) in section 2.2.1.

(a)

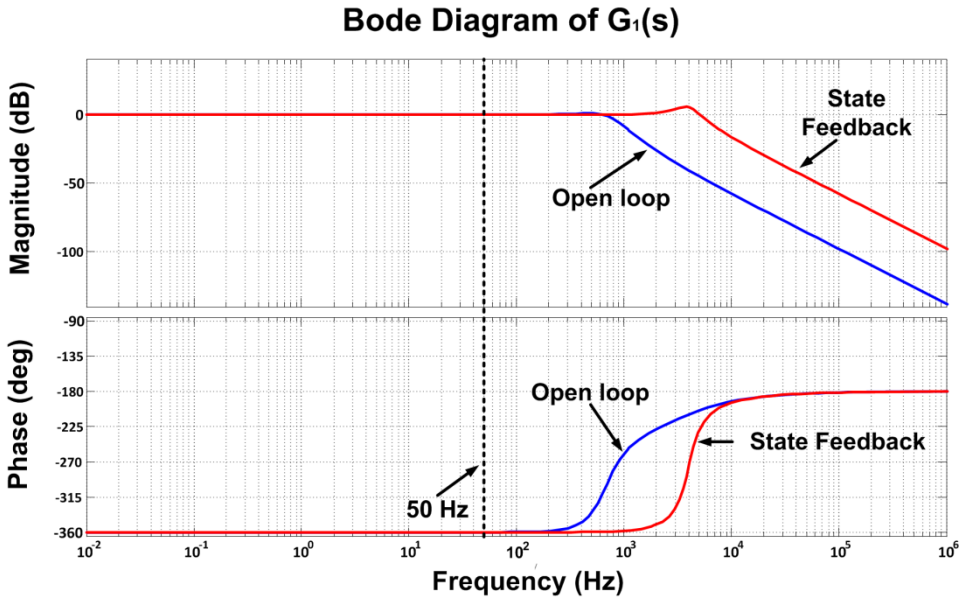

(b)

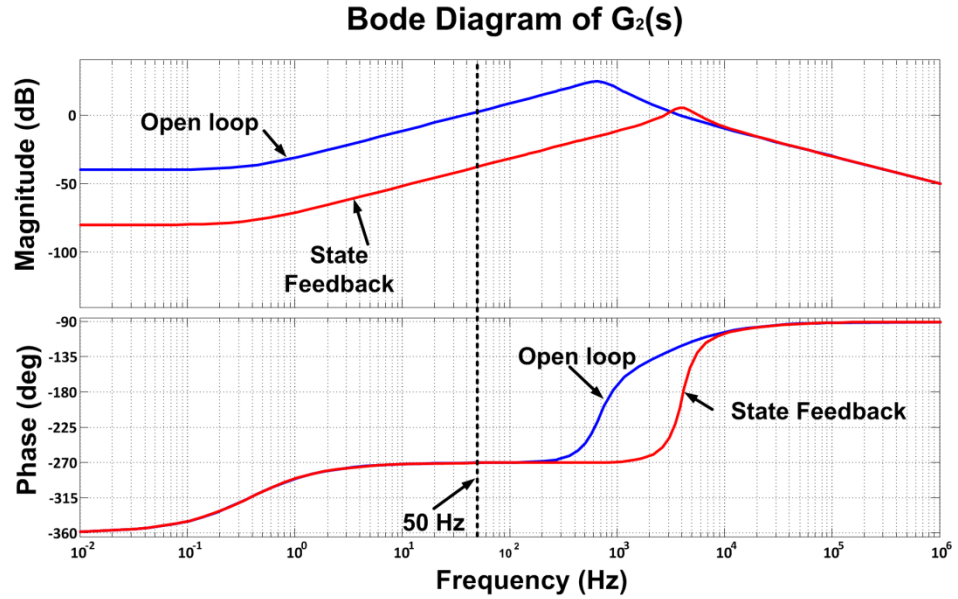

Fig. 2.10 (a) Open loop and closed loop Bode diagram of $G_1(s)$, (b) Open loop and closed loop Bode diagram of $G_2(s)$.

2.2.4 Additional modules of the central controller

The secondary level control (central controller) communicates with the distribution network tertiary controller as well as the primary controller of all DERs within the microgrid. The main responsibility of the central controller is to provide the references and set points, required for the primary controller of each DER system. These set points are later used to define the output active and reactive power

of each DER system. This is valid for both grid-connected and off-grid operating modes. It is to be noted that the central controller does not operate instantaneously and has larger time steps (ΔT) compared to the primary controller of each DER system. Hence, it runs in a slower time frame compared to the primary controllers; however, it should be faster than the operation time of the under/overvoltage and under/over frequency relays within the microgrid.

In grid-connected mode, each DER generates an output power based on its MPPT or the level defined by the distribution network tertiary controller. Hence, in this case, the microgrid central controller receives the desired ratio of the output power of the DERs from the tertiary controller and passes those information (set points) to each DER system.

In off-grid mode, each DER has to generate a portion of the load requirements within the microgrid. This portion is again defined by the tertiary controller and passed to each DER system through the central controller. However, in this case, as the voltage and frequency in the microgrid is not decided by the grid, the central controller is also responsible for monitoring these two parameters. According to the load variations in the microgrid, the output power of each DER will vary; however, if the voltage and frequency of the microgrid increases above or drops below the acceptable thresholds, the central controller defines new settings for the primary controller of each DER system and then sends these set points to them. It is to be noted that this procedure should take place faster than the pre-defined operation time for under/over frequency relays in the microgrid.

The central controller consists of several modules, as described in detail below.

2.2.4.1 Circuit breaker status monitoring module

Depending on the state of the main circuit breaker, the microgrid operates in either grid-connected or off-grid mode. In this research, islanding detection is realized by monitoring the status of the circuit breaker assuming the communication infrastructure availability to transfer the information to the DERs.

2.2.4.2 Dynamic power ratio adjustment module

From (2.5), assuming L_{conv} and L_{line} are much smaller than L_{coup}, the ratio of the average active power between these two DERs can be given as

$$\frac{P_1}{P_2}=\frac{L_{T,2}}{L_{T,1}}\frac{|V_1|\sin\delta_1}{|V_2|\sin\delta_2} \tag{2.42}$$

Now, let us assume the desired active power ratio between these two DERs is $P_1/P_2 = k_p$ where $k_p > 0$. In many references such as [3][32], for simplicity, it is assumed that

$$\begin{cases}\dfrac{P_1}{P_2}=k_p\\ \dfrac{L_{T,2}}{L_{T,1}}=k=k_p\end{cases}\quad\Rightarrow\quad |V_1|\sin\delta_1=|V_2|\sin\delta_2 \tag{2.43}$$

Similaly, assuming L_{conv} and L_{line} are much smaller than L_{coup}, the ratio of the reactive power output between two DERs can be calculated from (2.5) as

$$\frac{Q_1}{Q_2}=\frac{L_{T,2}}{L_{T,1}}\frac{|V_1|\cos\delta_1-|V_3|}{|V_2|\cos\delta_2-|V_3|} \tag{2.44}$$

Now, let us assume that the reactive power ratio between these two DERs is $Q_1/Q_2 = k_q$ where $k_q > 0$. In many references such as [3][32], for simplicity, it is assumed that

$$\begin{cases}\dfrac{Q_1}{Q_2}=k_q=k_p\\ \dfrac{L_{T,2}}{L_{T,1}}=k=k_q\end{cases}\quad\Rightarrow\quad |V_1|\cos\delta_1=|V_2|\cos\delta_2 \tag{2.45}$$

However, in general, it can be assumed that coupling inductances of the two DERs can have a ratio of k' where $k' > 0$. In such a case, we have

$$\begin{cases}\dfrac{P_1}{P_2}=k_p\\ \dfrac{L_{T,2}}{L_{T,1}}=k'\end{cases}\quad\Rightarrow\quad |V_1|\sin\delta_1=\frac{k_p}{k'}|V_2|\sin\delta_2=k''|V_2|\sin\delta_2 \tag{2.46}$$

where $k'' = k_p/k'$. From (2.46), it can be seen that under such conditions, the voltages at the outputs of both of the DERs are correlated by a factor of k''. It is to be noted that under such condition, the ratio among the reactive powers of the two DERs will be as

$$\begin{cases} \dfrac{Q_1}{Q_2} = k_q \\ \dfrac{L_{T,2}}{L_{T,1}} = k' \end{cases} \Rightarrow \quad |V_1|\cos\delta_1 - |V_3| = \frac{k_q}{k'}\left(|V_2|\cos\delta_2 - |V_3|\right) \tag{2.47}$$

Hence, from (2.46) and (2.47), it can be seen that in general $k_p \neq k_q$. Therefore, the output active power of the two DERs can be controlled to be equal to the desired value of k_p while the ratio of the reactive power outputs among these two DERs will not be equal to k_p. Hence, if only active power ratio is going to be changed dynamically, any ratio of the coupling inductances can be selected (considering the system stability). In addition to the active power, if the reactive power ratio is also desired to be changed dynamically, a virtual impedance technique as discussed in [35] can be utilized.

In grid-connected mode as well as the off-grid mode, the distribution network tertiary controller defines the desired output power ratio among the DERs within a microgrid. Hence, the ratio among the output powers of two DERs can change dynamically based on the commands from the tertiary controller which are transferred to the DERs through the microgrid central controller. Let us assume that at $t = t_1$, the ratio of the output active power of two DERs (i.e. DER-1 and DER-2 of Fig. 2.1) is k_{p1}. Hence, from (2.21), we have $P_{\text{rated},2}/P_{\text{rated},1} = m_1/m_2 = k_{p1}$. In this case, from (2.9), we have

$$f_1^{t_1} = f_{\text{rated}} + m_1\left(P_{\text{rated},1} - P_1^{t_1}\right) \tag{2.48}$$

The tertiary controller decides to change this ratio to k_{p2} at $t = t_2$. Hence, from (2.9), we have

$$f_1^{t_2} = f_{\text{rated}} + m_1\left(P_{\text{rated},1} - P_1^{t_2}\right) \tag{2.49}$$

Since the load demand in t_1 and t_2 is the same, the total active power generation by the DERs will be the same during these two time intervals. Hence, we have

$$P_1^{t_1} + P_2^{t_1} = P_1^{t_2} + P_2^{t_2} \tag{2.50}$$

Replacing the power ratios in (2.50), it can be simplified as

$$P_1^{t_1} + k_{p1}P_1^{t_1} = P_1^{t_2} + k_{p2}P_1^{t_2} \Rightarrow P_1^{t_1}(1+k_{p1}) = P_1^{t_2}(1+k_{p2})$$
$$\Rightarrow P_1^{t_2} = P_1^{t_1}\frac{1+k_{p1}}{1+k_{p2}} \tag{2.51}$$

From (2.48), (2.49) and (2.51), the frequency variation due to this ratio change is calculated as

$$\Delta f^t = f_1^{t_2} - f_1^{t_1} = m_1\left(P_1^{t_1} - P_1^{t_2}\right) = P_1^{t_1}m_1\left(1-\frac{1+k_{p1}}{1+k_{p2}}\right)$$
$$= \frac{k_{p2}-k_{p1}}{1+k_{p2}}m_1P_1^{t_1} \tag{2.52}$$

It is to be noted that this frequency variation is acceptable as far as the new frequency of the microgrid is between $f_{\max}$ and $f_{\min}$. Therefore, we have

$$f_{\min} \le f_1^{t_1} + \Delta f^t \le f_{\max} \Rightarrow f_{\min} - f_1^{t_1} \le \Delta f^t \le f_{\max} - f_1^{t_1}$$
$$f_{\min} - f_1^{t_1} \le \frac{k_{p2}-k_{p1}}{1+k_{p2}}m_1P_1^{t_1} \le f_{\max} - f_1^{t_1} \tag{2.53}$$

Assuming

$$H_1 = \frac{f_{\min} - f_1^{t_1}}{m_1P_1^{t_1}} \text{ and } H_2 = \frac{f_{\max} - f_1^{t_1}}{m_1P_1^{t_1}}$$

in order to prevent non-acceptable frequency in the microgrid, k_{p2} must fulfil the following constraints.

$$\begin{cases} k_{p2} > 0 \\ k_{p2} \le \left(k_{p1} + H_1\right)/\left(1-H_1\right) \\ k_{p2} \le \left(k_{p1} + H_2\right)/\left(1-H_2\right) \end{cases} \tag{2.54}$$

The similar study can be repeated for the voltage magnitude in the microgrid. Assuming at $t = t_1$, the ratio of the output reactive power of DER-1 and DER-2 of Fig. 2.1 is k_{q1}, from (2.21), we have $Q_{\text{rated},2}/Q_{\text{rated},1} = n_1/n_2 = k_{q1}$. In this case, from (2.9), we have

$$\left|V_1\right|^{t_1} = V_{\text{rated}} + n_1\left(Q_{\text{rated},1} - Q_1^{t_1}\right) \tag{2.55}$$

The tertiary controller decides to change this ratio to k_{q2} at $t = t_2$. Hence, from (2.9), we have

$$|V_1|^{t_2} = V_{\text{rated}} + n_1\left(Q_{\text{rated},1} - Q_1^{t_2}\right) \tag{2.56}$$

Since the load demand in t_1 and t_2 are the same, the total reactive power generation by the DERs will be the same during these two time intervals. Hence, we have

$$Q_1^{t_1} + Q_2^{t_1} = Q_1^{t_2} + Q_2^{t_2} \tag{2.57}$$

Replacing the power ratios in (2.57), it can be simplified as

$$\begin{aligned} &Q_1^{t_1} + k_{q1}Q_1^{t_1} = Q_1^{t_2} + k_{q2}Q_1^{t_2} \Rightarrow Q_1^{t_1}(1+k_{q1}) = Q_1^{t_2}(1+k_{q2}) \\ &\Rightarrow Q_1^{t_2} = Q_1^{t_1}\frac{1+k_{q1}}{1+k_{q2}} \end{aligned} \tag{2.58}$$

From (2.55), (2.56) and (2.58), the voltage variation due to this ratio change is calculated as

$$\begin{aligned} \Delta|V_1|^t &= |V_1|^{t_2} - |V_1|^{t_1} = n_1\left(Q_1^{t_1} - Q_1^{t_2}\right) = Q_1^{t_1} n_1\left(1 - \frac{1+k_{q1}}{1+k_{q2}}\right) \\ &= \frac{k_{q2} - k_{q1}}{1+k_{q2}} n_1 Q_1^{t_1} \end{aligned} \tag{2.59}$$

It is to be noted that this voltage magnitude variation is acceptable as far as the new voltage magnitude of the microgrid is between $|V|_{\max}$ and $|V|_{\min}$. Therefore, we have

$$\begin{aligned} &|V|_{\min} \le |V_1|^{t_1} + \Delta|V|^t \le |V|_{\max} \\ &\Rightarrow |V|_{\min} - |V_1|^{t_1} \le \Delta|V|^t \le |V|_{\max} - |V_1|^{t_1} \\ &\Rightarrow |V|_{\min} - |V_1|^{t_1} \le \frac{k_{q2} - k_{q1}}{1+k_{q2}} n_1 Q_1^{t_1} \le |V|_{\max} - |V_1|^{t_1} \end{aligned} \tag{2.60}$$

Assuming

$$G_1 = \frac{|V|_{\min} - |V_1|^{t_1}}{n_1 Q_1^{t_1}} \text{ and } G_2 = \frac{|V|_{\max} - |V_1|^{t_1}}{n_1 Q_1^{t_1}}$$

in order to prevent non-acceptable voltage magnitude in the microgrid, k_{q2} must fulfil the following constraints.

$$\begin{cases} k_{q2} > 0 \\ k_{q2} \le \left(k_{q1} + G_1\right)/\left(1 - G_1\right) \\ k_{q2} \le \left(k_{q1} + G_2\right)/\left(1 - G_2\right) \end{cases} \tag{2.61}$$

If k_{p2} causes violations in the microgrid frequency and voltage magnitude, the f_{rated} and V_{rated} parameters for the DERs should be adjusted properly to recover the voltage magnitude and frequency to the acceptable ranges, as discussed below. Fig. 2.11 shows schematically the dynamic power ratio adjustment principle.

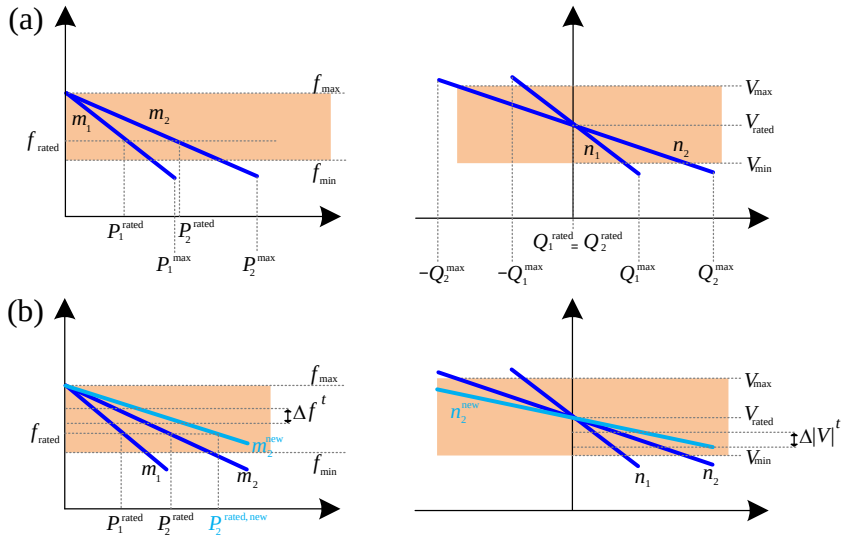

Fig. 2.11 (a) Active and reactive power sharing using droop between two DER converters, (b) Adjustments in the droop curve for dynamic power ratio variations among the two converters.

2.2.4.3 Droop curve adjustment module

In grid-connected mode, the voltage and frequency of the microgrid is dictated by the grid. However, in off-grid mode, these parameters are regulated indirectly by the output active and reactive power of the DERs. Hence, the droop curve adjustment module is only active when the microgrid is in off-grid mode. In this case, if the voltage magnitude or frequency within the microgrid rises above or drops below the acceptable thresholds, the central controller takes action to shift up or down the rated values of the droop characteristic. It is desired that for the same output powers of the DER system, the microgrid voltage magnitude and frequency is retained close to the desired values. For this, the difference between the frequency of the microgrid with

its desired value should be calculated. Let us call this difference as Δf. To adjust the microgrid frequency to the desired value, a new rated frequency can be defined by adding Δf to the previous (old) rated frequency as

$$f_{\text{rated}}^{\text{new}} = f_{\text{rated}}^{\text{old}} + \Delta f = f_{\text{rated}}^{\text{old}} + \left(f_{\text{desired}} - f\right) \tag{2.62}$$

Similarly, the difference between the voltage magnitude of the microgrid with its desired value should be calculated. Let us call this difference as ΔV. To adjust the microgrid voltage magnitude to the desired value, a new rated voltage can be defined by adding ΔV to the previous (old) rated voltage magnitude as

$$V_{\text{rated}}^{\text{new}} = V_{\text{rated}}^{\text{old}} + \Delta V = V_{\text{rated}}^{\text{old}} + \left(V_{\text{desired}} - |V|\right) \tag{2.63}$$

This is shown schematically in Fig. 2.12.

It is to be noted that, restoring the voltage magnitude and frequency to the rated values can also be achieved using a PI regulator. However, using the proposed method, the new references can be directly calculated and transmitted to the primary controllers of each DER system.

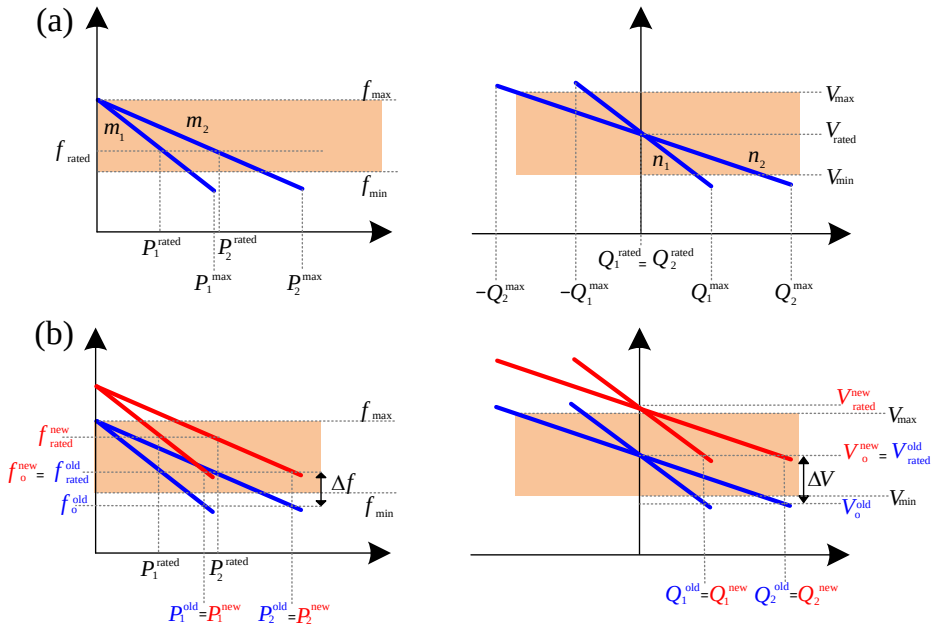

Fig. 2.12 (a) Active and reactive power sharing using droop between two DER converters, (b) Adjustments in the droop curve for regulating the network voltage and frequency within the acceptable limits.

2.2.4.4 Load shedding module

For the microgrid in off-grid mode, if the voltage magnitude and/or frequency in the ac bus reach a value below the pre-defined minimum acceptable limits even after droop curve adjustment is applied, the load shedding is required. In this research, a three-level load-shedding algorithm is developed which monitors the network frequency. If the frequency drops below the lower limit in any of the phases, the module applies the first level of load-shedding after a short delay (i.e. 0.2 s in this study). This may bring the frequency into the acceptable range. Otherwise, the second load-shedding is applied after a long delay (i.e. 1 s in this study). In a similar way, the third load shedding is applied after another long delay (i.e. 1 s delay), in case the second load-shedding also fails to recover the frequency.

2.2.5 DSTATCOM control

As discussed in section 2.1.1.5, voltage regulation in the microgrid is achieved by a DSTATCOM installed at the secondary side of the distribution transformer, which regulates its pcc voltage to a desired value. The utilized DSTATCOM in this research has an LCL filter in its converter output and voltage regulation is achieved by exchanging reactive power with the network. The reactive power exchange can be controlled in two different methods. These two methods are:

- Voltage control strategy: The first method is based on directly controlling the pcc voltage. In this method, the difference between the pcc root mean square (rms) voltage ($V_{T\text{-}DSTAT}$) and its desired value ($V_{T\text{-}DSTAT,desired}$) is utilized to generate the required voltage magnitude across ac filter capacitor in DSTATCOM as

$$\left|V_{cf-DSTAT}\right| = V_{cf-DSTAT,ref} + \left(K_P + \frac{K_I}{s}\right)\left(V_{T-DSTAT,desired} - V_{T-DSTAT}\right) \tag{2.64}$$

where $V_{cf\text{-}DSTAT,ref}$ is the assumed reference value for this voltage, K_P and K_I are PI regulator parameters and the suffix *DSTAT* represents DSTATCOM.

- Power factor correction strategy: The second method is based on power factor correction at pcc. This method is not a direct voltage control method since the DSTATCOM is controlled to exchange a desired reactive power with the network ($Q_{DSTAT,ref}$) which is equal to the network reactive power demand in

downstream side of the DSTATCOM. Hence, the required voltage magnitude across ac filter capacitor in DSTATCOM can be calculated as

$$\left|V_{cf-DSTAT}\right| = V_{cf-DSTAT,ref} + \left(K'_P + \frac{K'_I}{s}\right)\left(Q_{DSTAT,ref} - Q_{DSTAT}\right) \tag{2.65}$$

where Q_{DSTAT} is the measured injected reactive power by the DSTATCOM.

Now, let us consider a radial medium voltage network supplying 5 distribution transformers with a low voltage feeder in their downstream as shown in Fig. 2.13. All feeders have a similar impedance load of 88 kW with power factor 0.95 lagging. We refer to them as F1 to F5. The network does not include any DERs. Initially, no DSTATCOM is connected to any of the distribution feeders. In this case, voltage profile of the medium voltage side along the feeder drops from 0.97 pu, at the beginning of the feeder, to 0.92 pu, at the end of the feeder, as shown in Table 2.1.

Now, let us assume that the DSTATCOMs are connected to the secondary side of each distribution transformers, as shown in the figure. The operation of each DSTATCOM is independent from other DSTATCOMs and they all operate in voltage control mode. Once a DSTATCOM regulates its pcc voltage, the voltage in the primary side of that transformer (V_{MVF*}) is also regulated accordingly. Hence, in the considered system, the DSTATCOMs can be utilized to regulate the voltage, along the medium voltage feeder to a desired voltage profile. This voltage profile can be chosen as a flat voltage (i.e. 1 pu for all connection points) or a gradually decreasing voltages (e.g. 1, 0.99,…, 0.96 pu) along the medium voltage feeder. The fixed voltage set points are assigned for each DSTATCOM. It is to be noted that no optimization method is utilized to select these set points in this analysis. Since the DSTATCOMs hold the voltage along the medium voltage feeder, the node voltages are not affected by load changes.

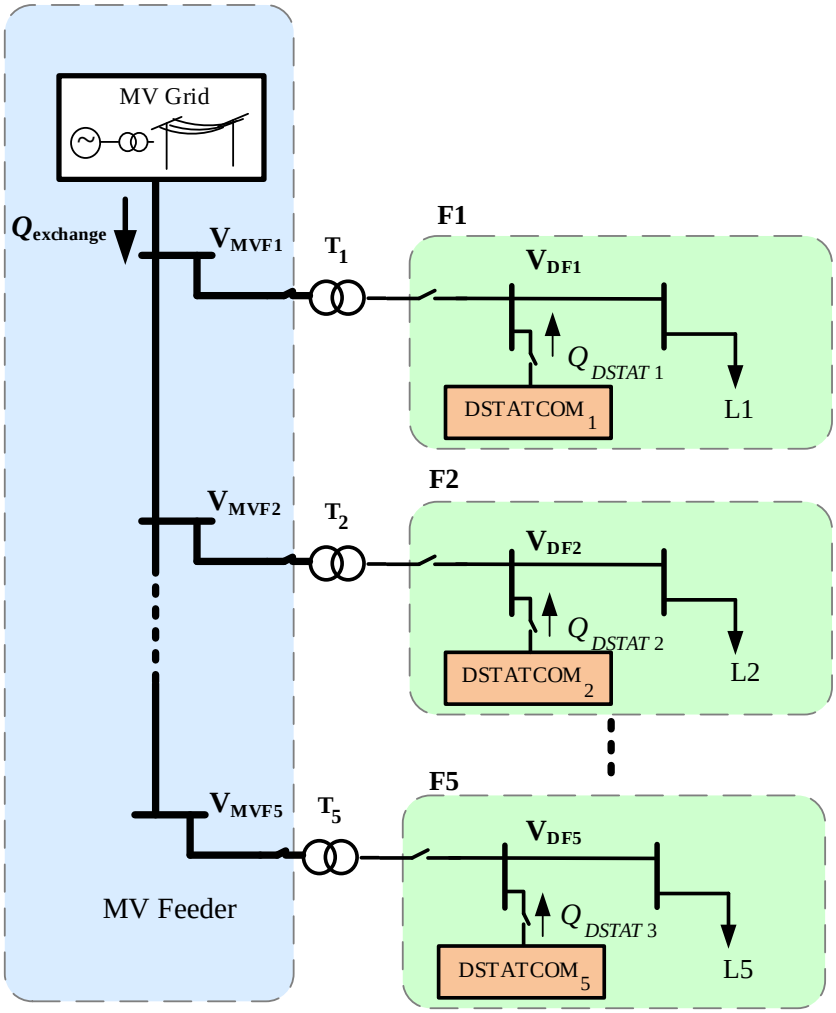

Fig. 2.13 Radial MV network with five distribution feeders.

The voltage profiles in the primary and secondary side of the transformers for the above two cases are given in Table 2.1 and the reactive power injection of each DSTATCOM, along with the reactive power exchange with the grid ($Q_{exchange}$) are shown in Table 2.2. From Table 2.1, it can be seen that both cases have similar results with regard to the voltage profile of the medium voltage feeder. However, in the case of flat voltage profile, the amount of reactive power injected by DSTATCOMs gradually increases towards the end of the medium voltage feeder. Therefore, the DSTATCOMs at feeder end nodes have relatively higher ratings compared to DSTATCOMs in feeder at beginning when the flat voltage profile is used. On the other hand, at the beginning of the medium voltage feeder, a huge reverse reactive power flow ($Q_{exchange}$) is observed in the case of the flat voltage line

compared to the other two cases considered, as shown in Table 2.2. This will affect the medium voltage feeder current carrying capacity.

Now, let us assume that all DSTATCOMs are operating in power factor correction strategy. In this case, they will inject the reactive power required by the loads in their downstream. Since the loads have similar impedances and the voltage drops along the medium voltage feeder, the amount of the reactive power injected by the DSTATCOMs slightly decreases from the beginning towards the end of the feeder. However, the voltage profile is improved compared to the case without DSTATCOMs. On the other hand, no reverse reactive power flow is observed at the beginning of the medium voltage feeder, as shown in Table 2.2.

Based on this discussion, controlling DSTATCOMs with power factor correction strategy results in indirect improved voltage profile in both medium voltage and low voltage feeders, prevents reverse reactive power flow in medium voltage feeder and minimizes the rating of DSTATCOMs.

Table 2.1 Voltages at different locations in the power system shown in Fig. 2.13 for different DSTATCOM control modes (pu).

DSTATCOM Control Mode	**Location**	**F1**	**F2**	**F3**	**F4**	**F5**
No DSTATCOM	Medium voltage side (V_{MVF*})	0.97	0.96	0.94	0.93	0.92
	Distribution voltage side (V_{DF*})	0.95	0.94	0.93	0.91	0.90
Flat Voltage	Medium voltage side (V_{MVF*})	1	1	1	1	1
	Distribution voltage side (V_{DF*})	0.98	0.97	0.97	0.96	0.96
Gradually Decreased	Medium voltage side (V_{MVF*})	1	0.99	0.98	0.97	0.96
	Distribution voltage side (V_{DF*})	0.98	0.97	0.96	0.96	0.95
Power Factor Correction	Medium voltage side (V_{MVF*})	0.98	0.96	0.95	0.94	0.94
	Distribution voltage side (V_{DF*})	0.98	0.96	0.95	0.94	0.94

Table 2.2 Reactive power injection from DSTATCOMs and reactive power flow from grid to medium voltage feeder, for different DSTATCOM control modes [kVAr].

DSTATCOM Control Mode	Q_{DSTAT1}	Q_{DSTAT2}	Q_{DSTAT3}	Q_{DSTAT4}	Q_{DSTAT5}	$Q_{exchange}$
Flat Voltage	51.37	66.36	76.51	82.62	85.65	-160.07
Gradually Decreased	55.98	59.02	56.97	50.43	39.11	-73.73
Power Factor Correction	28.69	27.79	27.16	26.76	26.38	41.33
No DSTATCOM	-	-	-	-	-	170.75

The dc capacitor voltage (V_{dc}) in DERs is stabilized by their dc sources; however, there is no such a dc source in DSTATCOMs. V_{dc} in DSTATCOM can be kept equal to its reference value ($V_{dc,ref}$) when the ac system does not exchange any power with the dc capacitor [91]. This can be reassured if the ac system replenishes the DSTATCOM converter losses. For this, the angle of the voltage across the ac filter capacitor (δ_{cf}) must be varied with respect to the dc capacitor voltage variations as

$$\delta_{cf-DSTAT,ref} = \left(K_P'' + \frac{K_I''}{s}\right)\left(V_{dc-DSTAT,ref} - V_{dc-DSTAT}\right) \tag{2.66}$$

2.3 Summary

In this chapter, the primary and secondary control levels for the DERs in a microgrid are presented. The DERs are all converter-interfaced and voltage-controlled. The DERs operate in constant power mode when the microgrid is grid-connected and operate in power sharing mode based on droop during off-grid mode. The DERs are utilizing an LQR-based state feedback control system which is a robust and optimal control method. Based on the output active and reactive power of the DERs, the network voltage and frequency is regulated in the off-grid mode of operation. Once the voltage and frequency violate the acceptable limits, the secondary level control takes action to adjust the set points of the droop controller. If the voltage and frequency fall below the minimum acceptable threshold even after

the adjustments are applied by the secondary controller, the non-critical loads need to be shed to prevent the system collapse. In addition, the secondary control can dynamically modify the ratio of the active power output of the DERs in off-grid mode by adjusting the droop control settings. A DSTATCOM can be utilized to maintain the microgrid voltage both in grid-connected as well as off-grid operation. Three different control strategies for a DSTATCOM control are discussed.

Chapter 3 Primary and Secondary Level Control Results

The proposed primary and secondary control levels in Chapter 2 are applied for a microgrid system and the system performance is investigated in grid-connected and off-grid modes of operation. Several simulation case studies are built in PSCAD/EMTDC to verify the operation of the microgrid with the proposed hierarchical control system. In addition, other issues such as DER resynchronization, presence of unbalanced and harmonic loads in the microgrid and the dynamic power sharing ratio adjustment among the DERs are also investigated through these case studies.

3.1 Microgrid operation in grid-connected and off-grid modes

Let us consider the system shown in Fig. 2.1 to investigate the DERs operation during grid-connected and off-grid modes. Technical data for this case study is given in Table 3.1 below. In grid-connected mode, each DER will generate its rated power and the extra load demand will be supplied by the grid or the excess DER generation will flow back to the grid. In off-grid mode, the load demand of the microgrid is shared among the DERs with in the microgrid proportional to their rating. It is to be noted that the maximum generation capacities of the DERs are not considered in the preceding study. However, if the system frequency is dropped below the acceptable level, the load shedding module should disconnect some of the non-critical loads.

Table 3.1 Technical data of the DERs and droop control coefficients for the network under consideration in Fig. 2.1.

DER Type	DER Rating [kW]	Coupling Inductance (L_{coup}) [mH]	*m* [rad/kW]	*n* [V/kVAr]
Fuel Cell (DER-1)	4	5.61	1.5708	0.9
PV (DER-2)	3	7.48	2.0944	1.17
Battery (DER-3)	2	11.22	3.1416	1.8

Let us assume in the system shown in Fig. 2.1, CB_G and CB_M are closed. The system is assumed to be in steady state condition at t = 0 s and all the DERs are running at their rated conditions. The DSTATCOM is not connected to the system.

At t = 1 s, the grid is disconnected (i.e. CB_G is opened) and the microgrid starts to operate in off-grid mode. Therefore, the DERs increase their output power to satisfy the load demand within the microgrid. At t = 2 s a 25% load increase (i.e. 3 kW) and at t = 3 s a load decrease of 25% are applied in the microgrid. It can be seen that all DERs are sharing the load change proportional to their ratings. At t = 4 s, it is desired that the microgrid reconnects to the grid. In order to prevent fluctuations in the current and power, the resynchronization method described in section 2.1.1.6 is used. The resynchronization is achieved at t = 10.1 s and CB_G closes. It can be seen the system reaches to the steady state condition after each change within 5 cycles. Fig. 3.1a shows the active power dispatch of grid and the existing DERs in the microgrid during 0 to 11 seconds in the above-mentioned network while Fig. 3.1b shows the reactive power dispatch for the same time period.

The voltage profile of the network is also shown in Fig. 3.1c. As it can be seen in this figure, during the off-grid mode, there might be an uncontrolled voltage drop/rise in the network, as none of the DERs are regulating the network voltage. In this research, a DSTATCOM is utilized to regulate the network voltage. To investigate the efficacy of DSTATCOM, let us now assume that in Fig. 2.1, CB_S is closed and the DSTATCOM is connected. For this condition, the active and reactive power dispatch of grid and DERs are shown in Fig. 3.2a and Fig. 3.2b, respectively. The voltage profile of the network is now highly improved and remains close to the desired value of 1 pu, as shown in Fig. 3.2c. The difference in the active powers in figures Fig. 3.1a and Fig. 3.2a is due to the fact that voltage is varying before DSTATCOM installation. The voltage profile of DSTATCOM dc capacitor is shown

in Fig. 3.2d which has a negligible drop of 1% in off-grid mode. The output active and reactive power of DSTATCOM is also shown in Fig. 3.2e. The oscillations in the results of Fig. 3.2 are due to the dynamic characteristics of DSTATCOM.

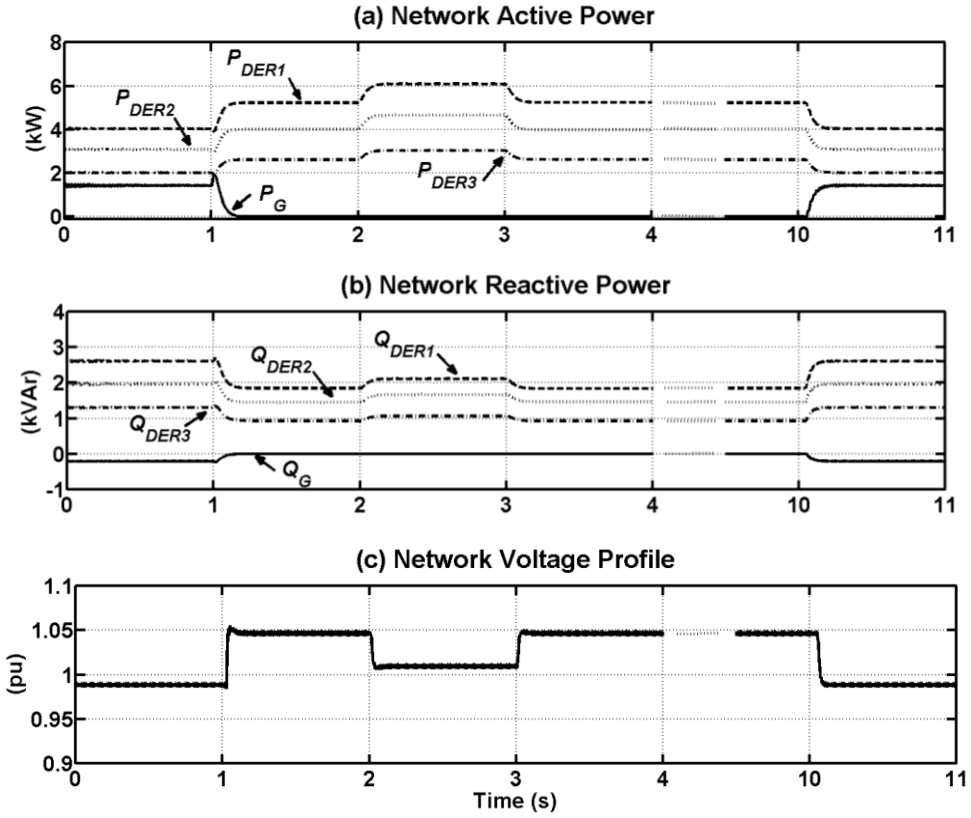

Fig. 3.1 Simulation results for MG before DSTATCOM connection:

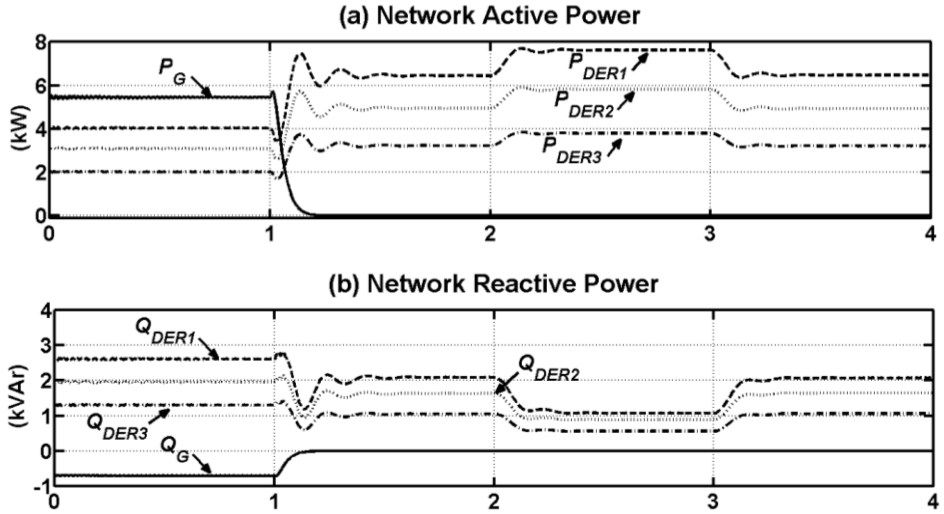

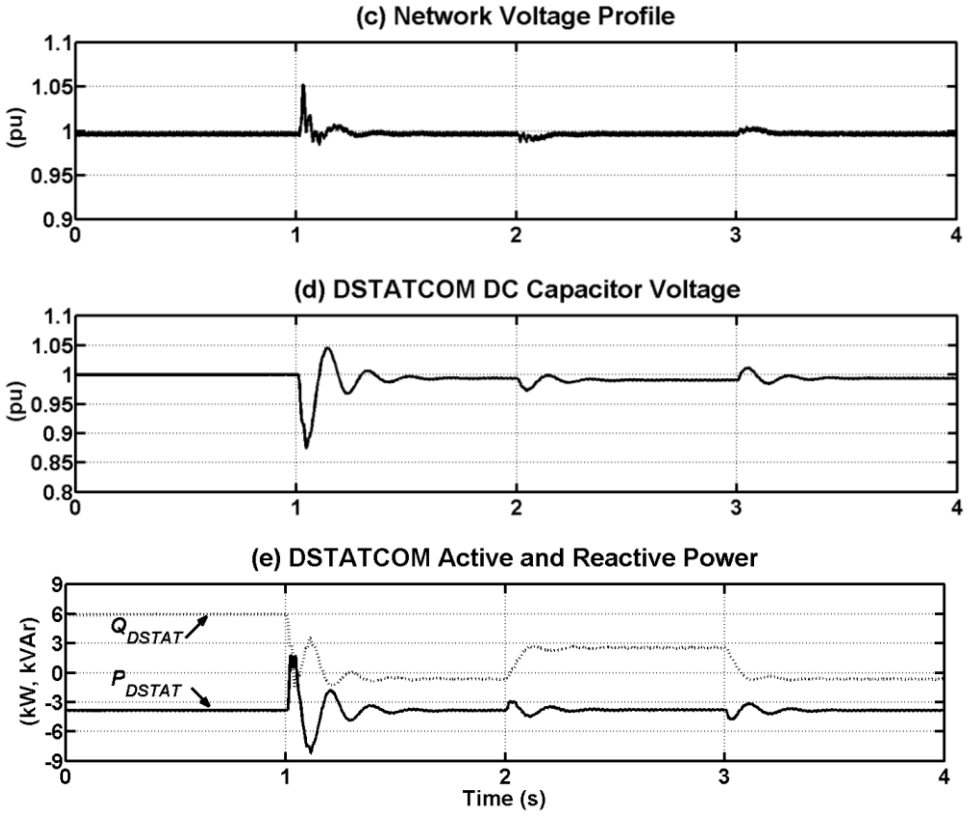

Fig. 3.2 Simulation results of MG after DSTATCOM connection:

3.2 DER and microgrid isolation and resynchronization

Another case study is carried out to verify the dynamic performance of DER converters during getting isolated from the grid and resynchronization before reconnecting with the grid. It is assumed that the microgrid in section 3.1 is grid-connected and in steady state condition at $t = 0$. The technical data of the DERs and their droop coefficients for this study are given in Table 3.2 below. The rated capacities of the DERs are selected arbitrarily.

Table 3.2 Technical data of the DERs and droop control coefficients for the network under consideration in section 3.2.

DER Type	DER Rating [kW]	Coupling Inductance (L_{coup}) [mH]	*m* [rad/kW]	*n* [V/kVAr]
Fuel Cell (DER-1)	6.6	3.4	0.95	0.54
PV (DER-2)	3.3	6.8	1.9	1.08
Battery (DER-3)	3.3	6.8	1.9	1.08

At t = 1 s, the microgrid main switch (CB_M) opens and the microgrid falls into off-grid mode. At t = 2 s, DER-3 which is supplying 28 % of total load demand (i.e. 4.3 kW), is disconnected from the microgrid. At t = 3 s, the resynchronization of DER-3 to the microgrid is initiated and at t = 3.68 s, it is connected back to the microgrid. At t = 4 s, resynchronization of the microgrid to the grid is activated and at t = 4.15 s, it is reconnected to the grid.

The simulation results are shown in Fig. 3.3. The instantaneous voltage on both sides of DER-3 circuit breaker and their difference, during reconnection of DER-3 to the microgrid, are shown in Fig. 3.3a and Fig. 3.3b. The output current of phase-A of the DERs during reconnection of DER-3 to the microgrid is also shown in Fig. 3.3c. The instantaneous voltage on both sides of DER-3 circuit breaker and their difference, during reconnection of the microgrid to the grid, are shown in Fig. 3.3d and Fig. 3.3e.

DER-3 synchronizes with the microgrid as the voltage difference across DER-3 circuit breaker becomes zero (Fig. 3.3a). The resynchronization takes 0.68 s in the studied case and due to the proper resynchronization, no abnormal fluctuations are observed in the output current of DERs (Fig. 3.3c). The microgrid synchronizes with the grid as the voltage difference across the microgrid main circuit breaker becomes zero (Fig. 3.3d). The resynchronization takes 0.15 s in the studied case.

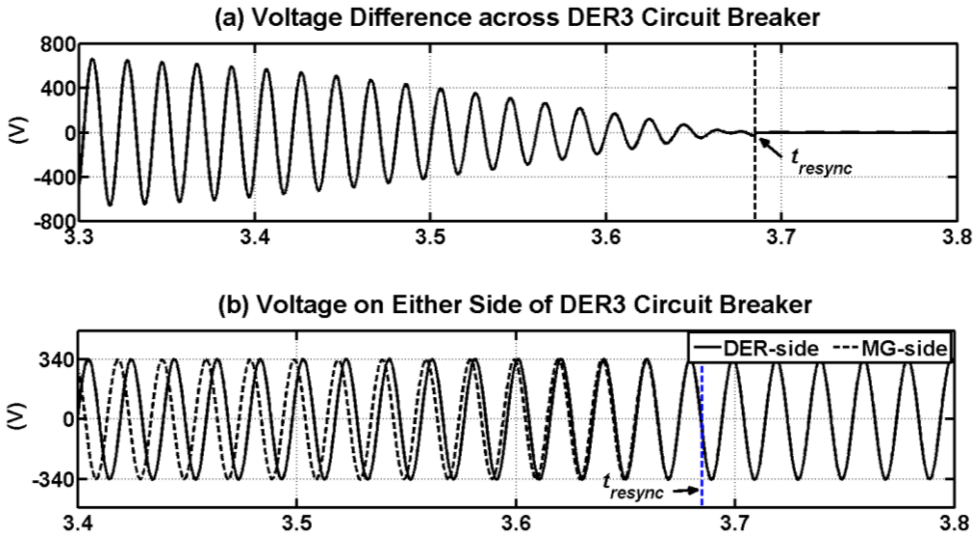

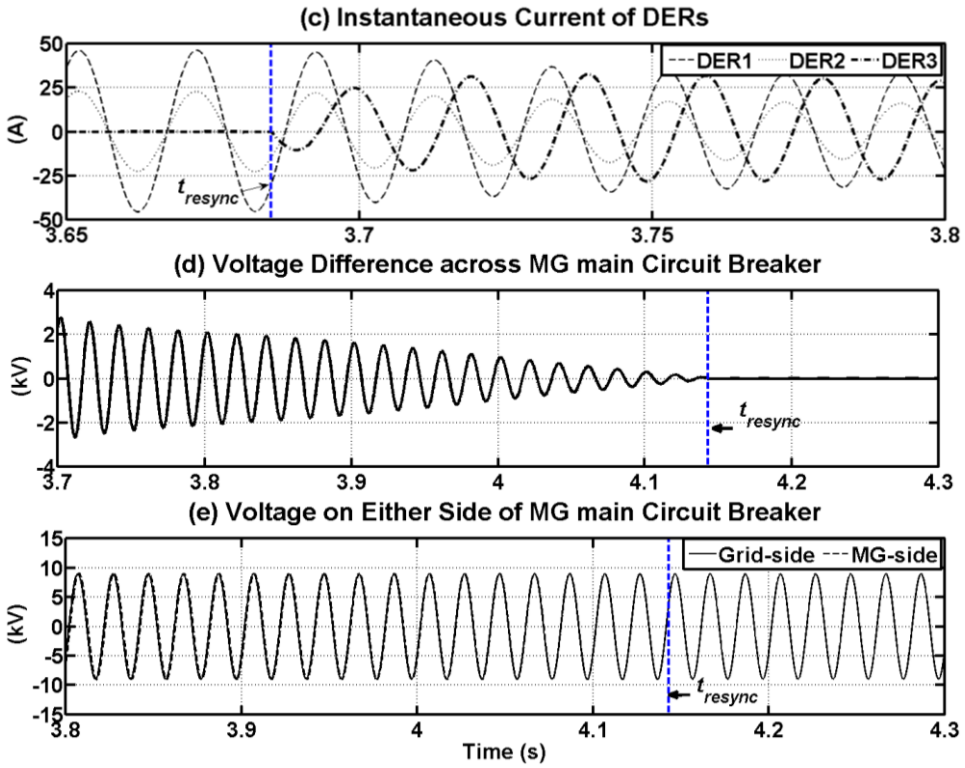

Fig. 3.3 Simulation results for resynchronization of DER-3 and the microgrid:

3.3 Microgrid with unbalanced and harmonic loads

For investigating the performance of the microgrid with several converter-interfaced DERs for different types of loads in the network such as balanced, unbalanced and harmonic, several case studies are considered. A few of them are discussed below. The technical data of the DERs and their droop coefficients for this case study are tabled in Table 3.3 below. The rated capacities of the DERs are selected arbitrarily.

Table 3.3 Technical data of the DERs and droop control coefficients for the network under consideration in section 3.3.

DER Type	DER Rating [kW]	Coupling Inductance (L_{coup}) [mH]	*m* [rad/kW]	*n* [V/kVAr]
Fuel Cell (DER-1)	2	76.2	3.14	1.8
PV (DER-2)	4	38.1	1.57	0.9
Battery (DER-3)	3	49.8	2.05	1.17

3.3.1 Microgrid with unbalanced loads

In this case, let us assume that at t = 0 s CB_G, CB_M and CB_S are closed in the system shown in Fig. 2.1, and it is in steady state condition. At t = 0.5 s, CB_G is opened to disconnect the grid hence the microgrid operates in off-grid mode.

3.3.1.1 Non-isolated distribution transformer

Let us assume that the circuit breaker in the secondary side of the distribution transformer still remains connected to the low voltage side. At t = 1.5 s a new single-phase 2 kW load is connected to phase-A. Later, at t = 2.5 s another single-phase 2 kW load is connected to phase-C.

Fig. 3.4a shows the active power dispatch of the grid and the existing DERs in the microgrid between 0 and 3.5 seconds in the above-mentioned network. From this figure, it can be seen that, the total amount of active power generation among DERs are maintained on the desired power sharing ratio among them.

The active power output of one of the DERs (e.g. DER-1) is shown in Fig. 3.4b for each phase individually. From this figure, it can be seen that for t < 1.5 s, all three phases of DER-1 have an equivalent amount of generated active power. However, at t = 1.5 s when a single-phase load is connected to phase-A, the active power output of all phases of the DER increases. This increase is slightly higher for phase-A. In a similar way, at t = 2.5 s when another single-phase load is connected to phase-C, the output active power of all phases of the DER increases but this increase is more for phase-C. Similar results are monitored in all the DERs of the microgrid. From this figure it can be seen that single phase load power demand is shared among the three phases of the DERs.

Fig. 3.4c shows the active power output of all DERs in their phase-A for the studied case. From this figure, it can be seen that for a load change in the network, the contribution of each phase of the DERs in power generation also follows the desired sharing ratio among them.

It is to be noted that, all phases of the DERs contribute to a single-phase (or unbalanced) load change in the network since there is a possibility of power circulation from one phase of microgrid to the other two phases through the windings of the distribution transformer. Fig. 3.4d shows the active power supplied by the distribution transformer in the studied case. From this figure, it can be seen that the

distribution transformer output power is zero when the microgrid is working in off-grid mode with balanced loads (i.e $0.5 < t < 1.5$ s). However, it can be seen that for $1.5 < t < 2.5$ s there is a negative active power flow into the distribution transformer in phase-B and C which is circulated and retuned to phase-A where the single phase load is connected. Similarly, during $2.5 < t < 3.5$ s there is a negative active power flow into the distribution transformer in phase-B which is circulated and retuned to phase-A and C where the single phase loads are connected to.

The three-phase instantaneous current output of a sample DER (e.g. DER-1) is shown in Fig. 3.4e which shows the DERs are generating unbalanced current in their output.

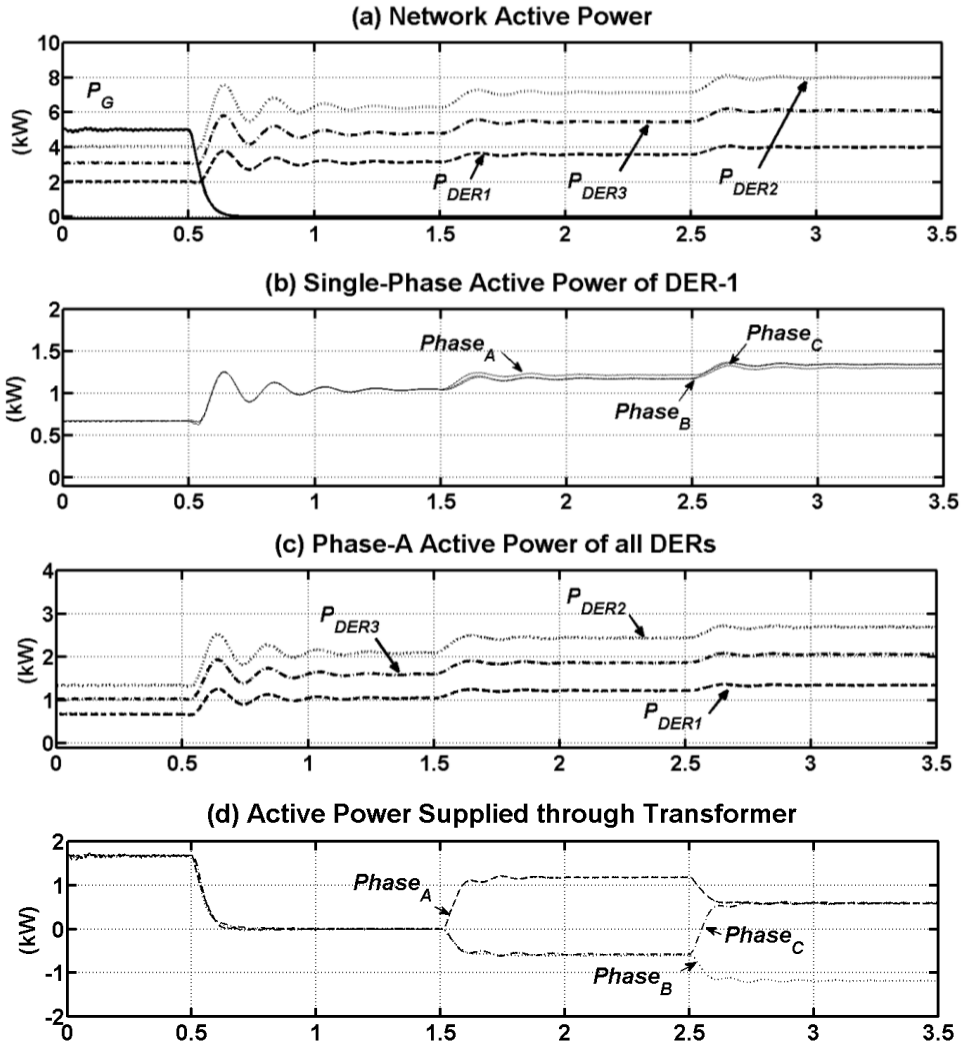

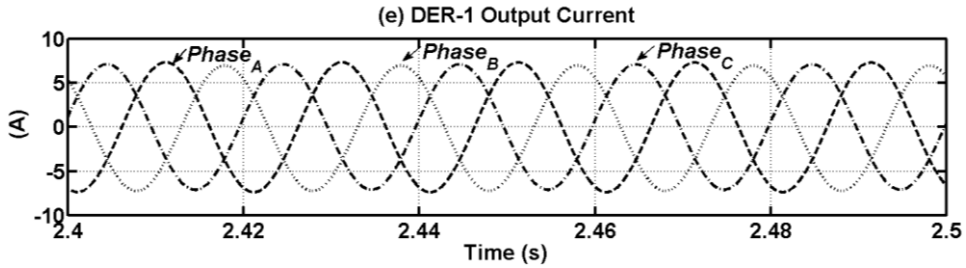

Fig. 3.4 Simulation results of microgrid discussed in section 3.3.1.1.

3.3.1.2 Isolated distribution transformer

Now, let us consider the network of section 3.3.1.1 where the distribution transformer is isolated from the low voltage side when the grid is disconnected. Therefore, let us assume that at t = 0.5 s, CB_G and CB_M open and microgrid operating in off-grid mode.

As the distribution transformer is isolated from the low voltage side, no power circulation can take place among the three phases during the off-grid mode operation. Therefore, it is expected that a single-phase (unbalanced) load change in the network, the DERs will be contributed only by the same phase of the DER in which the single-phase load change is applied.

The active power output of one of the DERs (e.g. DER-1) is shown in Fig. 3.5a for each phase individually. From this figure, it can be seen that for t < 1.5 s, all three phases of DER-1 have an equivalent amount of generated active power. However, at t = 1.5 s when a single-phase load is connected to phase-A, only the active power output of phase-A increases. In a similar way, at t = 2.5 s when another single-phase load is connected to phase-C, only the output active power of phase-C increases. Similar results are monitored in all the DERs of the microgrid. From this figure, it can be seen that single phase load power demand is only supplied by the relevant single-phase of the DERs.

Fig. 3.5b shows the active power output of all DERs in their phase-A for the studied case. From this figure, it can be seen that for a load change in the network, the contribution level of each phase of the DERs in power generation is based on the desired sharing ratio among them.

Fig. 3.5c shows the active power supplied by the distribution transformer in the studied case. As the transformer is isolated at t = 0.5 s, its output power becomes zero.

The three-phase instantaneous current output of a sample DER (e.g. DER-1) is shown in Fig. 3.5d which shows the DERs are generating unbalanced current in their output.

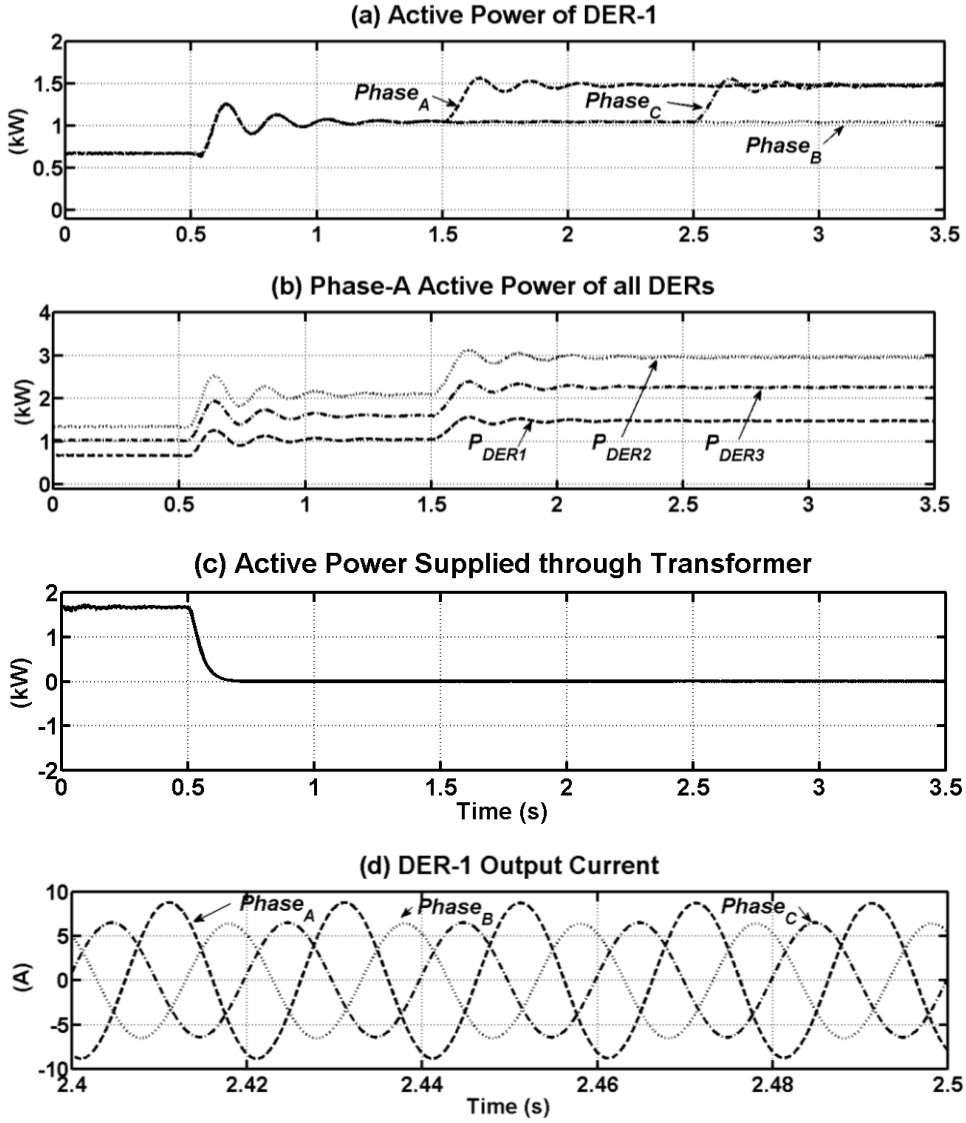

Fig. 3.5 Simulation results of microgrid considered in section 3.3.1.2.

3.3.2 Microgrid with harmonic loads

In this section, let us consider the microgrid of Fig. 2.1 with a three phase harmonic load. The system is in steady state condition at t = 0 s and at t = 0.5 s, the grid is disconnected (i.e. CB_G is opened) and the microgrid will work in off-grid mode. At t = 1.5 s a new three-phase harmonic load of 3 kW is connected to the network. At t = 2.5 s, its demand is increased to 6 kW. The harmonic load has a Total

Harmonic Distortion (THD) of 25.5% as shown in the Fast Fourier Transform (FFT) Spectrum in Fig. 3.6a.

Fig. 3.6b shows the active power dispatch of the grid and the existing DERs in the microgrid between 0 and 3.5 seconds in the above-mentioned network. The single-phase active power output of one of the DERs (e.g. DER-1) is shown in Fig. 3.6c. This is same for all phases of A, B and C. The active power output in phase-A of all three DERs are also shown in Fig. 3.6d. From these figures, it can be seen that as the load is supplied from the three-phase network, its demand is shared equally among the three phases of each DER. However, the DERs share the extra demand based on their desired power sharing ratio.

The three-phase instantaneous current output of a sample DER (e.g. DER-1) is shown in Fig. 3.6e which shows the output current of the DERs are distorted as required by the network harmonic load.

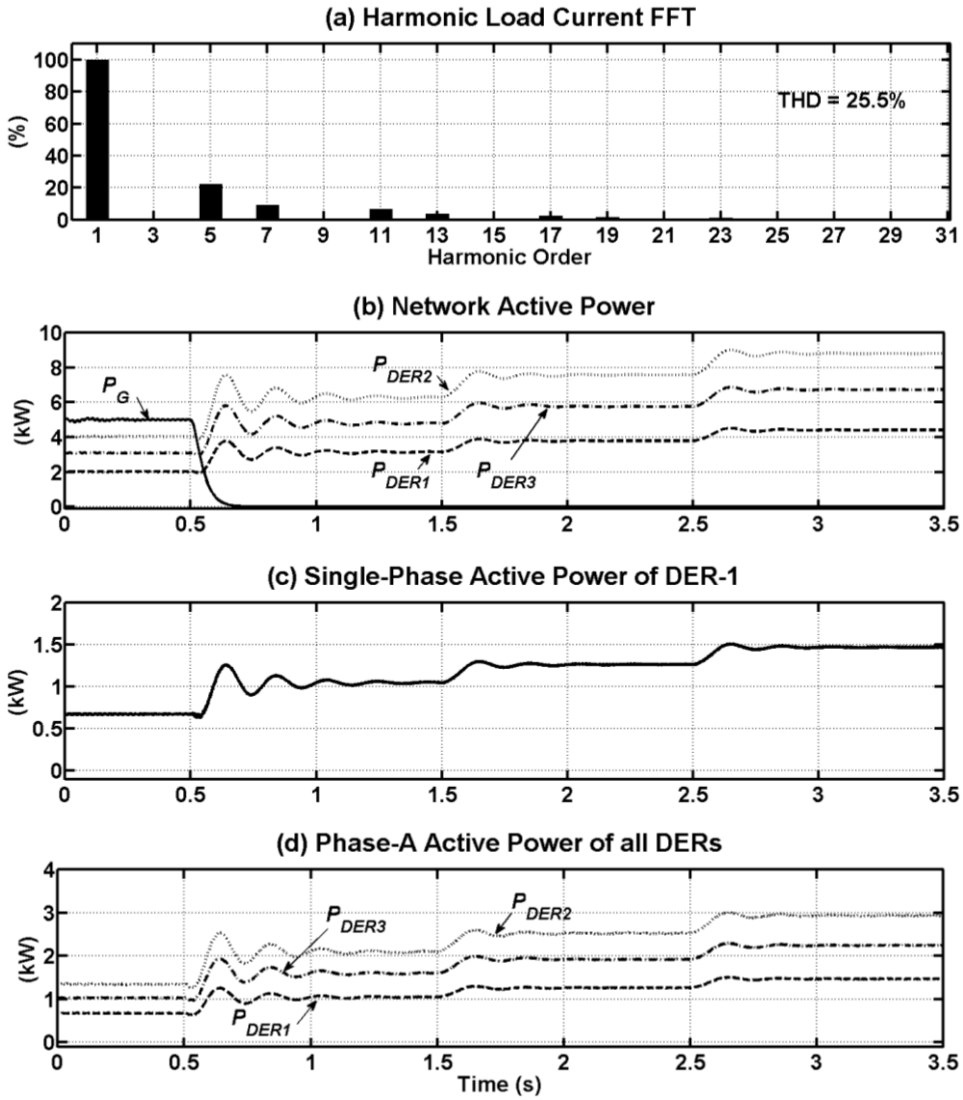

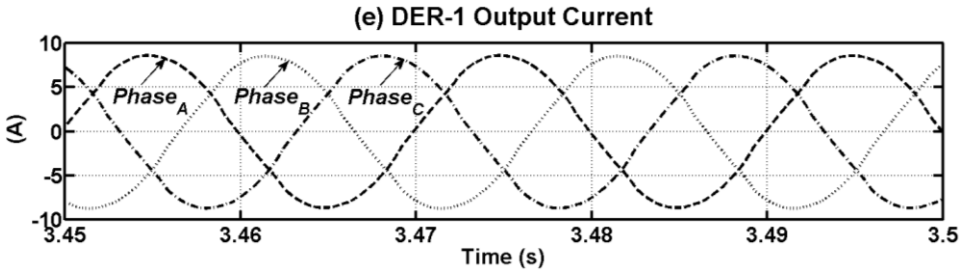

Fig. 3.6 Simulation results of microgrid considered in section 3.3.2:.

3.4 Droop curve adjustment in microgrid

The microgrid system shown in Fig. 2.1 with 2 DERs (i.e. DER-1 and DER-2) is considered in order to investigate the performance of the proposed microgrid central controller. The DSTATCOM is disconnected and the DERs are responsible for regulating the system voltage during off-grid mode. The single line diagram of the considered network is shown in Fig. 3.7. The parameters of network, DER converters and filters, coupling inductances, loads and the droop control coefficients are given in Table 3.4. It is to be noted that the droop coefficient "*n*" has been selected ten times greater than the normal value in order to exaggerate the terminal voltage variation to show the effectiveness of the secondary controller.

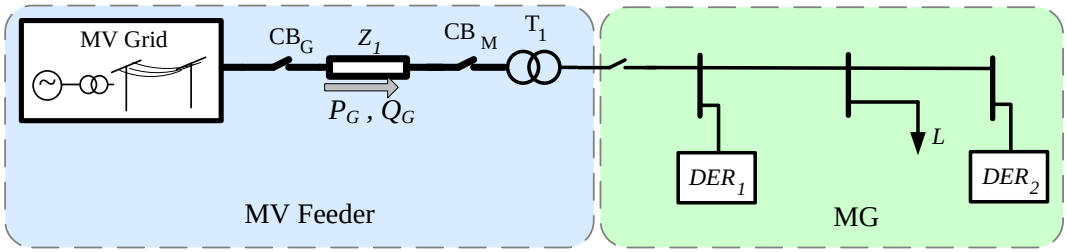

Fig. 3.7 Structure of the microgrid under consideration.

Table 3.4 Technical data of the DERs and droop control coefficients for the network under consideration in Fig. 3.7.

DER Type	DER Rating [kW]	Coupling Inductance (L_{coup}) [mH]	*m* [rad/kW]	*n* [V/kVAr]
DER-1	2	2.72	3.14	18
DER-2	4	1.36	1.57	9

3.4.1 Off-grid microgrid within acceptable voltage and frequency

It is assumed that the microgrid system is initially in steady-state condition, with a total load demand of approximately 0.41 pu where 1 pu is 6 kW. At t = 0.5 s, this load is increased to 1 pu and at t = 1 s, the network load is decreased to 0.53 pu. At t = 1.5 s, the load is further decreased to 0.17 pu.

The output active power ratio among DER-1 and 2, is maintained to 1:2, as assigned by the central controller (Fig. 3.8a) for all load changes. The microgrid voltage is within the acceptable limits during all load changes as shown in Fig. 3.8c. Similarly, the microgrid frequency is also within the acceptable limits during all load changes as shown in Fig. 3.8d. Hence, the central controller does not issue any new control commands and V_{rated} is kept as 1 pu (Fig. 3.8e) while the f_{rated} is kept as 50 Hz (Fig. 3.8f).

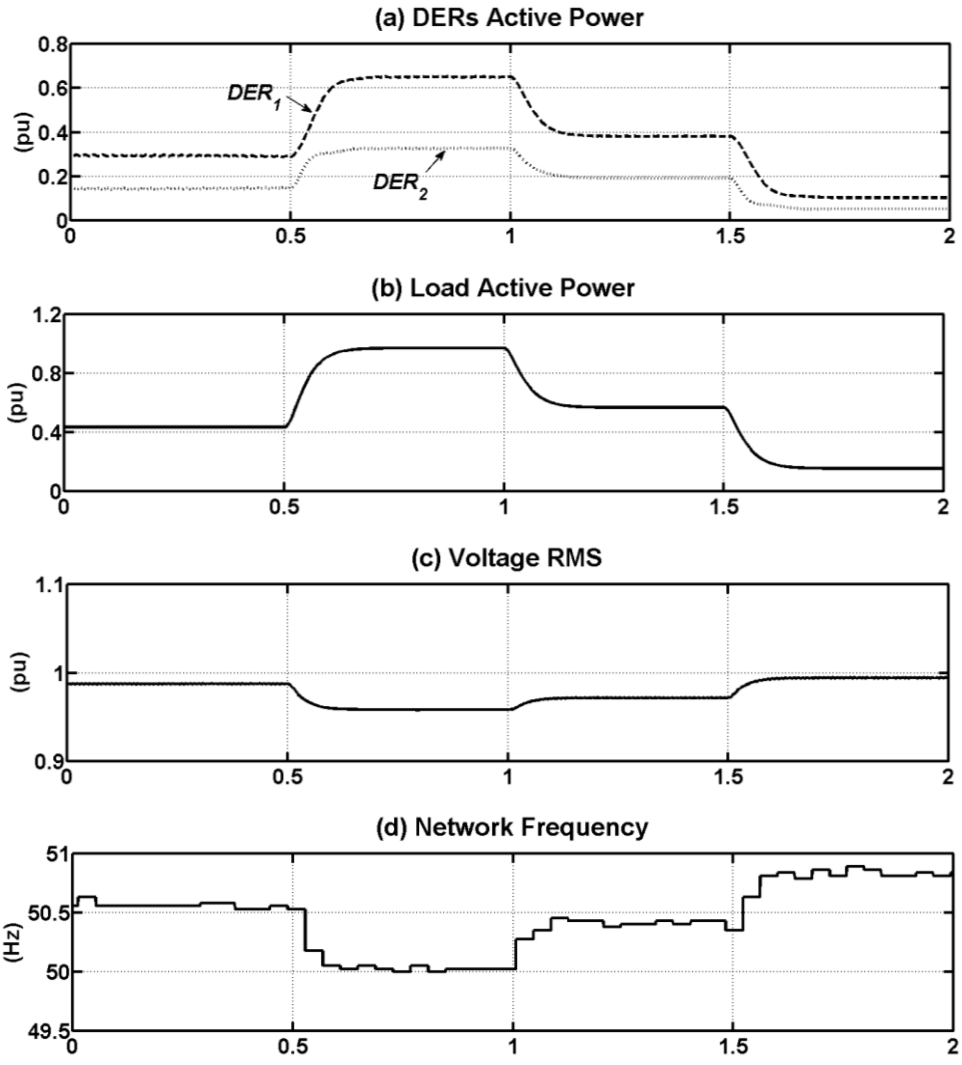

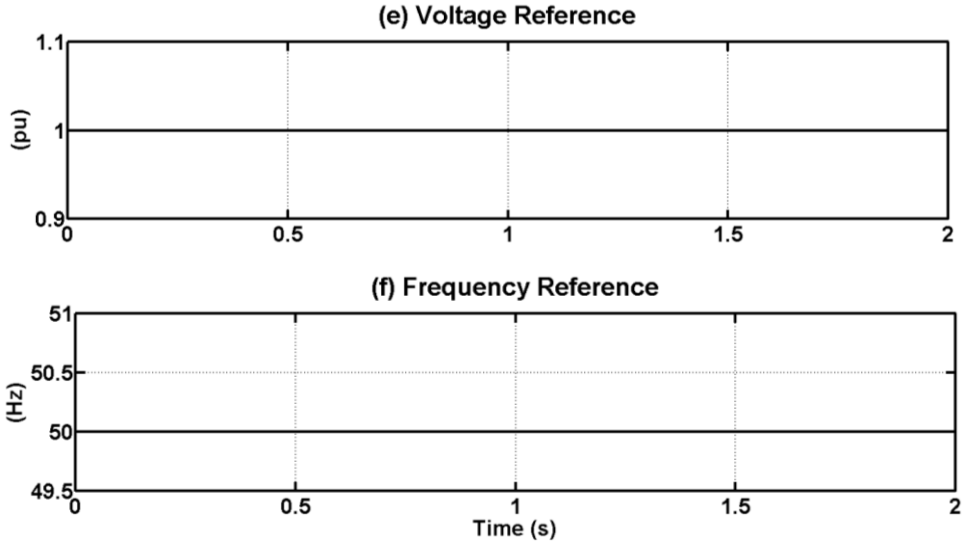

Fig. 3.8 Simulation results for considered microgrid in section 3.4.1:

3.4.2 Off-grid microgrid with unacceptable voltage and frequency

Now, let us assume that the microgrid system is initially in steady-state condition, with a total load demand of approximately 0.15 pu where 1 pu is 18 kW. The output power of DERs is maintained as 1:2, as assigned by the central controller (Fig. 3.9a).

At t = 0.5 s, the load is increased to 0.4 pu (Fig. 3.9b) and consequently, the network voltage drops to 0.89 pu (Fig. 3.9c) which is below the acceptable limit of 0.9 pu. The microgrid frequency is still within the acceptable range (Fig. 3.9d). Since the central controller operates with a larger time step, as discussed before, it modifies V_{rated} for the system (Fig. 3.9e) at the first operating time after the load change (i.e. t = 1 s). Hence, V_{rated} is updated to 1.1. It can be seen that, as the central controller increases the voltage reference for the droop control, the network voltage is restored to 1 pu.

At t = 1.5 s, another load increase is applied and the system undergoes the same sequence of events as at t = 0.5 s. The central controller increases the voltage reference to recover the voltage drop at t = 2.0 s. In this case, the microgrid frequency decreases beyond its acceptable limit and hence the central controller updates f_{rated} to 51.9 Hz at t = 2.6 s (Fig. 3.9f). Therefore, the microgrid frequency is restored back to 50 Hz t = 2.6 s. It is to be noted that since the loads were modelled as constant impedance load, after each V_{rated} increase at t = 1 and t = 2 s, the load active power consumption is also increased.

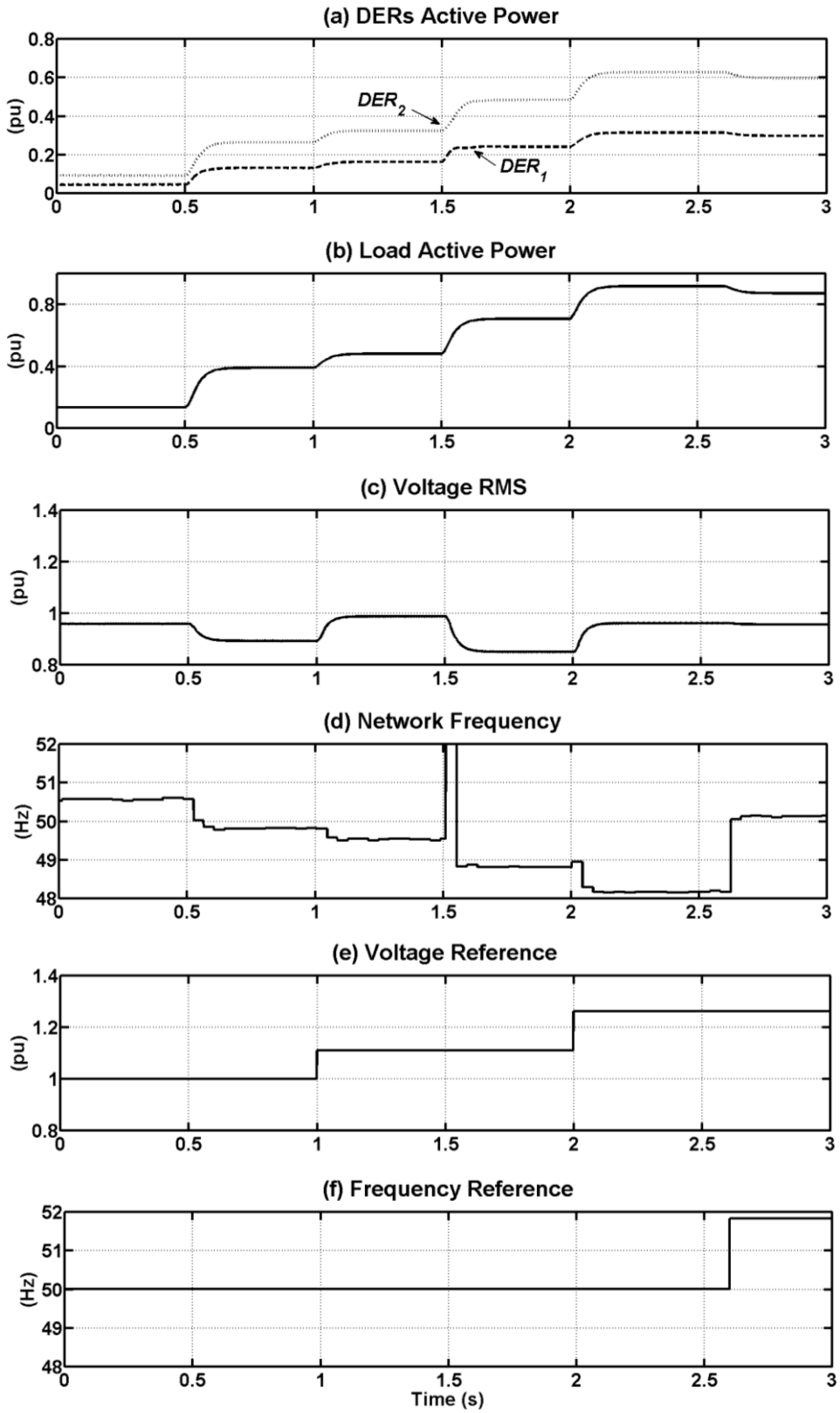

Fig. 3.9 Simulation results for considered microgrid in section 3.4.2:

3.5 Dynamic power ratio adjustment in microgrid

It is assumed that, at t = 0 s, the microgrid system is in steady-state condition. The two DERs have the same coupling inductance of L_{T1} = L_{T2} = 6.8 mH at their outputs. Initially, the tertiary controller has defined the output active power ratio among DER1:DER2 to be 1:2 (Fig. 3.10a). Hence, the droop coefficient ratio of the two DERs is selected as $m_{\text{DER1}}/m_{\text{DER2}}$ = 2/1 (Fig. 3.10b). In addition, it selects $P_{\text{rated1}}/P_{\text{rated2}}$ = 2/1. These two ratios are passed to the primary controllers of each DER system.

At t = 0.5 s, the tertiary controller changes the output active power ratio among DER1:DER2 to be as 1:1 and passes this information to the central controller. Hence, the *P-f* droop coefficients ratio and rated active power ratio between the two DERs are selected as $m_{\text{DER1}}/m_{\text{DER2}}$ = 1/1 and $P_{\text{rated1}}/P_{\text{rated2}}$ = 1/1 and then passed to the primary controllers of each DER system.

At t = 1 s, the tertiary controller orders the microgrid central controller to facilitate the active power output ratio among DER1:DER2 to be as 3:1. Hence, the droop coefficient ratio and rated active power ratio between the two DERs are selected as $m_{\text{DER1}}/m_{\text{DER2}}$ = 1/3 and $P_{\text{rated1}}/P_{\text{rated2}}$ = 1/3 and then passed to the primary controllers of each DER system.

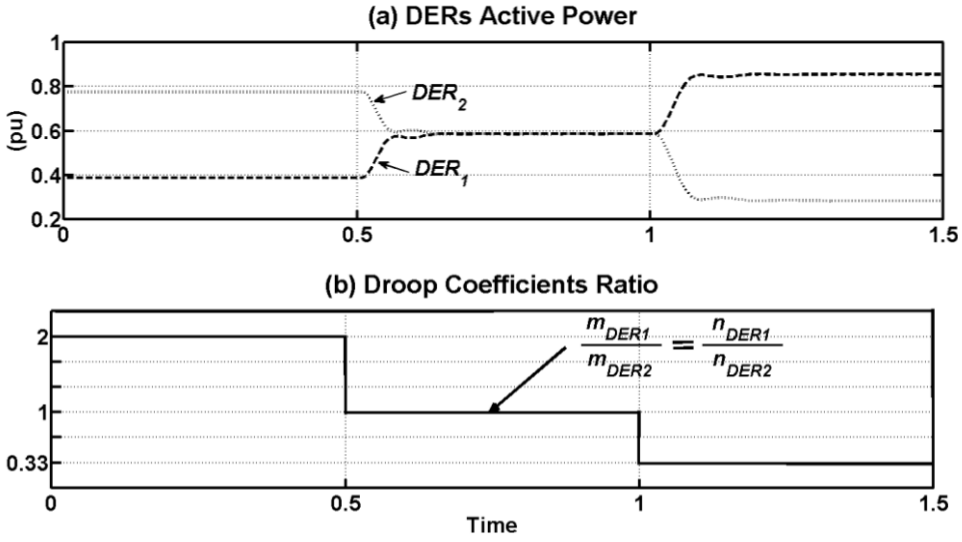

Fig. 3.10 Simulation results for considered microgrid in section 3.5:

3.6 Summary

In this chapter, the demonstrated simulation case studies verified the proper dynamic operation of the DERs through the proposed hierarchical control system. The DERs can be connected to the microgrid with minimum transients with the help of the developed synchronization technique. The DERs based on the voltage-controlled concept can supply the harmonic and unbalanced loads in the network without any further complexity in the reference generation process. In grid-connected mode of operation, the DERs generate the maximum (rated) power while they effectively share the local load in off-grid mode based on the designed droop settings. The secondary level control successfully adjusts the microgrid voltage and frequency if they are violated the acceptable limits. In addition, the secondary control is capable of adjusting the active power sharing ratio among the DERs, in case it is desired.

Chapter 4 Interconnecting Neighboring Microgrids

This chapter discusses the dynamic operation and control of DERs in the system of interconnected microgrids. When several microgrids are located nearby, interconnection of two or more such neighboring off-grid microgrids can effectively reduce the load shedding requirement in a microgrid which has power deficiency, if the neighboring microgrids have excess generation capacity. Microgrids interconnection command is issued by the network tertiary controller, which is beyond the scope of this chapter. Several case studies are carried out in PSCAD/EMTDC to verify the successful operation of the DERs in the system of interconnected microgrids.

4.1 Requirement of interconnecting neighboring microgrids

It is expected that in the near future, there will be several microgrids in each distribution network. They will be located in a neighborhood and the networks will be facilitated with self-healing capabilities. In such a scenario, an off-grid operation of a microgrid is not anymore desired and the concept of microgrids supporting each other becomes more viable option. If the DERs generation capacity in an off-grid microgrid is less than the local load demand but there is surplus generation capacity in DERs of neighboring off-grid microgrids, interconnecting these two microgrids can reduce the load shedding requirement in the microgird with deficiency of generation. In the system of interconnected microgrids, the DERs should be properly controlled to share the total load demand in the interconnected system. The following assumptions are required when interconnecting two such off-grid microgrids:

- Availability of communication infrastructure among DERs, protection devices and circuit breakers,

- Self-healing capability in the network,
- Surplus generation capacity in the DERs in one of the microgrids,
- Possibility of bypassing some of the current technical requirements for DER interconnection.

The main contribution of this chapter is demonstrating that the developed and proposed primary control level for DER converters in Chapter 2 neither results any undesired dynamic performance nor instability in DER operations when interconnecting two or more off-grid neighboring microgrids together forming a cluster of microgrid.

It is to be noted that the linear quadratic regulator (LQR) based technique is utilized for controlling the DER converters instead of the traditional PID based controllers. The main characteristic of the PID based controllers is their dependency on the network and the load parameters. Therefore, tuning the PID control parameters is vital to achieve an acceptable dynamic performance [90][92][93]. In case of interconnected microgrids, the initially tuned PID control parameters may not result in an acceptable dynamic performance and even may lead to instability due to the changes take place in the network parameters. Therefore, an adaptive or intelligent PID controls are required which increase the complexity of the controller. However, LQR is an optimal and robust controller [90] and its control parameters only depend on the DER converter parameters and are independent from network and load characteristics. In addition, a per-phase (i.e. *abc*) based control technique is utilized in this research instead of the traditional *dq* transformation in which a PID controller is not effective in tracking sinusoidal waveforms. Using the proposed per-phase control technique, even unbalanced systems can be phase controlled individually. These are the main advantages of the developed and proposed primary control level in Chapter 2 with regard to the existing DER converter control strategies. Using the proposed and developed control technique, the desired dynamic performance of DER converters is achieved in the interconnected off-grid microgrids operation.

4.2 System of interconnected off-grid microgrids

Let us consider a medium voltage feeder connected to two low voltage microgrids, namely MG-1 and MG-2, through distribution transformers T1 and T2,

as shown in Fig. 4.1. MG-1 has 3 DERs (i.e. DER_1 to DER_3) and 5 loads while MG-2 has 2 DERs (i.e. DER_4 to DER_5) and 4 loads. A DSTATCOM is installed at the secondary side of the distribution transformer in each microgrid to regulate the voltage at its pcc. The loads are assumed to be residential loads and all DERs are assumed to be converter-interfaced DERs.

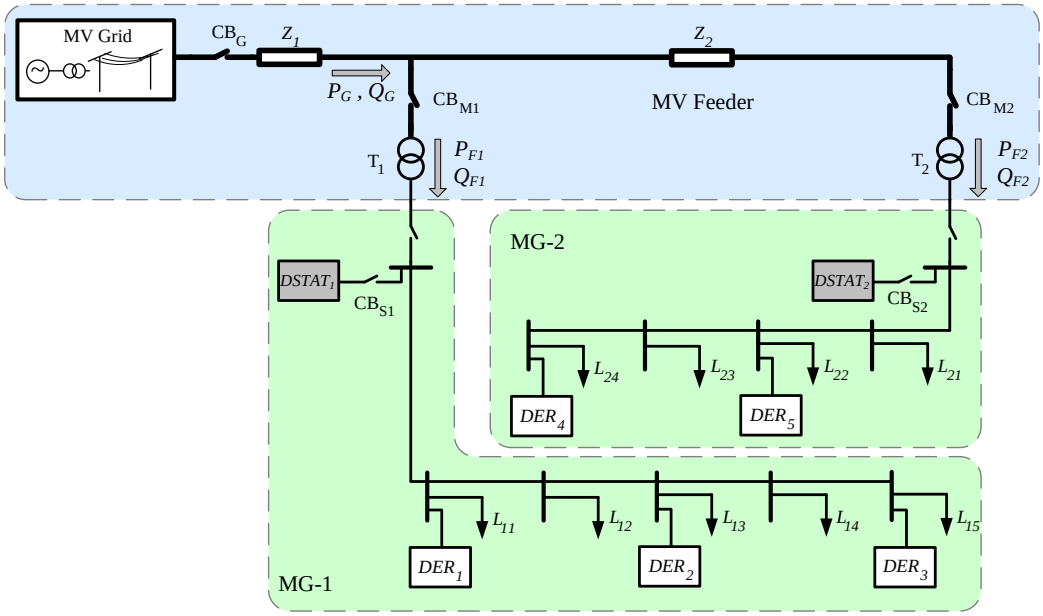

Fig. 4.1 Structure of the interconnected microgrid system.

During grid connected mode, all DERs will be operating at their rated capacities or the capacities determined by the economic analyses. During planned maintenance or unplanned fault situations on the medium voltage feeder, the microgrids will operate in off-grid mode. In this mode, when CB_{M1} and CB_{M2} are open, the DERs in each microgrid will share the loads of that microgrid individually. If the load demand in one microgrid is higher than the generation capacity of the DERs in that microgrid, load shedding must be applied to some of the (non-critical) loads in that microgrid.

Now, let us assume a scenario in which the power generation in MG-2 is less than its demand; while the power generation capacity of the DERs in MG-1 is higher than its demand. Assuming the network has self-healing and automatic supply restoration capability, CB_{M1} and CB_{M2} can be closed while CB_G will remain open. In this way, the two microgrids will be interconnected together. Hence, the DERs in MG-1 can share some of the loads in MG-2 and prevent/reduce load shedding in MG-2.

As an example, let us assume that in system shown in Fig. 4.1, at t = 0 s, circuit breakers CB_G, CB_{M1}, CB_{M2}, CB_{S1} and CB_{S2} are closed and the network is at steady state condition. The considered system has self-healing capability. Now, let us also assume that due to a fault in the medium voltage grid, after self-healing process, CB_G is open while CB_{M1} and CB_{M2} are closed at t = 1. As mentioned before, the operation of the protection devices and circuit breakers and resynchronization of interconnecting microgrids during self-healing process is beyond the scope of this study. In this study, this transition period is not considered. At t = 2 s a load increase of 25% and at t = 3 s a load decrease of 25% are also applied in MG-1.

The total active power supply from the grid in addition to the active power flow into each microgrid is shown in Fig. 4.2a. From this figure, it can be seen that MG-2 has a negative power flow and is delivering, approximately, 20% of the load demand in MG-1. The active power output of all the DERs in MG-1 and MG-2 are shown separately in Fig. 4.2b and Fig. 4.2c, respectively. It can be seen that all DERs in MG-1 and MG-2 are sharing the load demand of the system of interconnected microgrids proportional to their ratings. The voltage profile in the secondary side of the distribution transformers in each microgrid is regulated to the desired value of 1 pu as shown in Fig. 4.2d and Fig. 4.2e. The active and reactive power drawn by a sample load in the network, with a 2.7 kW demand and power factor of 0.95, is also shown in Fig. 4.2f.

Now, let us assume another case in which the two DERs in MG-2 are running in their maximum capacity (i.e. 4 and 8 kW, respectively). Let us also assume that at t = 1 s, due to a fault in the medium voltage, CB_G is open while CB_{M1} and CB_{M2} are closed as in the previous case. It is to be noted that the self-healing transition period is not considered in this study. A 25% load increase and decrease in the network is applied at t = 2 and 3 s, respectively.

For this case, the total active power supply from the grid in addition to the active power flow into each microgrid is shown in Fig. 4.3a. From this figure, it can be seen that MG-1 has a negative power flow and is delivering, approximately, 30% of the load demand in MG-2. The active power output of all the DERs in MG-1 and MG-2 are shown separately in Fig. 4.3b and Fig. 4.3c, respectively. It can be seen that all DERs in MG-2 are running in their maximum rating at all times while the DERs in MG-1 are sharing the rest of the network load demand proportional to their ratings.

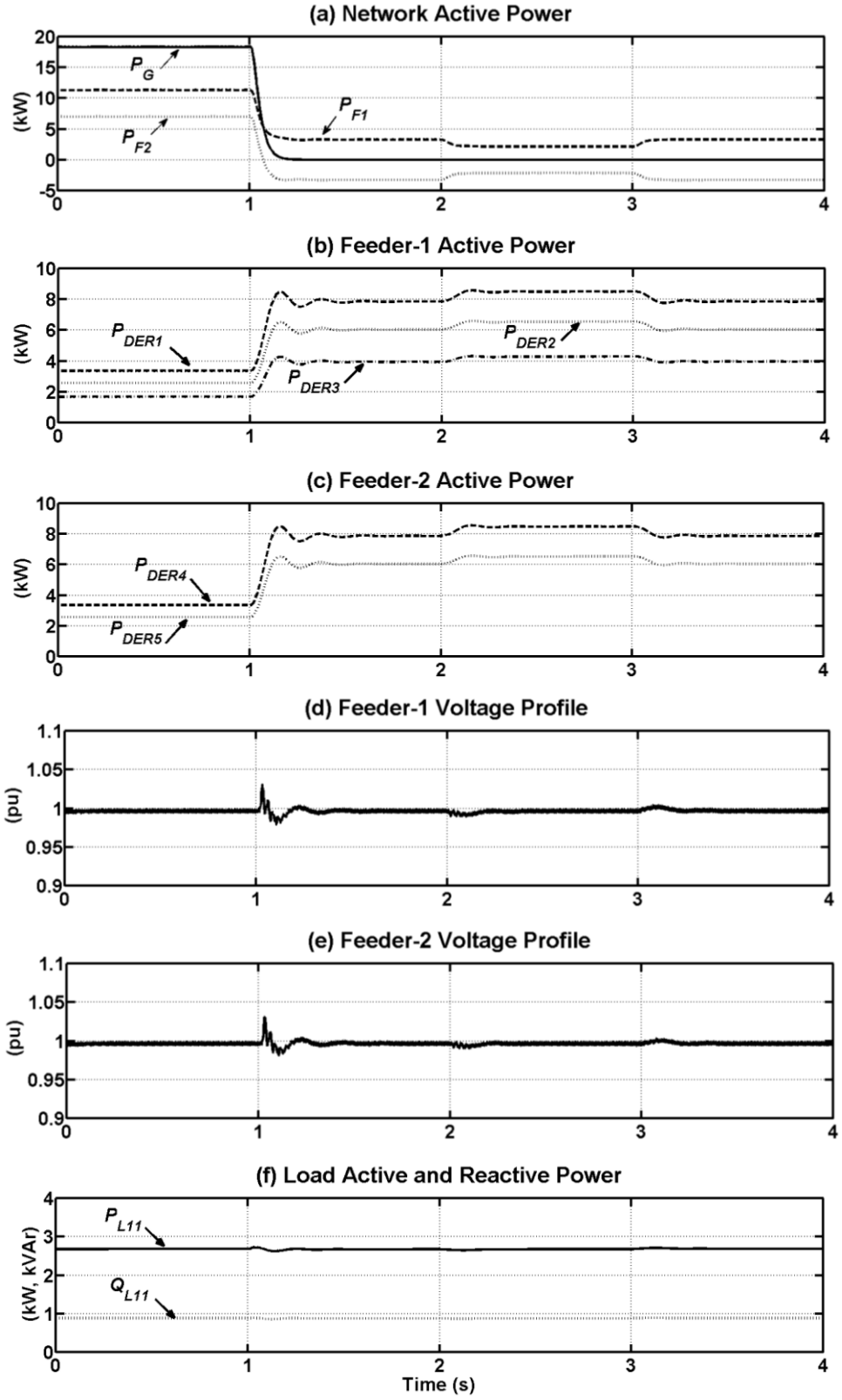

Fig. 4.2 Simulation results for system of interconnected MG-1 and MG-2:

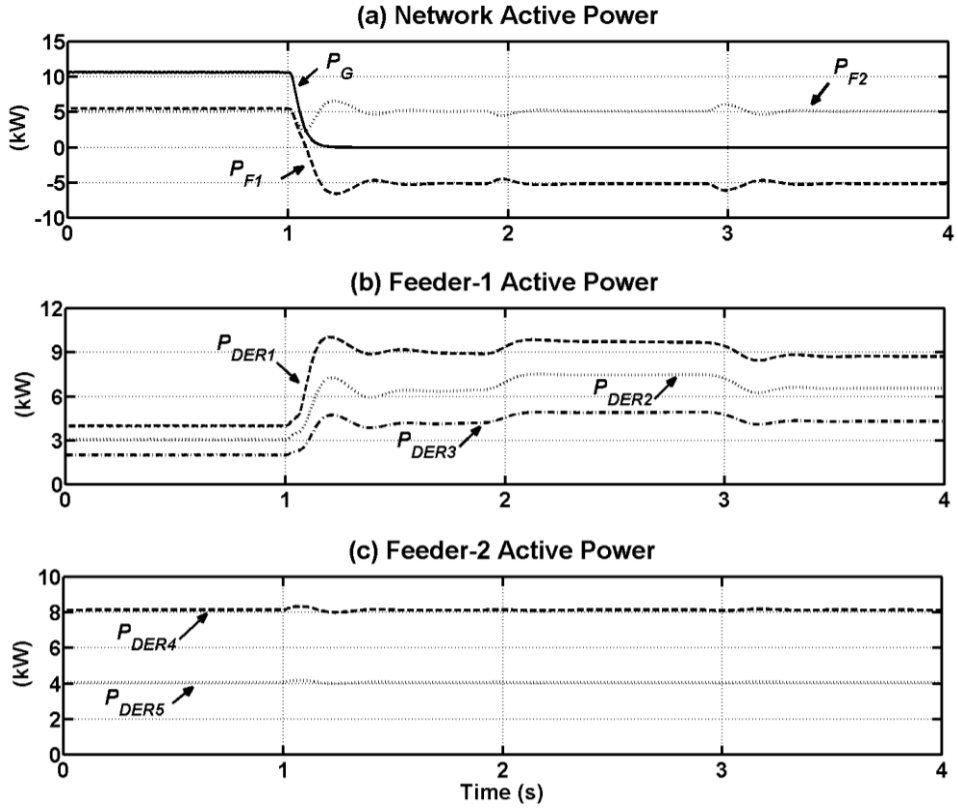

Fig. 4.3 Simulation results for the system of interconnected MG-1 and MG-2 when MG-2 DERs operate at their maximum capacity:

4.3 Large feeder with multiple interconnected microgrids

Now, let us assume a larger medium voltage feeder with self-healing capability with the single line diagram as shown in Fig. 4.4. The assumed network contains 9 microgrids which can be interconnected at certain times to fulfill the power demand requirement of each other. Each microgrid is a combination of several DERs and loads plus a DSTATCOM at the secondary side of their distribution transformer.

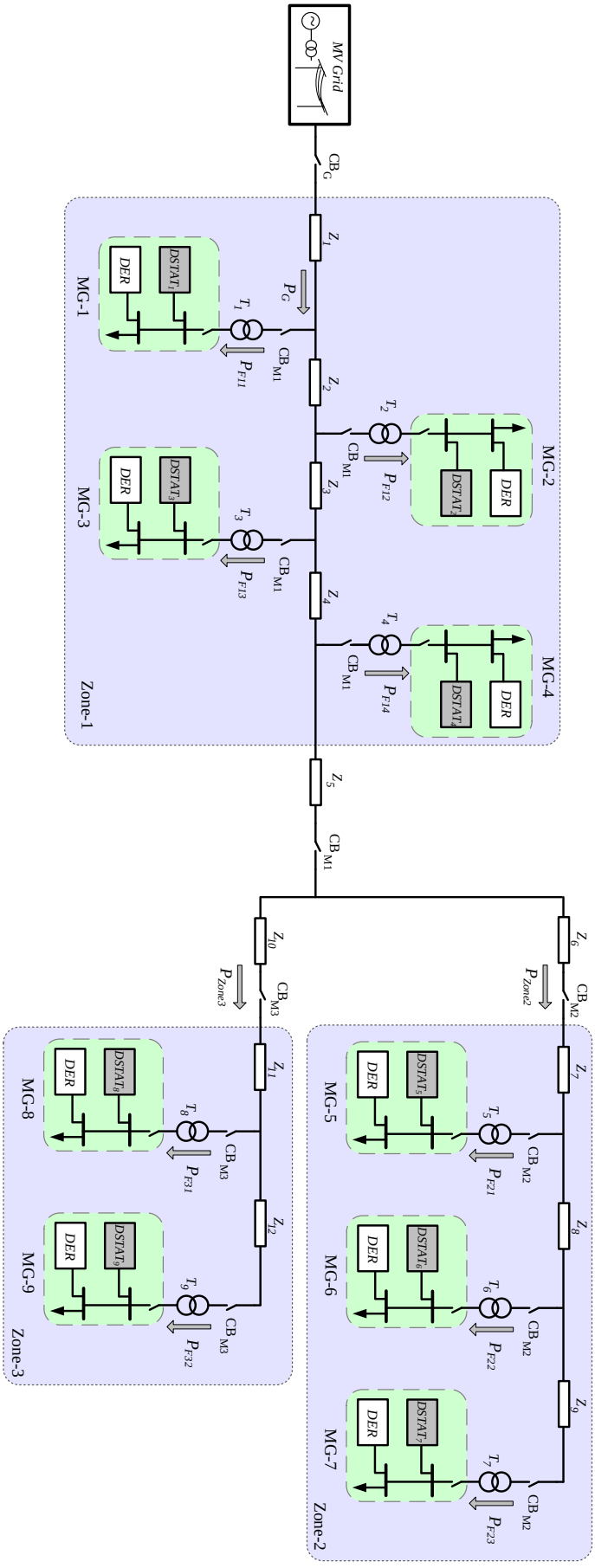

Fig. 4.4 Schematic diagram of the large medium voltage feeder with self-healing capability containing several interconnected microgrids.

The network is divided into 3 zones by proper installation and coordination of circuit breakers CB_G, CB_{M1}, CB_{M2} and CB_{M3}, as shown in this figure. This zone forming can be achieved by deploying the required protection and communication infrastructure, which is not the scope of this study.

Now, let us assume at t = 0 s the network is in steady state condition and all the circuit breakers are closed. In case of a fault within any microgrid, the faulty microgrid can be isolated from the rest of the network by the proper operation of the low voltage circuit breaker, located in the secondary side of the distribution transformer, of the relevant microgrid. Let us assume at t = 0.5 s, a fault is occurred on the medium voltage feeder which is cleared at t = 1 s. Based on the fault location, three separate cases are considered as below:

Case 1: The fault is on the medium voltage feeder within Zone-2.

Case 2: The fault is on the medium voltage feeder within Zone-1.

Case 3: The fault is on the medium voltage grid (i.e. upstream of Zone-1).

For case 1, when the fault is within Zone-2, it is expected that, based on the protection and circuit breaker coordination and self-healing process, CB_{M2} to be opened while all other circuit breakers are closed. In such a case, the DERs in MG-5, MG-6 and MG-7 have to independently supply their local load demand and a load shedding is required if their generation capacity is less than their load demand. At t = 1 s, CB_{M2} is reclosed after the fault is cleared. Fig. 4.5 shows the simulation results of the network for this case. The active power supplied from the grid in addition to the power supplied to Zone-2 and Zone-3 are shown individually in Fig. 4.5a. The active power flow into each microgrid feeder is also shown for all three zones separately, in Fig. 4.5b to Fig. 4.5d. From Fig. 4.5c, it can be seen that the active power flow into the microgrids within Zone-2 becomes zero between 0.5 and 1 second as CB_{M2} is opened, while no power variation is observed in Zone-1 and Zone-3 microgrids.

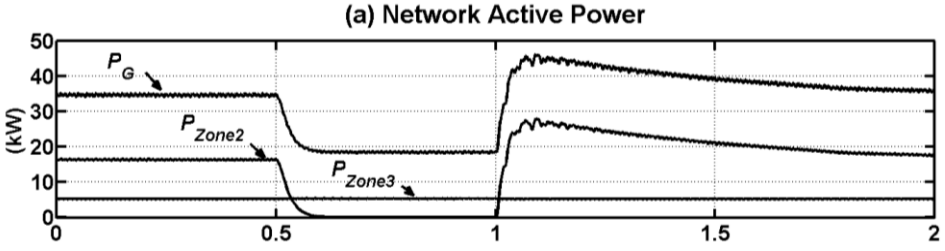

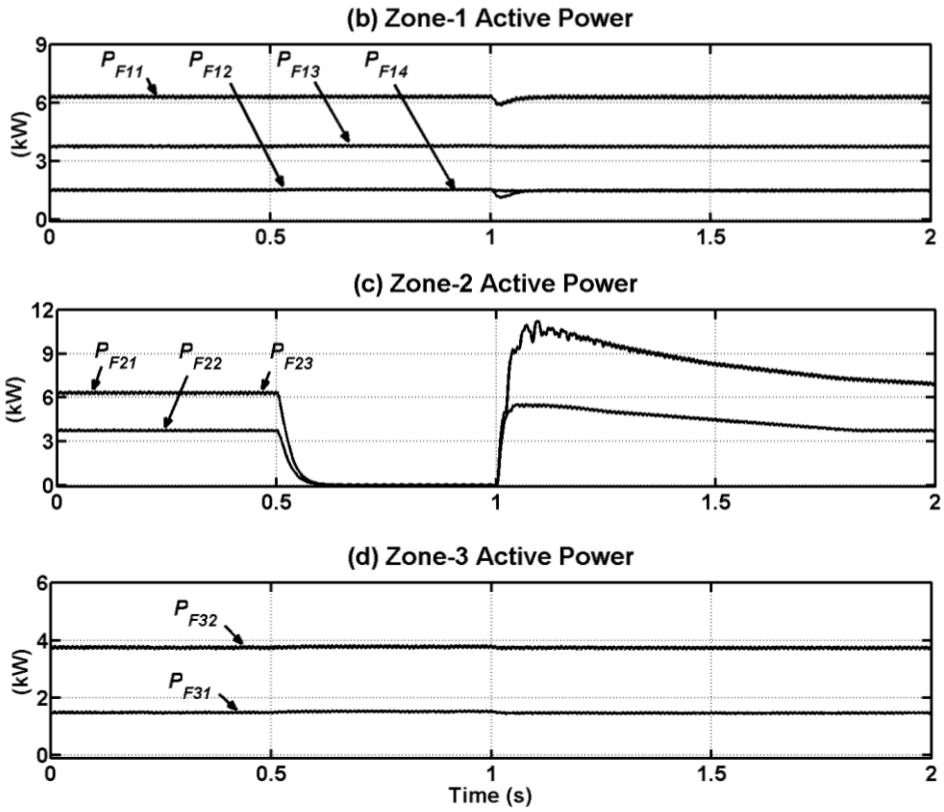

Fig. 4.5 Simulation results for the network in case 1:

For case 2, when the fault is within Zone-1, it is expected CB_G and CB_{M1} to be opened while all other circuit breakers are closed. In such a case, the DERs in MG-1 to MG-4 have to independently supply their local load demand. However, as Zone-2 and Zone-3 microgrids are interconnected, they can share the load demand altogether and this will prevent or reduce the load shedding for the loads of these two zones. Fig. 4.6 shows the simulation results for the network in this case. The active power supplied from the grid in addition to the power supplied to Zone-2 and Zone-3 are shown individually in Fig. 4.6a. The active power flow into each microgrid feeder is also shown for all three zones separately, in Fig. 4.6b to Fig. 4.6d. From the simulation results, it can be seen that the active power flow into the microgrids within Zone-1 becomes zero between 0.5 and 1 second as CB_G and CB_{M1} are opened. In addition, it can be seen that the DERs in MG-6, MG-8 and MG-9 have negative power flow. This indicates that these microgrids are delivering some portion of the loads within MG-5 and MG-7 in addition to their local loads. If this interconnection was not possible, then load shedding was inevitable for MG-5 and MG-7.

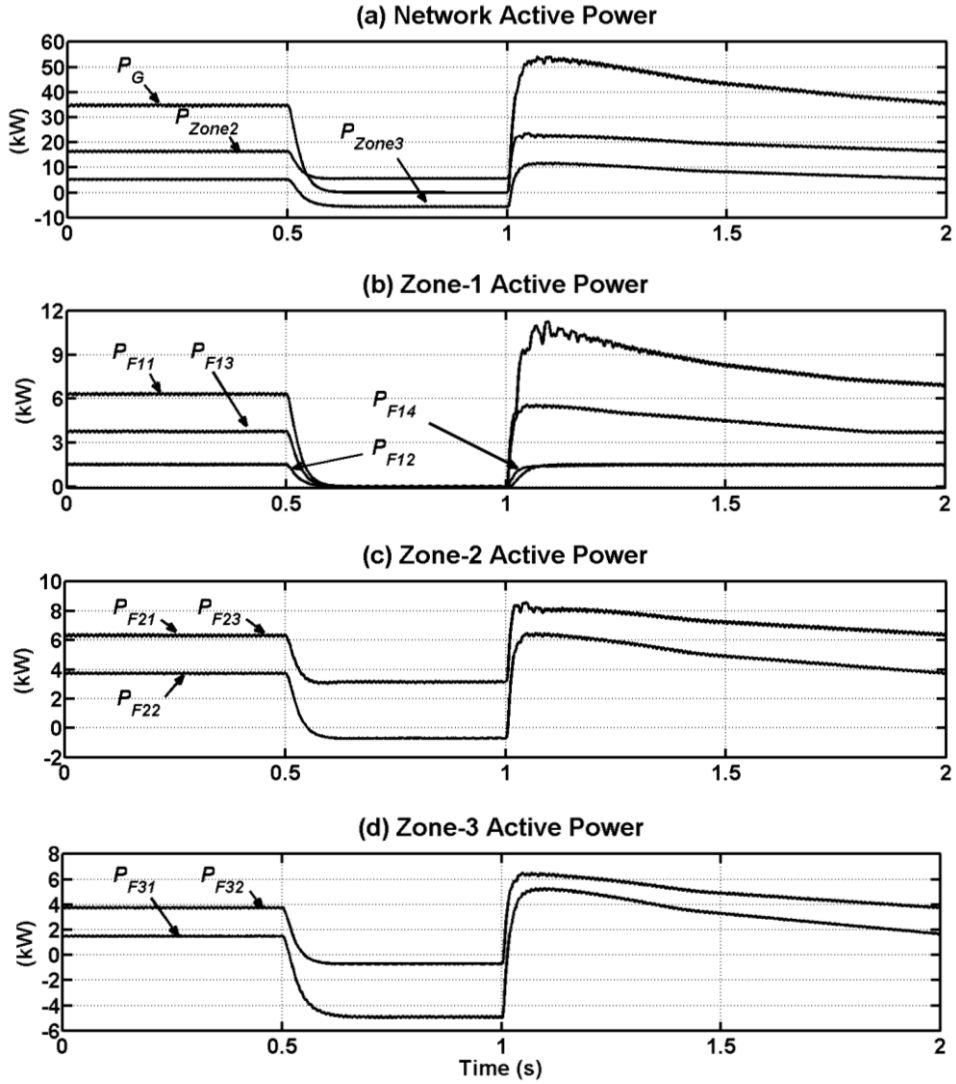

Fig. 4.6 Simulation results for the network in case 2:

For case 3, when the fault is in the upstream of Zone-1, it is expected only CB_G to be opened while all other circuit breakers are closed. In such a case, the microgrids in all three zones are interconnected and their DERs will share the load demand altogether. Hence, the load shedding for the loads of these three zones will be prevented or reduced. Fig. 4.7 shows the simulation results for the network in this case. The active power supplied from the grid in addition to the power supplied to Zone-2 and Zone-3 are shown individually in Fig. 4.7a. The active power flow into each microgrid feeder is also shown for all three zones separately, in Fig. 4.7b to Fig. 4.7d. From the simulation results, it can be seen that the active power flow supplied by the grid becomes zero between 0.5 and 1 second as CB_G is opened. Therefore, all DERs in the microgrids will increase their output power to pick up the required extra demand. From the simulation results, it can be seen that MG-3 and MG-9 have zero

active power flow. This indicates that all the generation capacity of their DERs is consumed by their local loads. On the other hand, it can be seen that MG-2, MG-4 and MG-8 have negative power flow. This indicates that these microgrids are delivering some portion of the loads within MG-1, MG-5, MG-6 and MG-7 in addition to their local loads. If this interconnection was not possible, then load shedding was inevitable for these microgrids. This verifies the efficacy of the proposed operation and control of the DER converters in the system of interconnected microgrids.

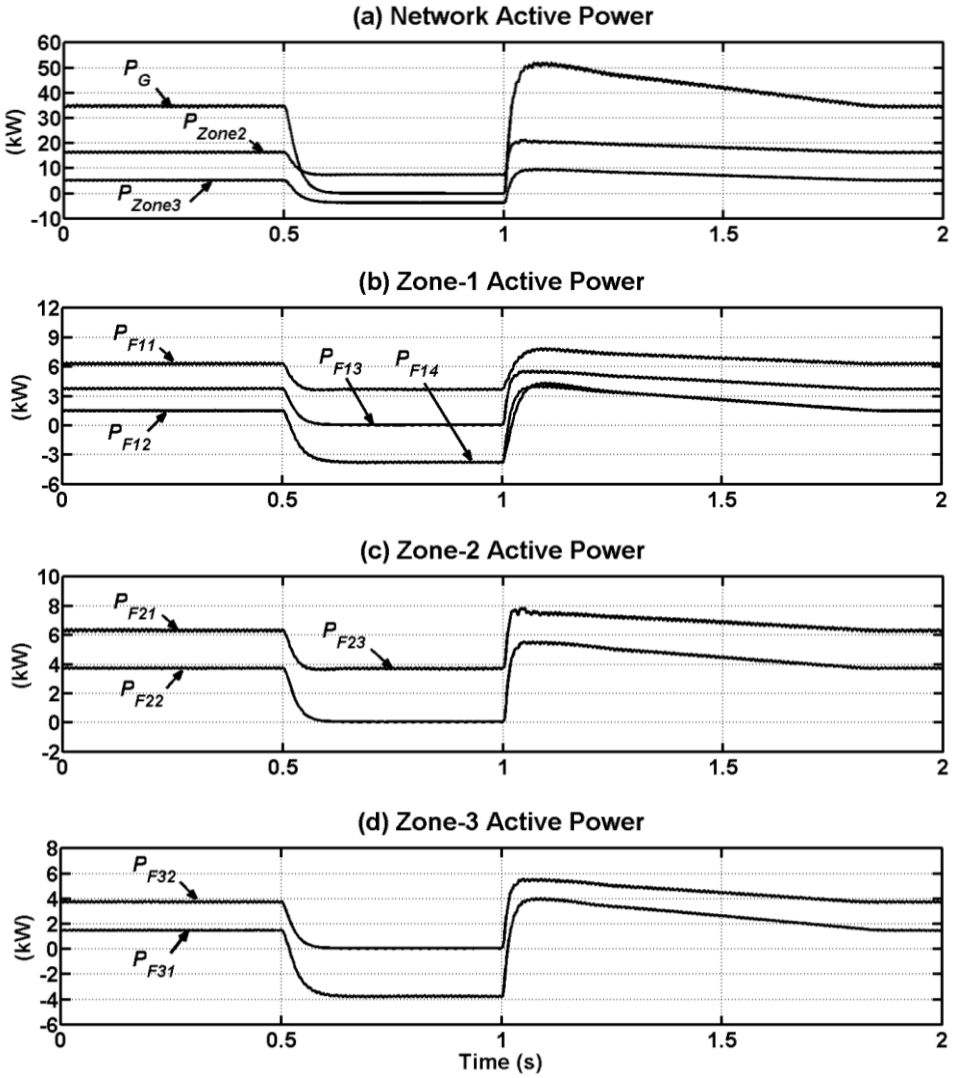

Fig. 4.7 Simulation results for the network in case 3:

4.4 Summary

In this chapter, through several simulation case studies, it is shown that two or more neighboring microgrids can successfully interconnect to each other in a smart grid network with self-healing capability. It is verified that the proposed primary control level for the DERs in Chapter 2 can successfully be employed by the DERs when the neighboring microgrids are interconnected. Based on this concept, it was shown that a large medium voltage feeder, can be successfully divided into several microgrid clusters containing few interconnected microgrids, in the event of a main grid failure.

Chapter 5 Microgrids with Single-phase DERs

The operation and control of single-phase DERs, distributed arbitrary among the three phases of a microgrid system are presented in this chapter. The power circulation mechanisms to circulate the excess generated single-phase power from one phase to the other phase(s) are discussed in detail. Through the simulation studies in PSCAD/EMTDC, it is verified that a microgrid with single phase DERs can operate successfully by supporting the loads in all the phases, by circulating the power to other phase through the proposed power circulation strategy.

5.1 Network under consideration

A group of residential neighboring houses are considered to form a house community, namely community-1, as shown in Fig. 5.1. It is supplied from a medium voltage feeder through a three-phase delta/wye-grounded (Dyn-type) distribution transformer, which is the common practice in Australia [94]. The houses are assumed to have single-phase supply and some of them are assumed to have converter-interfaced grid-connected DERs. The community acts as a three-phase microgrid and can operate in either grid-connected or off-grid mode. The microgrid connects to the grid or disconnects from the grid through a static transfer switch, referred to as microgrid main switch, which is installed in the upstream of the distribution transformer.

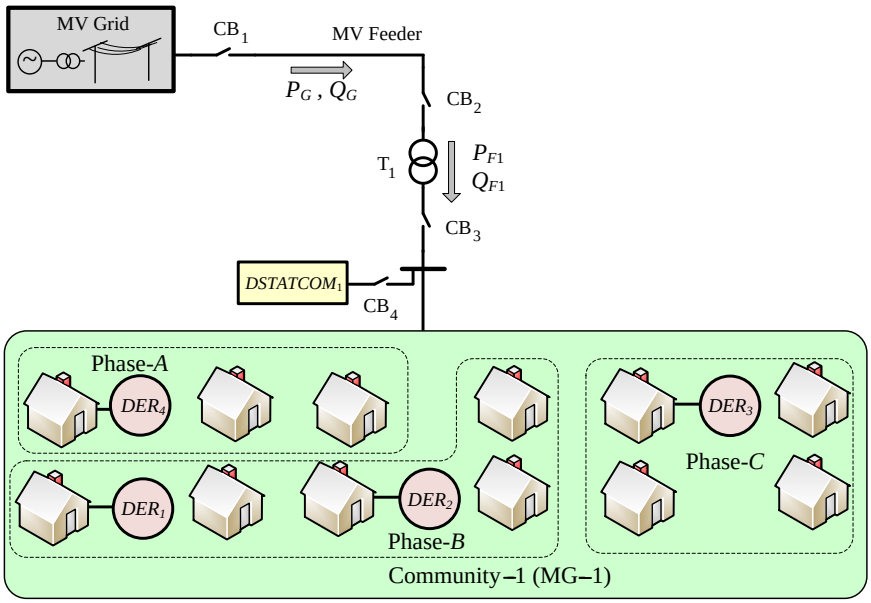

Fig. 5.1 Schematic diagram of the network under consideration.

It is assumed that four houses in community-1 are equipped with single-phase DERs and all are running in voltage-control mode. All the DERs are assumed to have energy storages with sufficient storage capacity.

A low voltage DSTATCOM is assumed to be installed at the secondary side of the distribution transformer, to regulate the voltage at its pcc as proposed in Chapter 2.

The single-phase DERs are connected to the low voltage network through VSCs with LCL filter at their output, as shown in Fig. 2.6a. The single-phase DER converter consists of a single-phase H-bridge, using IGBTs. Each IGBT has proper anti-parallel diode, snubber and protection circuits. The outputs of the H-bridge are connected to a single-phase transformer, with 1: *a* ratio. The transformer provides voltage boosting as well as galvanic isolation. The switching losses in the IGBTs and the core loss in the transformer are the main sources of power loss of the DER converter.

5.2 Interphase power circulation

The DERs in Fig. 5.1 are assumed to be single-phase and unequally distributed amongst the phases. Therefore, it is required to circulate the power generated by the DERs from the phase in which they are connected to the other phases with more load demand. This is referred to as interphase power circulation, in this thesis. In case the interphase power circulation is not available in the network, the three phases of the

microgrid will perform as three individual single-phase networks during off-grid operation. In such a condition, the loads in the phases with less DER generation capacity need to be shed to maintain the voltage and frequency of that phase within the acceptable limits. The interphase power circulation is achieved in two different methods, as introduced below:

5.2.1 Power circulation through distribution transformer

Interphase power circulation through a transformer is based on the concept of interphase coupling among the three windings in the transformer secondary. For a three-phase distribution transformer composed of a 3-limb unified magnetic core [95], each secondary winding has an interphase coupling with the other secondary windings. Therefore, the flux generated by a particular phase flows throughout the core and contribute for inducing voltage in the other secondary windings. For a three-phase distribution transformer composed of three single-phase transformers, there are three separate cores; hence, there is no interphase coupling among the secondary windings, unless the primary windings are connected in delta.

To hold a three-phase balanced voltage across the secondary terminals of the distribution transformer, a three-phase DSTATCOM is connected to the terminals. Under such conditions, if a single-phase DER is connected to one terminal and a load is connected to another terminal, the interphase power circulation takes place through the distribution transformer; hence, the load will be supplied by the single-phase DER in the other phase.

However, in this mode of operation, the distribution transformer experiences an excessive unbalanced condition and hence it may operate while it is heavily saturated. Hence the losses take place within the transformer could be significant. Further, at least two phases of the transformer secondary needs to be energized with proper voltages in order to obtain correct voltage across the third phase with the required phase difference. Additionally, there can be security and safety concerns involves with leaving the distribution transformer energized. Alternatively, the power circulation can be achieved through the DSTATCOM, which is described in detail below.

5.2.2 Power circulation through DSTATCOM

Alternatively, a DSTATCOM can be used to provide current (power) circulation among the phases. DSTATCOM can be connected to medium voltage as well as the low voltage feeders. This is shown schematically in Fig. 5.2.

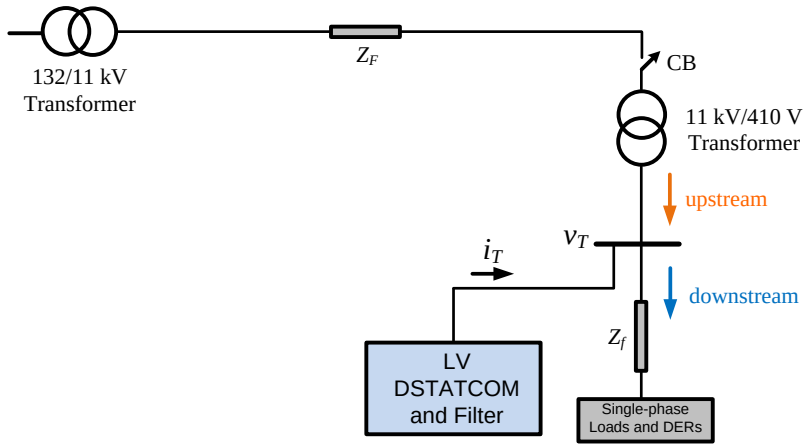

(a)

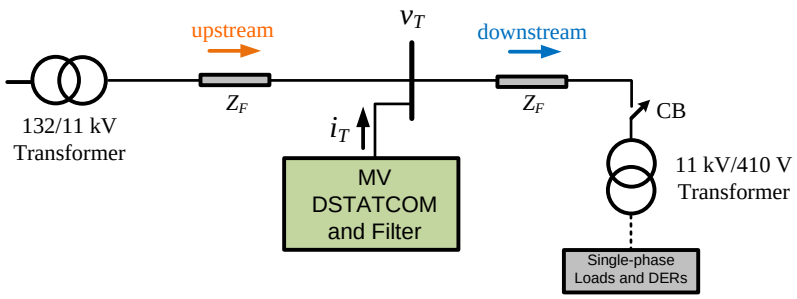

(b)

Fig. 5.2 Schematic diagram of a distribution network with DSTATCOM installed in: (a) low voltage feeder and (b) medium voltage feeder.

The main advantage of installing a DSTATCOM in a low voltage feeder is the elimination of the unbalance reverse power flow into the medium voltage network due to the unbalance excess generation of the single phase DERs connected to different phases. However, installation of a few DSTATCOMs in several adjoining low voltage feeders, supplied by the same medium voltage line, is not cost-effective. Hence, reduction in the initial investment costs is the main advantage of installing a DSTATCOM in the medium voltage feeder. In general, several criteria can be considered in choosing the connection of DSTATCOM to a low voltage or medium voltage feeder such as:

- Economic concerns: The cost of a DSTATCOM is highly dependent on its rating. Similar to other electrical devices, this cost increases significantly by the increase of the DSTATCOM rating. Hence, economic analyses can lead to choosing among the two options of installing one DSTATCOM, with a higher rating, in the medium voltage feeder or several DSTATCOMs, each with a smaller rating, in the low voltage feeders.
- The level and frequency of reverse power flow in the feeder: The reverse power flow may be experienced more frequently in the low voltage feeders with higher percentage. However, it may be neither very frequent nor a high percentage in the medium voltage feeders. Therefore, the level of reverse power flow in the medium voltage line can sometimes be insignificant while it is significant in some low voltage lines.
- Reliability concerns: Failure of a DSTATCOM in a low voltage feeder may only interrupt the power supply to a few customers in the feeder, however; its failure in a medium voltage feeder may result in power interruption to a larger number of customers of the medium voltage feeder.
- Operational and maintenance concerns: A DSTATCOM installed in a low voltage feeder will have less operational and maintenance costs and lower hazards for the personnel under hot line practices, in comparison to those of the medium voltage installation.

Two different topologies are considered for the DSTATCOM– one when it is used in low voltage feeder and the other when it is used in medium voltage feeder. The positioning of the boosting transformer in the output of the DSTATCOM is different for medium voltage and low voltage applications. This changes the filter characteristic in the output of the DSTATCOM. In this section, it is shown that voltage control strategy is suitable for low voltage applications from the output passive filter arrangement point of view. On the other hand, it is shown that current control strategy is well suited for medium voltage applications, considering the same.

The current and voltage output references of the DSTATCOM are generated such that a set of balanced currents are drawn from the upstream side, while facilitating the circulation of reverse power flow among the phases. In addition, the used topology for low voltage application provides a reliable path among the phases in off-grid applications. Hence, when the low voltage feeder is isolated from the

upstream side, the single-phase DERs, controlled in droop, can manage the power demand of the three-phase network irrespective to the phase they are connected. This is a novel application of DSTATCOM in addition to voltage control [96][97][98][99].

The main aim of the DSTATCOM, either in low voltage or in medium voltage, is to force the upstream currents balanced irrespective of the power flow in its downstream side. To achieve this, the DSTATCOM must circulate power from one phase to the other. In other words, it forces the power from the phase with excess generation to flow to the other phase(s) to avoid reverse power flow in that phase. Even when there is no reverse power flow and the power to the load is supplied by the grid, the DSTATCOM balances the upstream currents, but this also occurs as the power is circulated amongst the phases, through the DSTATCOM.

5.2.2.1 DSTATCOM in low voltage feeder

Let us consider a case that the distribution transformer is isolated form the downstream side when the microgrid operates in off-grid mode. In this case, the interphase power circulation is not available through the distribution transformer. However, it can be accomplished through the DSTATCOM [98]. For this purpose, the DSTATCOM is required to have a common dc bus, connected to the VSCs of all three phases. Note that, the structure of three single-phase DSTATCOMs, with three separate dc buses, cannot be utilized for this purpose.

Fig. 5.3 shows a three-phase DSTATCOM topology to be connected to the low voltage feeder. This DSTATCOM is connected to a common dc bus, which regulates its pcc to a balanced three-phase voltage of 1 pu. Since the transformer is isolated (i.e. CB-T_P and CB-T_S are open), the currents in the upstream of the DSTATCOM are all zero ($i_{tr\_a} = i_{tr\_b} = i_{tr\_c} = 0$). Then, the KCL at DSTATCOM pcc is written as

$$\begin{cases} i_{dstat\_a} + i_{tr\_a} - i_a = 0 \\ i_{dstat\_b} + i_{tr\_b} - i_b = 0 \\ i_{dstat\_c} + i_{tr\_c} - i_c = 0 \end{cases} \Rightarrow \begin{cases} i_{dstat\_a} = i_a \\ i_{dstat\_b} = i_b \\ i_{dstat\_c} = i_c \end{cases} \tag{5.1}$$

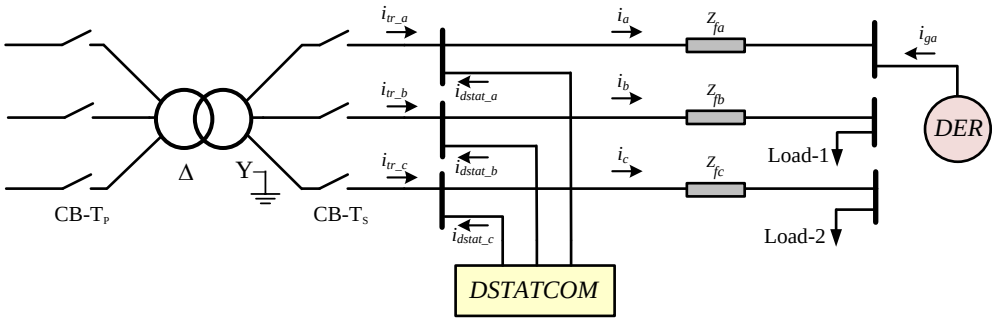

Fig. 5.3 Simplified network under consideration for power circulation through a DSTATCOM.

On the other hand, the three VSCs in the DSTATCOM are connected to a common dc bus and they are wye-connected through the three single-phase isolating transformers. Hence, the DSTATCOM consists a closed boundary circuit and based on KCL, the sum of the currents leaving this closed boundary is zero (i.e. $i_{dstat\_a} + i_{dstat\_b} + i_{dstat\_c} = 0$). Therefore, $i_a = -(i_b + i_c)$. On the other hand, as $i_a = -i_{ga}$, it is concluded that $i_{ga} = i_b + i_c$. This verifies that the loads in phase-B and C are supplied by the DER in phase-A and the interphase power circulation takes place through the DSTATCOM [98].

The main aim of the DSTATCOM is to force the upstream currents to be balanced irrespective of the power flow in its downstream side. This guarantees a proper power circulation through the DSTATCOM. To have a balanced set of current flowing in the medium voltage feeder, the voltage at the pcc of the DSTATCOM must be balanced. This can be achieved by controlling the DSTATCOM such that it generates and holds a balanced set of voltage at its pcc. A voltage control technique is utilized to hold a balanced set of voltages across the three filter capacitors (C_f). The three-phase reference voltage will then be [100]

$$[\boldsymbol{V}_{cf}]^{ref}_{ABC} = E_{DSTAT} \angle \delta^{ref}_{cf,A} \times [1 \quad \lambda^2 \quad \lambda]^T \tag{5.2}$$

where E_{DSTAT} is the desired phase rms voltage for the pcc (i.e. 240 V in this study), $\delta_{cf,A}$ is the angle of the terminal voltage, v_{TA} and $\lambda = 1 \angle 120^o$. This voltage is used as the reference for converter control, as discussed in the next section. The DSTATCOM exchanges reactive power with the low voltage feeder to hold the desired voltage at its pcc.

The main assumption above is the presence of a balanced voltage at the secondary side of the distribution transformer. This may not be true in a real network

where a medium voltage feeder supplies several low voltage feeders and each low voltage feeder injects some power back into the medium voltage feeder. In such a case, the medium voltage feeder may induce unbalanced voltages at the secondary side of the distribution transformer. Hence, installing one DSTATCOM at one of the low voltage feeders will not guarantee a set of balanced currents to flow in the upstream of the DSTATCOM. Thereby, a DSTATCOM is required to be installed in every low voltage feeder in which single-phase DERs are connected. This will restrict the injection of reverse power flow into the medium voltage feeder.

5.2.2.2 DSTATCOM in medium voltage feeder

Now, let us assume that the DSATATCOM is connected to the medium voltage feeder. Fig. 5.4 shows the DSTATCOM topology connected to the medium voltage feeder. A voltage control strategy, similar to the one discussed in section 5.2.2.1 can be utilized. However, in section 5.6, through simulation studies, it will be shown that although the DSTATCOM will have an acceptable level of tracking of the voltage across C_f, due to the leakage inductance of the coupling transformers, the DSTATCOM pcc voltage is not perfectly balanced. Hence, a balanced set of currents will not be observed in the upstream side.

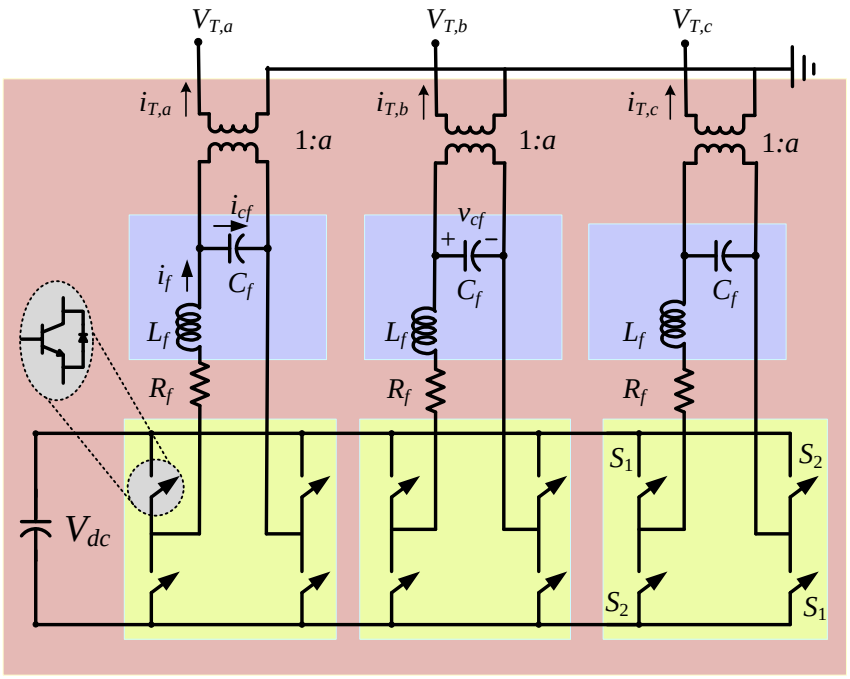

Fig. 5.4 Topology of the DSTATCOM connected to the medium voltage feeder

To avoid this problem, a current control strategy is utilized. In this method, the proper references for the output current for each phase of the DSTATCOM are calculated and the DSTATCOM is controlled to ensure the desired current is injected into the pcc.

The reference output currents of the DSTATCOM are generated such that power circulation takes place between the phases. As a consequence, the upstream currents become balanced. For this purpose, the theory of instantaneous symmetrical component is utilized [101]. In order to apply this theory, first the fundamental positive sequence of the pcc voltage is obtained [102]. Let the instantaneous positive sequence voltages be denoted by v_{A1}, v_{B1} and v_{C1}. The reference currents can then be calculated as [91]

$$[i_T]_{ABC}^{ref} = [i_L]_{ABC} - \frac{v_{A1}i_{LA} + v_{B1}i_{LB} + v_{C1}i_{LC}}{v_{A1}^2 + v_{B1}^2 + v_{C1}^2}[v_1]_{ABC} \tag{5.3}$$

where i_L is the current in the downstream of DSTATCOM. This current is used as the reference for converter control.

Let us consider only one phase of the DSTATCOM circuit shown in Fig. 5.4, in which the state vector is defined as [90]

$$x(t) = \begin{bmatrix} i_T(t) & i_f(t) & v_{cf}(t) \end{bmatrix}^T \tag{5.4}$$

where i_T is the output current of the DSTATCOM. Then, the state space equation of the system is written as

$$\begin{aligned} \dot{x}(t) &= Ax(t) + B_1u_c(t) + B_2v_T(t) \\ y(t) &= Cx(t) \end{aligned} \tag{5.5}$$

where

$$A = \begin{bmatrix} 0 & 0 & \frac{a}{L_T} \\ 0 & -\frac{R_f}{L_f} & -\frac{1}{aL_f} \\ -\frac{a}{C_f} & \frac{a}{C_f} & 0 \end{bmatrix}, \quad B_1 = \begin{bmatrix} 0 & \frac{V_{dc}}{aL_f} & 0 \end{bmatrix}^T, \quad B_2 = \begin{bmatrix} -\frac{1}{L_T} & 0 & 0 \end{bmatrix}^T, \quad C = \begin{bmatrix} 1 & 0 & 0 \end{bmatrix}$$

are system matrices.

As the system behavior is governed by the poles of its transfer function (i.e. the eigenvalues of matrix *A*), it is often desirable to modify the poles of the system in order to obtain certain properties such as rise/settling time, damping, overshoot and stability. In this study, the control system is designed using a discrete-time output feedback pole-shift control [96]. In this technique, the open-loop poles are shifted radially towards the origin (i.e. more stable locations) to form the closed-loop poles. Later, (5.5) is represented in discrete-time domain. Assuming the feedback control has the form of Fig. 5.5 the system of converter and filter is represented in transfer function domain as

$$\frac{y(k)}{u_c(k)} = \frac{G_1(z^{-1})}{F(z^{-1})} = \frac{g_1 z^{-1} + g_2 z^{-2} + g_3 z^{-3} + \ldots}{1 + f_1 z^{-1} + f_2 z^{-2} + f_3 z^{-3} + \ldots} \tag{5.6}$$

where z^{-1} is the delay operator. Now, let the control law be given by

$$u_c(k) = \frac{S(z^{-1})}{R(z^{-1})}\{y_{ref}(k) - y(k)\} \tag{5.7}$$

where y_{ref} is the desired (reference) output current. From Fig. 5.5, the closed-loop characteristic equation of the system, $\Delta(z^{-1})$, is given as

$$\Delta(z^{-1}) = F(z^{-1})R(z^{-1}) + G(z^{-1})S(z^{-1}) \tag{5.8}$$

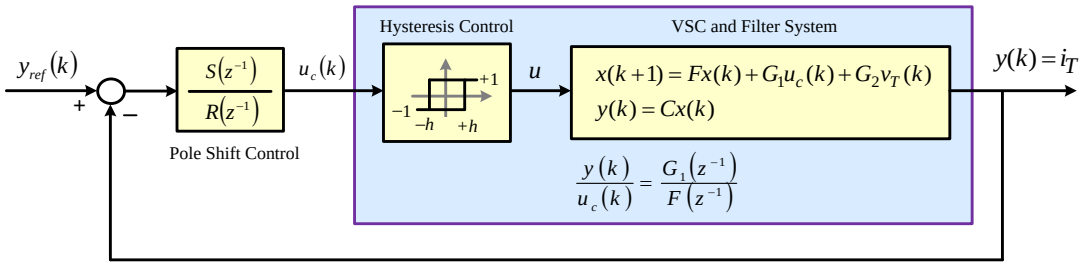

Fig. 5.5 Closed-loop switching control block diagram for current control strategy based on pole-shift.

Unlike the pole-placement technique where $\Delta(z^{-1})$ is pre-defined by the user, pole-shift technique takes the form of

$$\Delta(z^{-1}) = F(\lambda z^{-1}) = 1 + \lambda f_1 z^{-1} + \lambda^2 f_2 z^{-2} + \lambda^3 f_3 z^{-3} + \ldots \tag{5.9}$$

where the poles are shifted by λ towards the origin. In this technique, the closed-loop poles are obtained by multiplying the open-loop eigenvalues by $0 < \lambda < 1$ where λ is

a scalar, close to one (e.g. λ = 0.8), which is called the pole-shift factor. The pole-shift factor is the only parameter to be defined in the controller and its value determines the control gain. It is adjusted such that the controller is limited only for the first few swings following a large impact on the system. Given β is the absolute of the largest characteristic root of $F(z^{-1})$, for guaranteeing the closed-loop system stability, λ is limited as [103]

$$-\frac{1}{\beta} < \lambda < \frac{1}{\beta} \tag{5.10}$$

Since the penalty on control action can be easily adjusted by λ as in (5.10), the closed-loop system will unlikely be instable. This is an advantage of the pole-shift technique compared to other techniques such as deadbeat control which forces all the closed-loop poles to the origin, requiring excessive control effort.

Equating (5.8) with (5.9), the controller coefficients in $R(z^{-1})$ and $S(z^{-1})$ can be obtained. For the system of converter and filter under consideration in this study, based on the system order in (5.5)-(5.6), $S(z^{-1})$ and $R(z^{-1})$ in (5.7) are of the form

$$\frac{u_c(k)}{y_{ref}(k) - y(k)} = \frac{S(z^{-1})}{R(z^{-1})} = \frac{s_0 + s_1 z^{-1} + s_2 z^{-2}}{1 + r_1 z^{-1} + r_2 z^{-2}} \tag{5.11}$$

Based on these calculated values, the reference tracking error, $u_c(k)$ is defined from (5.7) and used to achieve a reference tracking error less than the maximum specified as described in (2.37).

5.3 Grid-connected and off-grid operation

First, a case study is carried out to verify the proper performance of the single-phase DER converters, during both grid-connected and off-grid modes of operations. The network of Fig. 5.1 is considered in which it is assumed to be initially grid-connected and in steady-state condition at t = 0. At t = 1 s, circuit breaker CB_{M1} opens and the microgrid falls into off-grid mode. At t = 2 s, a balanced three-phase load demand increase of 60% (i.e. 9 kW) is applied in the network. At t = 3 s, a single-phase load demand increase of 13.3% (i.e. 2 kW) is applied in phase-A. At t = 4 s, a new single-phase load is connected to phase-B with a demand of 4 kW. Finally,

at t = 5 s, a single-phase load demand decrease of 6.65% (i.e. 1 kW) is applied in phase-C.

The simulation results are shown in Fig. 5.6. The total active power demand of community-1 is shown in Fig. 5.6a. The active power supplied by the grid and the power generation by the single-phase DERs are shown in Fig. 5.6b. Fig. 5.6c and Fig. 5.6d show the active power flow in the primary and secondary sides of the distribution transformer. The network frequency is shown in Fig. 5.6e. The rms voltage in the DSTATCOM pcc is shown in Fig. 5.6f while the active and reactive power output of the DSTATCOM are shown in Fig. 5.6g.

For t < 1 s, the total surplus of DERs generation is 2.4 kW which is fed back to the (upstream) grid. The total active power demand remains the same after grid is disconnected at t = 1 s (Fig. 5.6a) and this demand is supplied by the DERs. The DERs active power generation drops as the grid is disconnected, since no power is delivered to the grid at this time (Fig. 5.6b). The three-phase power in the transformer primary is zero but in secondary, the three phases carry different amounts of power due to the unbalanced distribution of DERs and loads in the microgrid (Fig. 5.6c-d). The network frequency is 50 Hz when operating in grid-connected mode while it is regulated by the DERs through the droop control in off-grid mode (Fig. 5.6e). The voltage at transformer secondary is regulated to 1 pu by the DSTATCOM at all times (Fig. 5.6f). The DSTATCOM absorbs approximately 5 kVAr reactive power during grid-connected mode while it injects reactive power in off-grid mode depending on the network load (Fig. 5.6g). It is to be noted that the DSTATCOM consumes a constant amount of 3 kW, approximately, for replenishing the losses in its VSCs [31].

At 1 < t < 2 s, community-1 has 5 kW of demand in each phase while the DERs generation in phase-A, B and C is respectively 2.9, 8.7 and 4.4 kW. Hence, phase-B has excess of generation whereas phase-A and C have more demand. In the secondary side of the distribution transformer, there is a 2.1, –2.7 and 0.6 kW power flow in phase-A, B and C, respectively (Fig. 5.6d). This shows an interphase power circulation through the distribution transformer from phase-B to the other phases and as a result, the single-phase DERs in phase-B not only contribute to the load demand in this phase, but they also share some of the load demand in the other two phases. Note that in this condition, the DSTATCOM does not contribute to interphase power circulation.

At $2 < t < 3$ s, all single-phase DERs share the three-phase load increase proportional to their ratings (Fig. 5.6b). At $3 < t < 4$ s, all single-phase DERs increase their output power to share the single-phase load increase (Fig. 5.6b). At $4 < t < 6$ s, the load changes are shared by the DERs connected to different phases; however, the DERs in phase-B contribute for the load changes in the other phases based on the interphase power circulation through the distribution transformer (Fig. 5.6d).

The DERs update their output power based on droop control in response for different load changes in the network; hence different levels of interphase power circulation through the distribution transformer are observed (Fig. 5.6d).

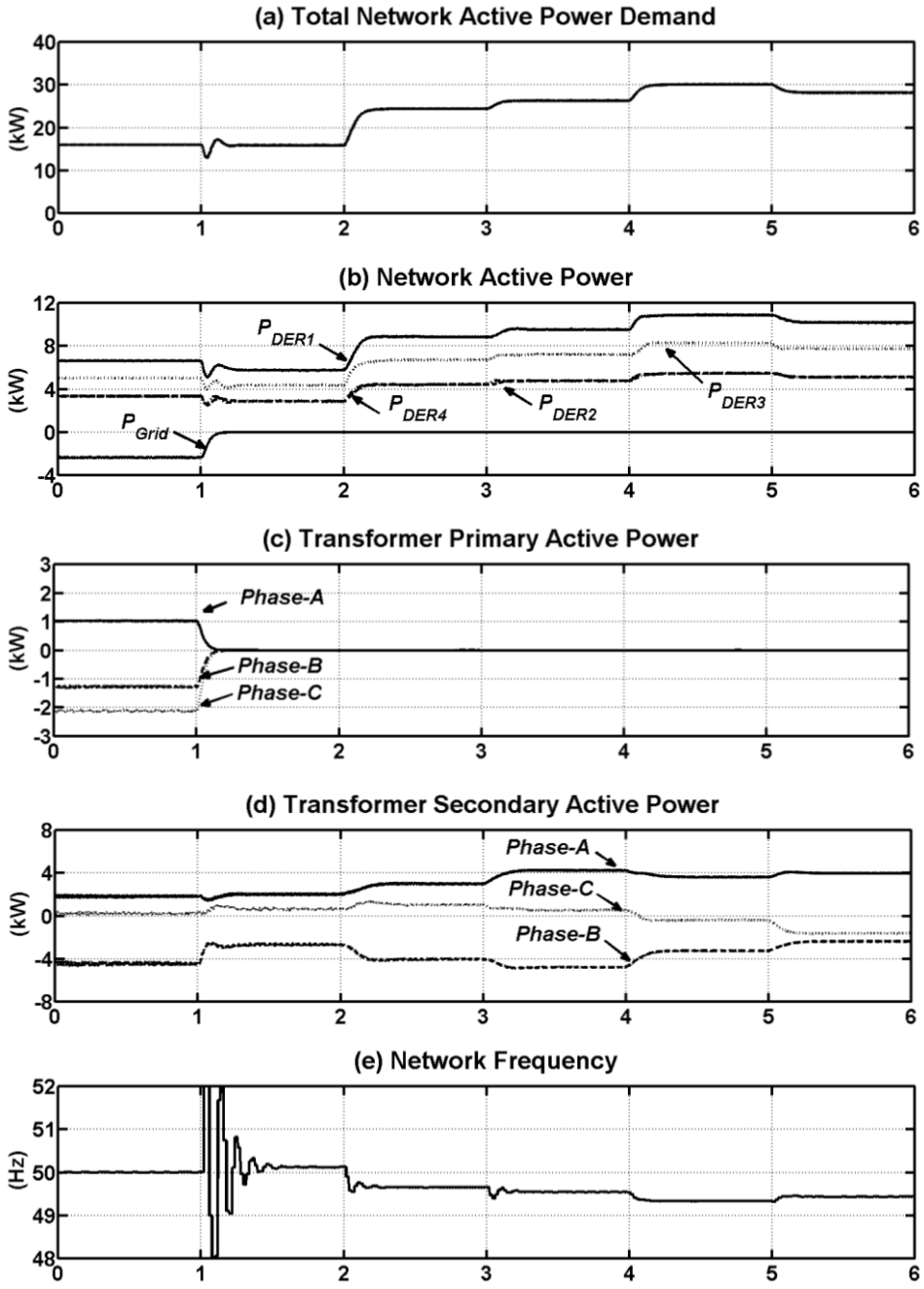

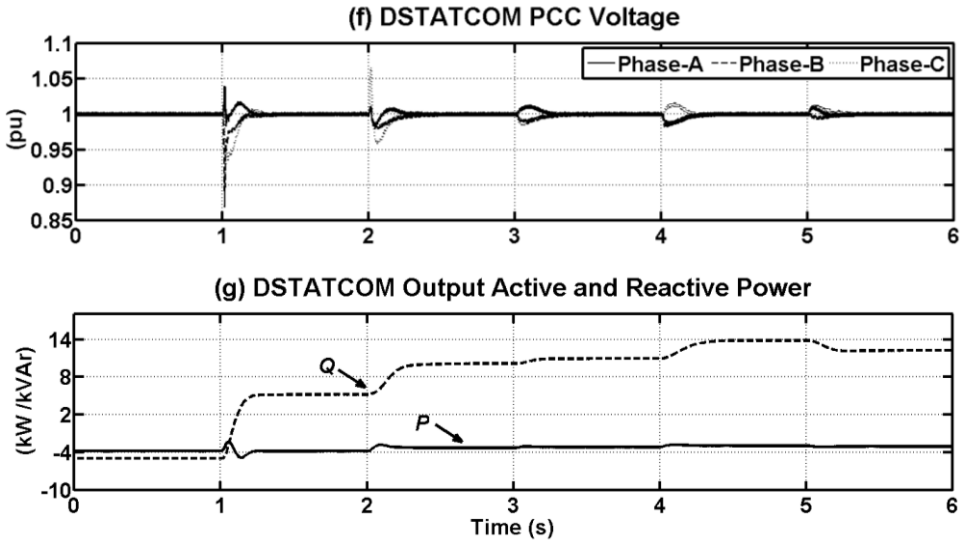

Fig. 5.6 Simulation results for community-1 in case-1:

5.4 Single phase DER and microgrid isolation and resynchronization

Another study case is carried out to verify the dynamic performance of single phase DER converters during transitions from grid-connected to off-grid and vice versa. It is assumed MG-1, in section 5.3, is grid-connected and in steady state condition at t = 0. At t = 1 s, the microgrid main switch (CB_M) opens and the microgrid falls into off-grid mode. At t = 2 s, DER-3 which is connected to phase-C and supplying 28 % of total load demand (i.e. 4.3 kW), is disconnected from MG-1. At t = 3 s, the resynchronization of DER-3 to the microgrid is initiated and at t = 3.68 s, it is connected back to the microgrid. At t = 4 s, resynchronization of the MG-1 to the grid is activated and at t = 4.15 s, it is reconnected to the grid.

The simulation results are shown in Fig. 5.7. The total active power demand of community-1 is shown in Fig. 5.7a. The active power supplied by the grid and the power generation by single-phase DERs are shown in Fig. 5.7b. Fig. 5.7c and Fig. 5.7d show the active power flow in the primary and secondary sides of the distribution transformer.

The total active power demand remains the same all the time of the study (Fig. 5.7a). At $1 < t < 4.2$ s, CB_M is open and the microgrid is operating in off-grid mode; hence, the power flow across the transformer primary is zero (Fig. 5.7c). As DER-3, the only generator connected to phase-C, disconnects at t = 2 s, the DERs connected to phase-*B* supply the loads on phase-C and an interphase power circulation is

observed through the distribution transformer (Fig. 5.7d). As DER-3 disconnects, its output power drops to zero and DER-1, 2 and 4 increase their generation proportional to the desired power sharing ratio to match the local demand (Fig. 5.7b). The resynchronization took 0.15 s in the studied case. After microgrid resynchronization, DERs operate at their rated capacity which makes the grid to absorb 2.4 kW (Fig. 5.7b).

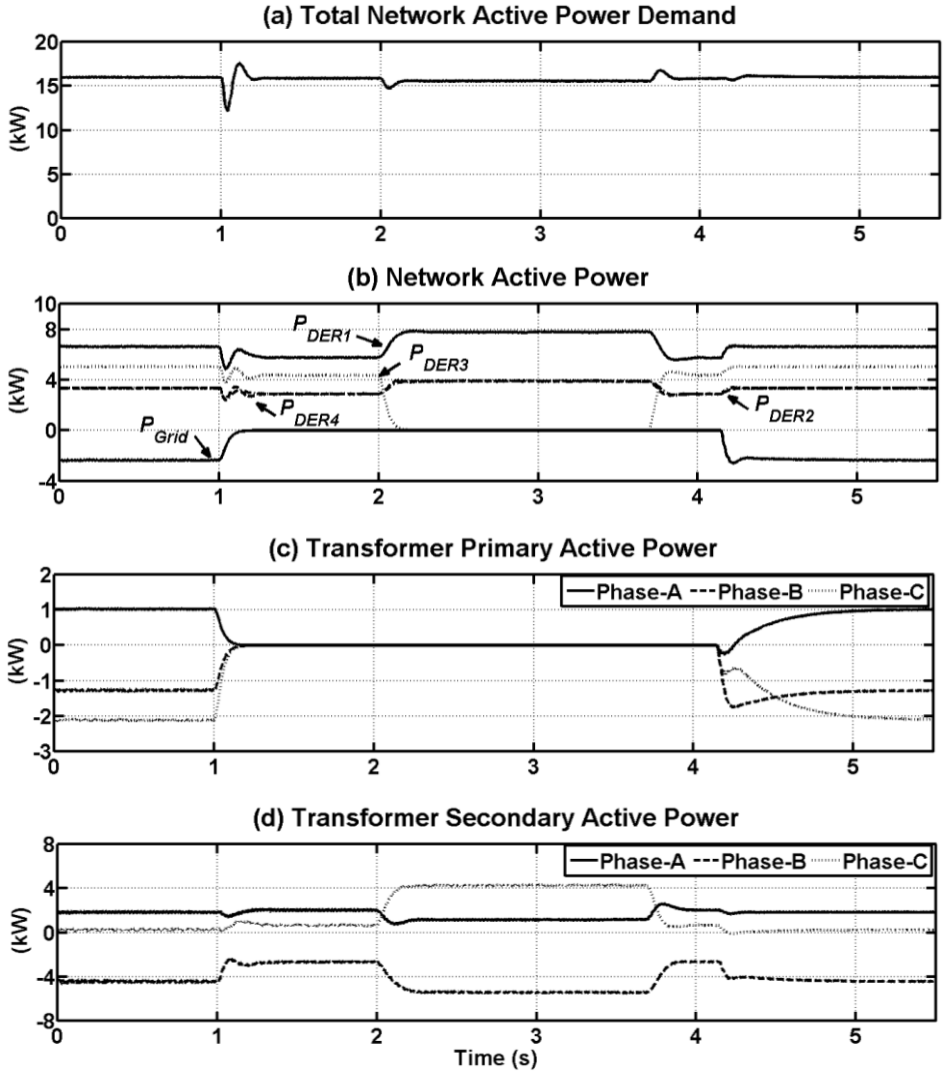

Fig. 5.7 Simulation results for community-1 in case-2:

5.5 Power circulation by a DSTATCOM in low voltage feeder

Another case study is carried out to verify the feasibility of power circulation through the DSTATCOM. Several case studies are demonstrated below to show the DSTATCOM operation in steady state and dynamic conditions. In addition, the network performance in the presence of single-phase DSTATCOMs instead of a three-phase DSTATCOM is demonstrated.

5.5.1 Steady state results

Let us consider the low voltage feeder of Fig. 5.1, with a delta/wye transformer and unbalanced loads where a DSTATCOM, with the topology shown in Fig. 2.4, is installed and controlled based on the voltage control strategy described in section 5.2.2.1. It is assumed that a reverse power flow in phase-A is observed due to the connection of excessive single-phase generation to this phase.

The steady-state, three-phase instantaneous current waveform in the upstream feeder, downstream load and the output of the DSTATCOM are shown in Fig. 5.8a-c, respectively. The phase active power flow along the above-mentioned locations is shown in Fig. 5.8d-f. Separate results are shown for the cases before and after connection of the DSTATCOM. The upstream currents are unbalanced due to the unbalanced downstream currents (Fig. 5.8a,b-left). The active power flow in the upstream of DSTATCOM is equal to the downstream (Fig. 5.8d,e-left).

The active power flow in the feeder is –20, 35 and 49 kW respectively in phase-A, B and C (Fig. 5.8d-left). After the DSTATCOM connection, the active power flow in the DSTATCPOM upstream is 27 kW in all phases (Fig. 5.8d-right). This is achieved as the DSTATCOM absorbs 43 kW from phase-A and injects 10 and 28.5 kW respectively to phase-B and C (Fig. 5.8f-right). Due to the proper power circulation through the DSTATCOM, a set of balanced phase current is also observed in the upstream feeder after the DSTATCOM connection (Fig. 5.8a-right). This case study demonstrates the principle of power circulation through the DSTATCOM which is based on absorbing active power from the phase with reverse flowing power and injecting that power (minus DSTATCOM internal losses) to the other phases. The output currents and active power flow from the DSTATCOM are shown in Fig. 5.8c,f-right. The summation of the active powers at the outputs of the

DSTATCOM represents the internal losses of the DSTATCOM (Fig. 5.8f-right). In this case, the DSTATCOM loss is equal to 4.5 kW.

It is to be noted that since the loads in these simulation results are assumed to be constant impedance loads, the downstream power before and after DSTATCOM connection is slightly modified due to the voltage correction by the DSTATCOM.

(a)

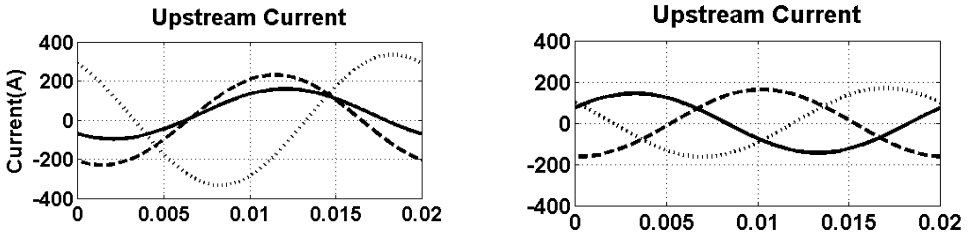

(b)

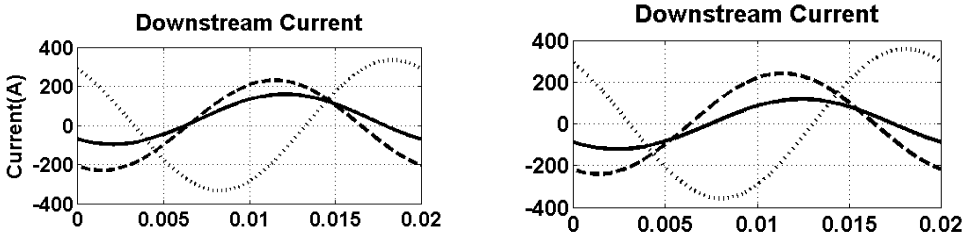

(c)

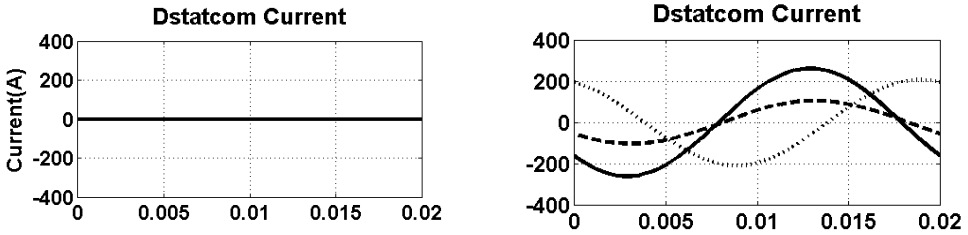

(d)

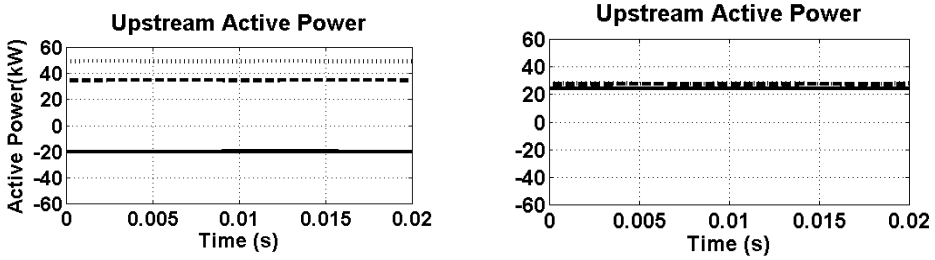

(e)

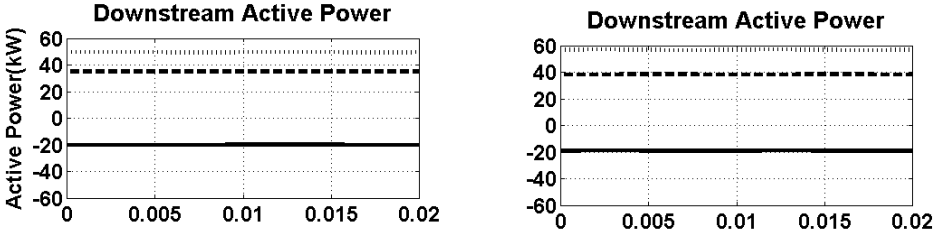

(f)

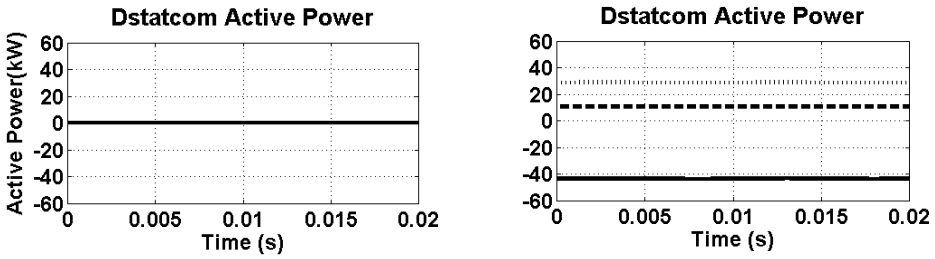

Fig. 5.8 Steady state simulation results before DSTATCOM connection (left column) and after DSTATCOM connection (right column). (solid line: Phase-A, dashed line: Phase-B, dotted line: Phase-C)

5.5.2 Dynamic results

Now, let us consider the network of Fig. 5.1. Community-1 is assumed with the same operation modes and load changes as in section 5.3. The only difference is that, CB_2 and CB_3 open simultaneously at t = 1 s; hence the distribution transformer is isolated from its downstream side, too.

First, let us assume that a three-phase DSTATCOM, with a common dc bus, is connected in the secondary side of the distribution transformer. The simulation results are shown in Fig. 5.9. The active power flow in the distribution transformer primary and secondary sides, are shown in Fig. 5.9a and Fig. 5.9b. The active power output of the DSTATCOM is shown in Fig. 5.9c.

For t > 1 s, during the off-grid mode of operation, phase-A is highly loaded while it has less generation capacity. This difference between its generation and demand level is supported by the DERs in other phases, through the DSTATCOM. This interphase power circulation level is different at the considered time periods (Fig. 5.9c) and depends on the network load and DERs generation. It is to be noted that DSTATCOM consumes approximately 3 kW to compensate its losses.

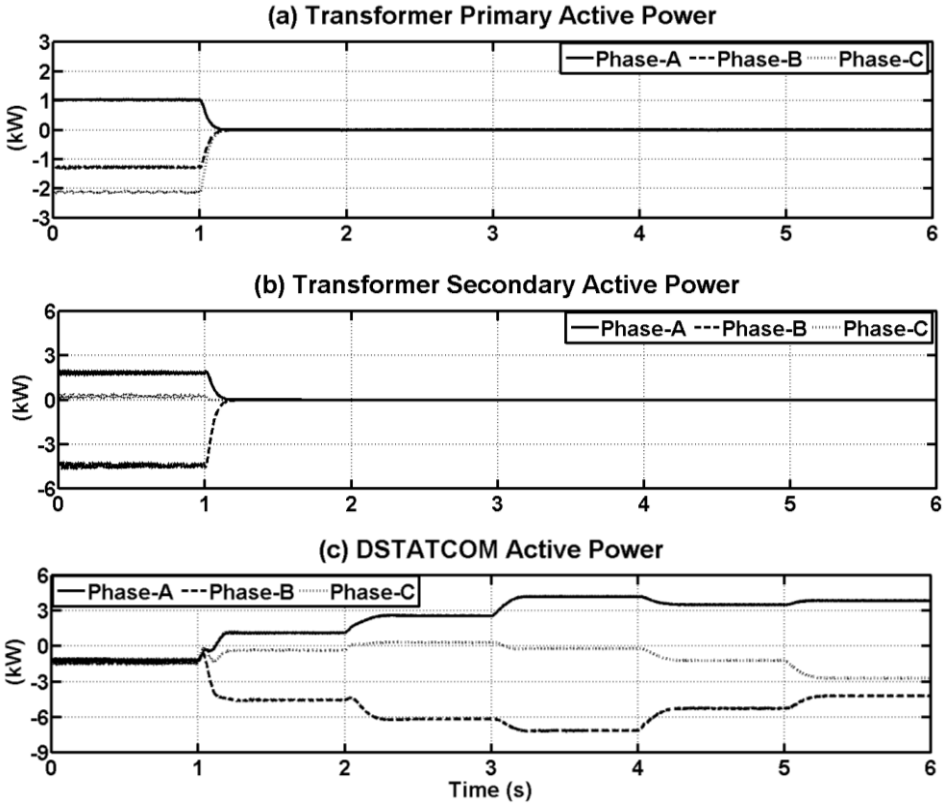

Fig. 5.9 Simulation results for House Community-1when the three-phase DSTATCOM is equipped with a common dc bus,

Now, let us assume a three-phase DSTATCOM, composed of three single-phase DSTATCOMs with separate dc buses, is connected in the secondary side of the distribution transformer. The simulation results are shown in Fig. 5.10. The active power supplied by the grid and the active power generation of the single-phase DERs is shown in Fig. 5.10a. The network frequency is shown in Fig. 5.10b.

Due to separate dc buses, the DSTATCOM cannot support interphase power circulation. Hence, in off-grid mode, the network becomes three unrelated single-phase networks, and the DERs in each network contribute only to the loads in that network (Fig. 5.10a). As a result a different frequency observed in each phase (Fig. 5.10b).

In such a condition, the frequency of a phase drops if the DERs connected to that phase generate more than their rated capacities. As an example, at $1 < t < 2$ s phase-A has 5 kW of demand whereas the rated capacity of DER-4, connected to this phase, is 3.3 kW. Hence, DER-4 increases its output power to meet the demand (Fig. 5.10a) while reducing the network frequency to 49.4 Hz (Fig. 5.10b). In contrast, the frequency rises if DERs generate less than their rated capacities. As an example, at 1

< t < 2 s phase-B has 9.9 kW of rated generation due to DER-1 and 2 connected to this phase, whereas it demand is 5 kW. Hence, DER-1 and 2 reduce their output power to meet the load demand in that phase (Fig. 5.10a); hence, the network frequency increases to 50.5 Hz (Fig. 5.10b). The frequency variation will be more if the difference between DER generation and its rated capacity is larger. As an example, for t > 2 s phase-A is heavily loaded; hence, the network frequency in this phase drops below 49 Hz (Fig. 5.10b). If proper interphase power circulating mechanism is in place, this frequency drop could have been avoided.

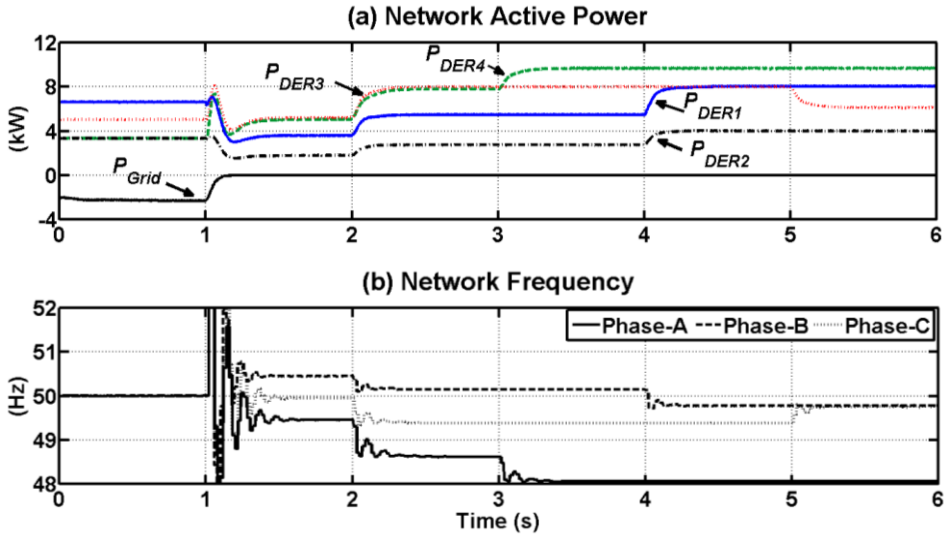

Fig. 5.10 Simulation results for House Community-1when the three-phase DSTATCOM is equipped with three separate dc buses,

This section discusses the performance of the microgrid when no power circulation takes place from one phase to another and hence three phases operate independently with its own generations. Since, no support is received from other phases; the heavily loaded phase (i.e. phase-A) experiences sever frequency drop to below the assumed acceptable level (i.e. 49 Hz in this study). Hence, if a proper load-shedding scheme is implemented; some loads will be disconnected from this phase. To verify the performance of the developed three-level load-shedding algorithm, discussed in section 2.2.4.4, the above case study is repeated assuming that the load-shedding algorithm is activated. It is assumed that each load-shedding level reduces approximately 20% of the network load in that phase. The simulation results are shown in Fig. 5.11. The network frequency is shown in Fig. 5.11a. The active power flow from the grid and the single-phase DERs is shown in Fig. 5.11b.

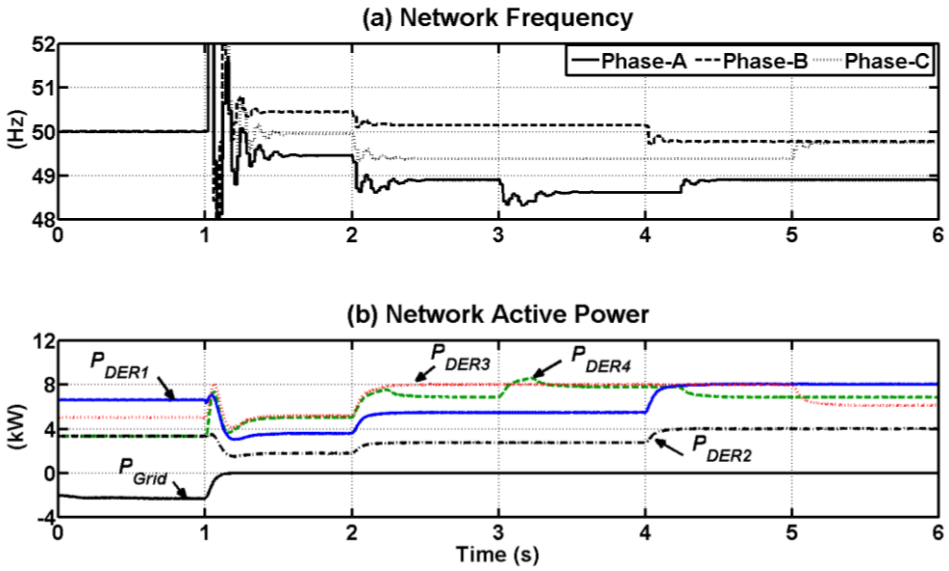

Fig. 5.11 Simulation results for House Community–1when the load shedding algorithm is active.

At t = 2 s, the frequency drops below 49 Hz in phase-A (Fig. 5.11a); hence, the load-shedding is initiated and disconnects the first set of loads in this phase at t = 2.2 s. As a result, the frequency is increased but still below 49 Hz. Therefore, at t = 3.2 s, the second set of load-shedding is applied. Similar to the previous time, since the frequency does not recover back to 49 Hz, the third and final set of load-shedding is applied at t = 4.2 s, which improves the frequency to the best possible value. The active power output from the DERs connected to phase-A is modified as the result of load-shedding in this phase (Fig. 5.11b). In phase-B and C, no load- shedding takes place since the frequency in these phases remains within the assumed acceptable range. The load shedding was applied as the interphase power circulation did not take place. Hence, the simulations in this case demonstrate the advantage of interphase power circulation for microgrids with single-phase DERs, distributed unequally among the three phases.

5.6 Power circulation by DSTATCOM in medium voltage feeder

Let us consider the medium voltage feeder of Fig. 5.2b with unbalanced loads where a DSTATCOM, with the topology shown in Fig. 2.4, is installed and controlled based on voltage control strategy. The simulation results are shown in Fig.

5.12. Before the DSTATCOM connection, the upstream currents are unbalanced and equal to those at the downstream of the DSTATCOM (Fig. 5.12a,b-left). Similarly, the active power flow in each phase is different (Fig. 5.12d-left). However, no reverse power flow is observed in any of the phases. Hence, the DSTATCOM only has to facilitate a set of balanced currents in its upstream. After the DSTATCOM is connected to the feeder, its upstream currents are balanced (Fig. 5.12a-right) while its downstream remains unbalanced (Fig. 5.12b-right). Similarly, the active power flow in the DSTATCOM upstream becomes equal to 4 MW in all phases (Fig. 5.12d-right) while those in the downstream side remain unbalanced (Fig. 5.12e-right). The output currents and active power flow from the DSTATCOM are shown in Fig. 5.12c,f-right.

Now, let us consider utilizing a DSTATCOM, with the topology shown in Fig. 5.4, in the medium voltage network of case-4, operating in voltage control strategy. In this configuration, the filter capacitor has a low voltage rating. Before DSTATCOM connection, the currents in DSTATCOM upstream are unbalanced (Fig. 5.13a-left). After the DSTATCOM connection, the actual and reference values of voltage across the filter capacitor are shown together in Fig. 5.13b-left and the tracking error is shown Fig. 5.13b-right. From this figure, it can be seen that the tracking error of the controller is about 8 V peak to peak. However, the upstream current is not balanced (Fig. 5.13a-right), as discussed earlier in section 5.2.2.2. Hence, for this configuration of DSTATCOM, voltage control strategy fails.

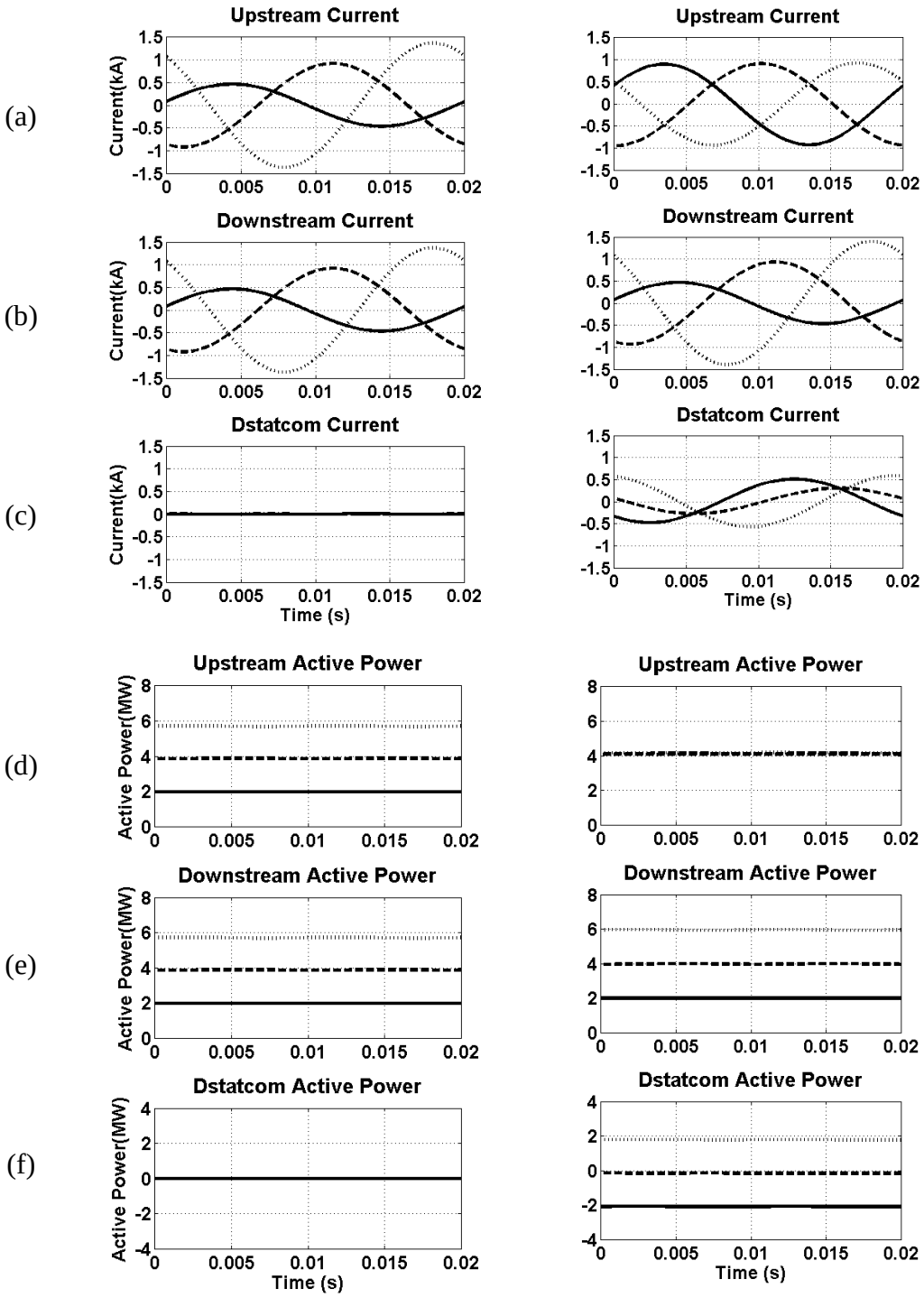

Fig. 5.12 Simulation results before DSTATCOM connection (left column) and after DSTATCOM connection (right column). (solid line: Phase-A, dashed line: Phase-B, dotted line: Phase-C).

(a)

(b)

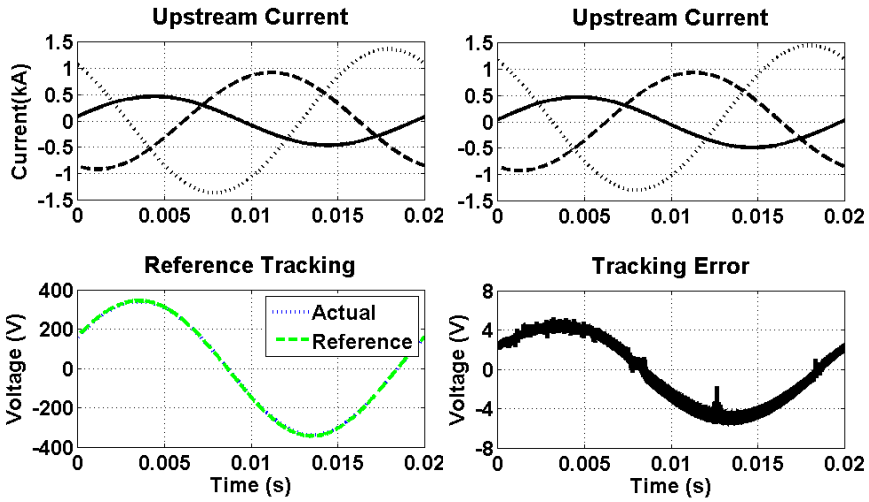

Fig. 5.13 Simulation results:

Top row: Upstream current before DSTATCOM connection (left) and after its connection (right) (solid line: Phase-A, dashed line: Phase-B, dotted line: Phase-C),

Bottom row: DSTATCOM output voltage and its reference (left),DSTATCOM output voltage tracking error (right)

Now, let us consider the network and DSTATCOM of Fig. 5.4, where a current control strategy, as discussed in section 5.2.2.2 is utilized instead of the voltage control strategy. The simulation results are shown in Fig. 5.14.

As it can be seen from the results, before the DSTATCOM connection, the currents at the upstream and downstream of the DSTATCOM are unbalanced (Fig. 5.14a,b-left). The active power flow is 2.8, 2.3 and 1.5 MW respectively in phase-A, B and C (Fig. 5.14d-left). After the DSTATCOM connection, the upstream current becomes balanced (Fig. 5.14a-left) and the active power becomes 2.3 MW in all phases (Fig. 5.14d-right). This is achieved as the DSTATCOM absorbs 1.18 MW from phase-C and injects 1.16 MW to phase-A while it has no power exchange with phase-B (Fig. 5.14f-right). In this case, the DSTATCOM has a loss of 20 kW, since it is connected to a medium voltage feeder.

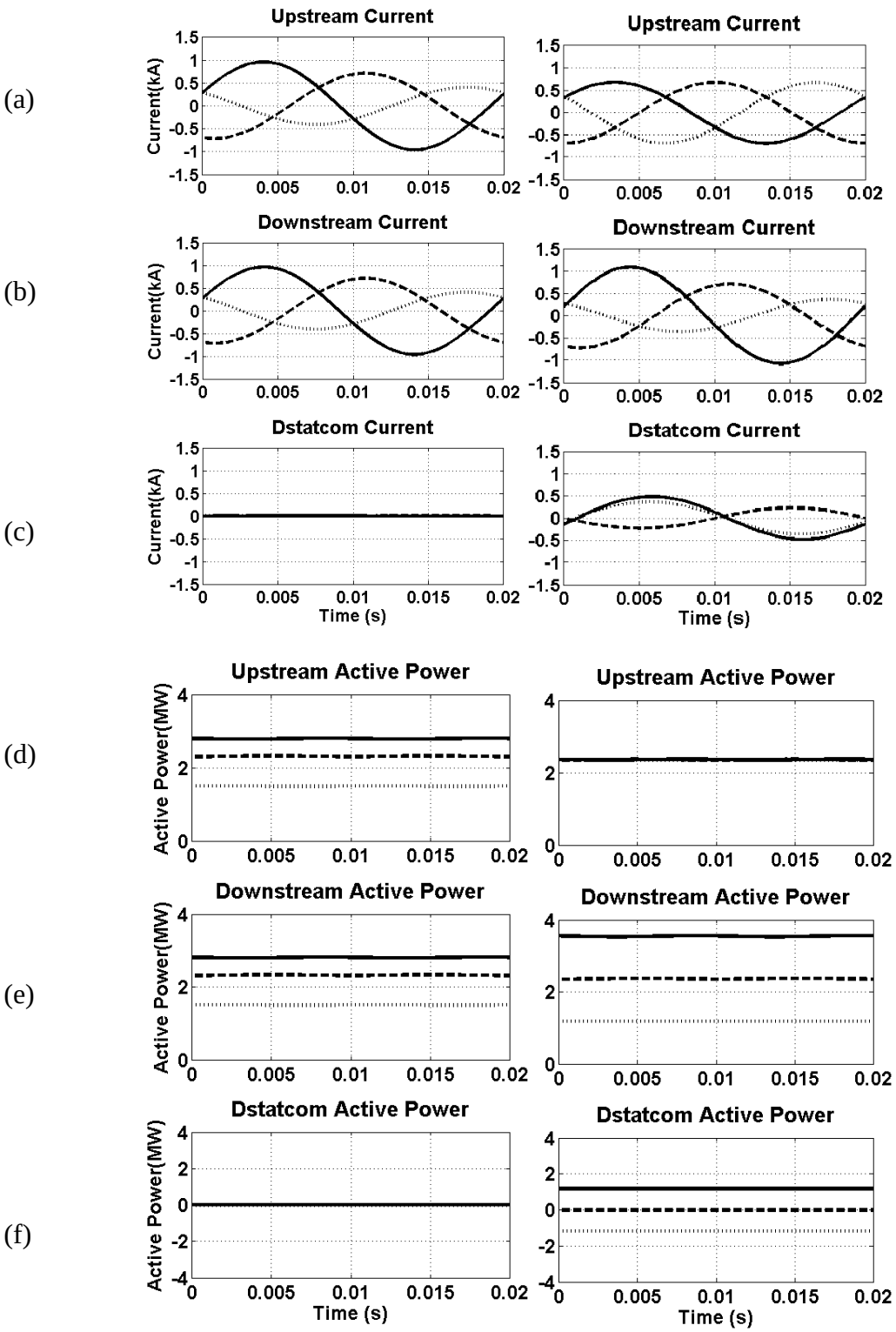

Fig. 5.14 Simulation results before DSTATCOM connection (left column) and after DSTATCOM connection (right column). (solid line: Phase-A, dashed line: Phase-B, dotted line: Phase-C).

5.7 Presence of different types of DERs in microgrid

A typical microgrid may consist of both voltage controlled and current controlled single phase and three phase DER converters. Another study case is carried out to investigate the feasibility of utilizing the proposed and developed control algorithm for single-phase DERs in a microgrid where different types of DERs exist.

A new group of residential neighboring houses are considered to form another house community, namely community-2, as shown in Fig. 5.15. It is assumed that seven houses in com munity-2 are equipped with DERs, where four of them are single-phase voltage-controlled, two are single-phase current-controlled and one is three-phase voltage-controlled. All the DERs are assumed to have energy storages with sufficient capacity. As before, a low voltage DSTATCOM is assumed to be installed at the secondary side of the distribution transformer.

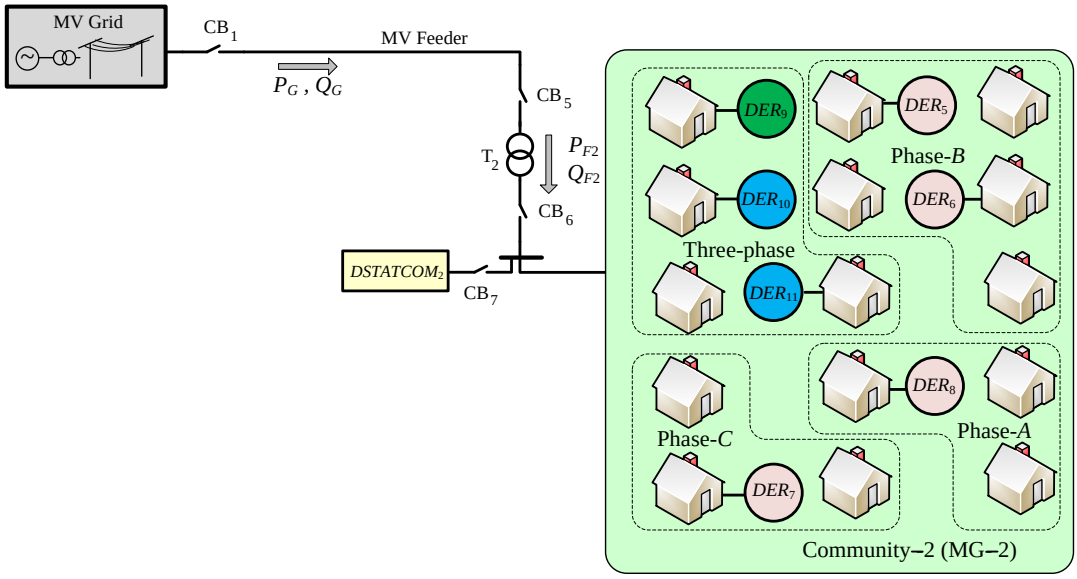

Fig. 5.15 Structure of the community-2 under consideration with different types of DERs.

The network is assumed to be grid-connected and in steady-state condition at t = 0. At t = 1 s, circuit breaker CB_5 opens and the microgrid falls into off-grid mode. At t = 2 s, DER-10 and 11 increase their output power respectively by 100% (i.e. 2 kW) and 60% (i.e. 2 kW). At t = 3 s, DER-10 reduces its output power by 85% (i.e. 3.4 kW) while DER-11 increases its output power by 40% (i.e. 2 kW). At t = 4 s, DER-10 and 11 output changes back to the same values as at $0 < t < 2$ s.

The simulation results are shown in Fig. 5.16. The active power generations of voltage-controlled and current-controlled DERs are shown in Fig. 5.16a and Fig. 5.16b. The network frequency is shown in Fig. 5.16c.

For t < 1 s, community-2 is operating in grid-connected mode and the DERs generate their rated power (Fig. 5.16a-b) and the grid supplies the rest of the network load demand (i.e. 16 kW or 36%) and the network frequency is 50 Hz (Fig. 5.16c). The output power of current-controlled DERs remains the same after the grid is disconnected at t = 1 s; hence, the voltage-controlled DERs increase their output power to share the loads. Hence, the network frequency drops to 49.4 Hz (Fig. 5.16c). As the output power of current-controlled DERs are varied during t > 1 s, the voltage-controlled DERs, update their output power accordingly to match the local load demand. Therefore, it can be seen that the single-phase voltage-controlled DERs, arbitrarily located among the three phases, can operate collaboratively with the other types of DERs in the microgrid by sharing the network load and regulating the network frequency based on the assigned droop control.

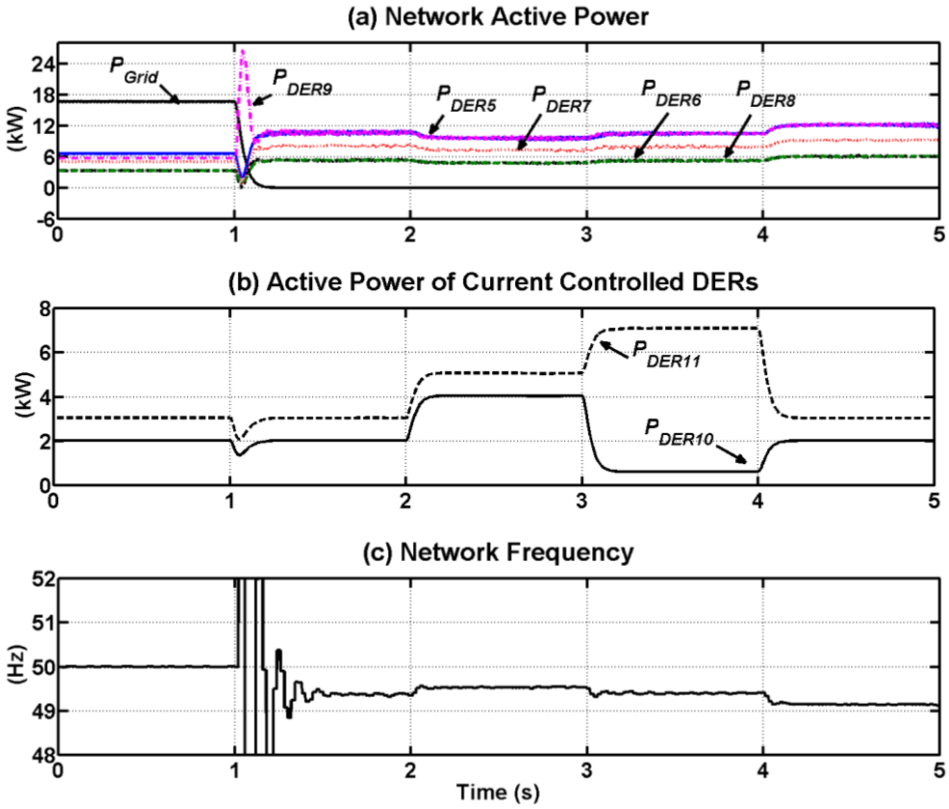

Fig. 5.16 Simulation results for community-2 in case-5:

5.8 Interconnection of neighboring microgrids with single phase DERs

The concept of interconnecting two off-grid neighboring microgrids is proposed in Chapter 4 to improve the network reliability and reduce load-shedding probability in self-healing networks. Based on the proposed concept, the single-phase DERs not only can share the loads in the other phases in the same microgrid, but they can also share the loads in any phase of a neighboring microgrid, if these two off-grid microgrids are interconnected together. Another case study is carried out to investigate the feasibility of such operations.

Let us consider the network of Fig. 5.17, with both of the house community 1 and 2. Both communities are assumed to have the same demand of 15 kW. Community-1 is assumed to have only single-phase DERs with a total generation capacity of 18.2 kW. In order to build up a worst case scenario, it is assumed that community-2 has only single-phase DERs (i.e. DER-5 and 7 discussed in section 5.7) with a total generation capacity of 11.6 kW.

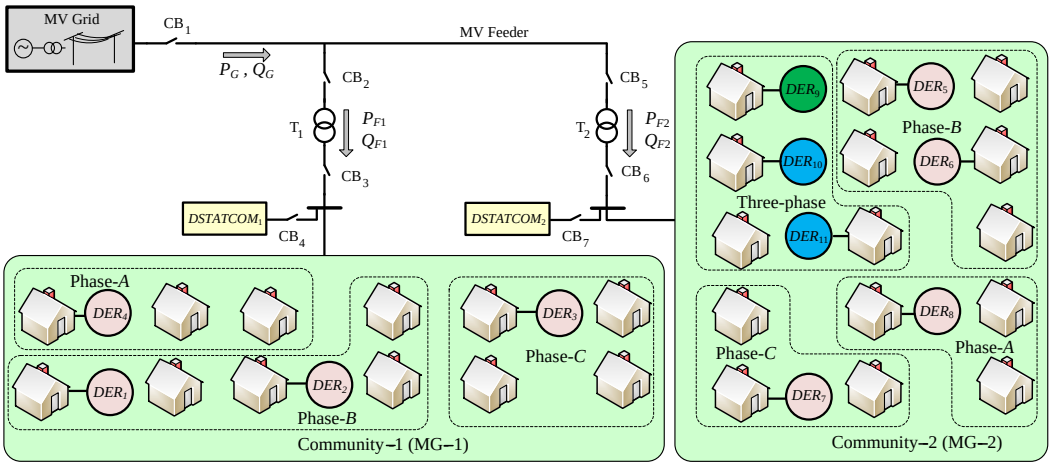

Fig. 5.17 Structure of the interconnected microgrid under consideration.

The network is assumed to be grid-connected and in steady-state condition at t = 0. At t = 0.8 s, circuit breakers CB_1, CB_2 and CB_5 open and both of the microgrids fall into off-grid mode. At t = 2 s, the resynchronization between the two microgrids is activated and at t = 2.9 s, they are synchronized and interconnect together by closing CB_2 and CB_5. At t = 4 s, a single-phase load of 4 kW is added to phase-B in community-2. At t = 5 s, another single-phase load of 2 kW is connected to phase-A in community-2.

The simulation results are shown in Fig. 5.18. The active power flow from the grid to each microgrid is shown in Fig. 5.18a. The active power flow supplied by the grid and the power generation by single-phase DERs are shown in Fig. 5.18b. Fig. 5.18c shows the total active power generation by the DERs in each microgrid. Fig. 5.18d-g show the active power flow in primary and secondary sides of the two distribution transformers, supplying the two microgrids. The network frequency in each microgrid is shown in Fig. 5.18h.

For $t < 0.8$ s, the microgrids operate in grid-connected mode and MG-1 exports 2.4 kW surplus of its DERs generation to the grid, while MG-2 imports 4.5 kW from the grid (Fig. 5.18a). Due to single-phase loads and DERs in each microgrid, different levels of power import/export is observed in the primary and secondary side of the distribution transformers in each phase (Fig. 5.18d-g) and the network frequency remains at 50 Hz (Fig. 5.18h).

At $0.8 < t < 2.9$ s, both microgrids are isolated from the grid and there is no power exchange with the grid (Fig. 5.18a). Hence, both microgrids operate in off-grid mode independently and the DERs in MG-1 reduce their power generation to match the local demand while the DERs in MG-2 increase their generation to meet their local demand (Fig. 5.18b). As a result, the DERs with the same rating in the two microgrids have different outputs (Fig. 5.18b). In this period, the single-phase DERs in each microgrid support the local loads based on the interphase power circulation through their distribution transformers (Fig. 5.18e,g). The two microgrids operate in two different frequencies in this period (Fig. 5.18h).

For $t > 2.9$ s, the two off-grid microgrids are interconnected based on the concept proposed in Chapter 4. In this period, the total load in the system of interconnected microgrids is shared by all the DERs in both microgrids. Therefore, a portion of the loads in MG-2 are supplied by the DERs located in MG-1; MG-1 exports approximately 4 kW to MG-2 (Fig. 5.18a). In addition, the DERs with the same rating in two microgrids have the same outputs, as desired by the power sharing ratio (Fig. 5.18b). Again, due to the different levels of demand and generation in each phase, different levels of power flow is observed in the primary and secondary sides of the distribution transformers (Fig. 5.18d-g). Both microgrids operate in the same frequency in this period (Fig. 5.18h).

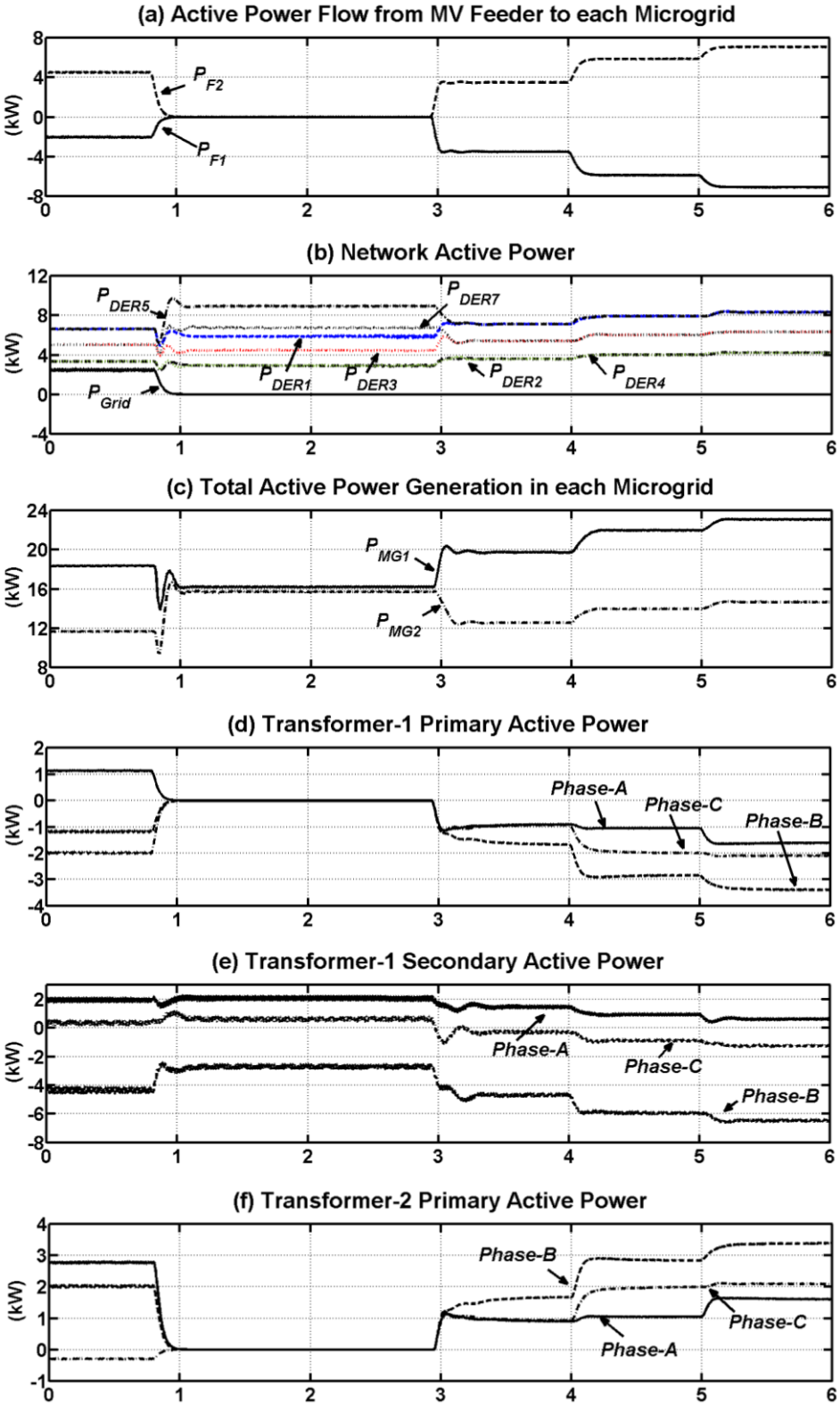
(a) Active Power Flow from MV Feeder to each Microgrid
(kW)
P_{F2}
P_{F1}
(b) Network Active Power
(kW)
P_{DER5}
P_{DER7}
P_{DER1}
P_{DER3}
P_{DER2}
P_{DER4}
P_{Grid}
(c) Total Active Power Generation in each Microgrid
(kW)
P_{MG1}
P_{MG2}
(d) Transformer-1 Primary Active Power
(kW)
Phase-A
Phase-C
Phase-B
(e) Transformer-1 Secondary Active Power
(kW)
Phase-A
Phase-C
Phase-B
(f) Transformer-2 Primary Active Power
(kW)
Phase-B
Phase-C
Phase-A

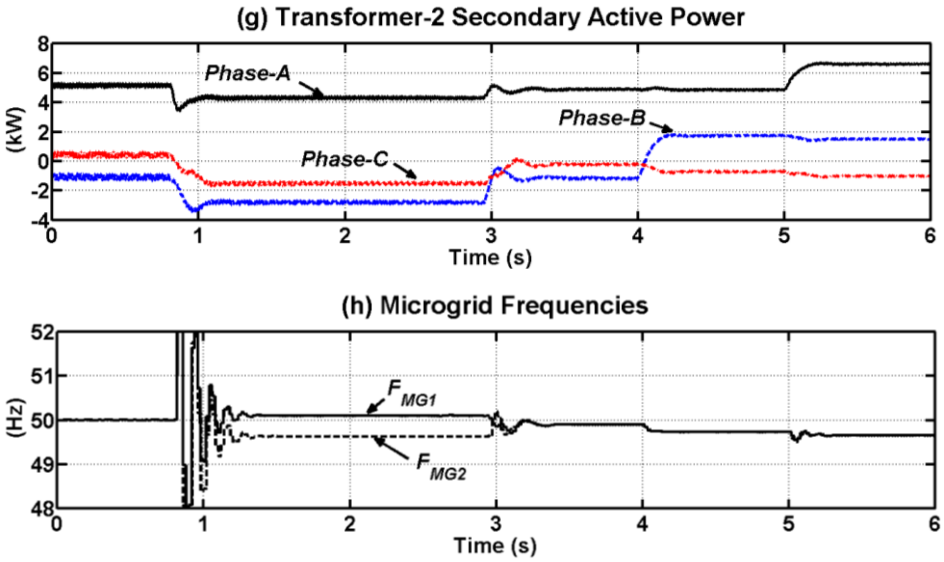

Fig. 5.18 Simulation results for community-1 and 2 in case-6:

5.9 Summary

In this chapter, the successful dynamic operation and control of a microgrid with single-phase DERs with different capacities, distributed randomly among the three phases of the network are demonstrated. The single-phase DERs are converter-interfaced and operated in voltage-control mode. The primary and secondary level controls proposed in Chapter 2 are employed for the single-phase DERs, too. It is shown that the excess generated power can be circulated successfully from one phase to the other phases(s) via the distribution transformer. For this purpose, the transformer needs to have a delta-wye connection (which is the normal case in distribution networks). Alternatively, the power circulation can be achieved by the help of a DSTATCOM installed on the low voltage or medium voltage feeder. Different topologies and control algorithms are proposed for the DSTATCOM when installed in the medium voltage feeder and in the low voltage feeder.

Chapter 6 AC-DC Hybrid Microgrid

In this chapter, the operation and control of a hybrid ac-dc microgrid is presented. The microgrid constitutes an ac bus interconnected to a dc bus via a tie-converter (TC). The DERs located in both buses operate in different modes of operation based on the grid availability and the conduction status of the TC. The objective of the TC is to maintain the dc bus voltage and ac bus voltage during the off-grid mode of operation of the ac-dc microgrid by controlling the active and reactive power flow through the TC. Several case studies are conducted in PSCAD/EMTDC to verify the proper operation of the hybrid ac-dc microgrid in different modes of operation.

6.1 AC-DC microgrid network

The hybrid ac-dc microgrid structure consists of an ac bus and a dc bus. All the ac loads and DERs within the microgrid are connected to the ac bus. Similarly, all dc loads and DERs are connected to the dc bus. A TC is used for interconnecting the ac bus and dc bus together. The ac bus is connected to grid through a circuit breaker and a three-phase transformer.

In this study, the ac bus is assumed to be a three-phase 400 V system, supplied by a 30 kVA, three-phase transformer. The dc bus is assumed to be a 350 V dc system. Two power-electronic interfaced ac DERs are assumed to be connected to the ac bus and two power-electronic interfaced dc DERs are assumed to be connected to the dc bus.

The introduced hybrid microgrid system should be able to operate successfully in the following modes of operation, as shown schematically in Fig. 6.1:

- Mode-1: Isolated ac and dc buses with the ac bus isolated from the grid,
- Mode-2: Isolated ac and dc buses with the ac bus connected to the grid,
- Mode-3: Interconnected ac and dc buses with the ac bus isolated from grid,

- Mode-4: Interconnected ac and dc buses with the ac bus connected to grid.

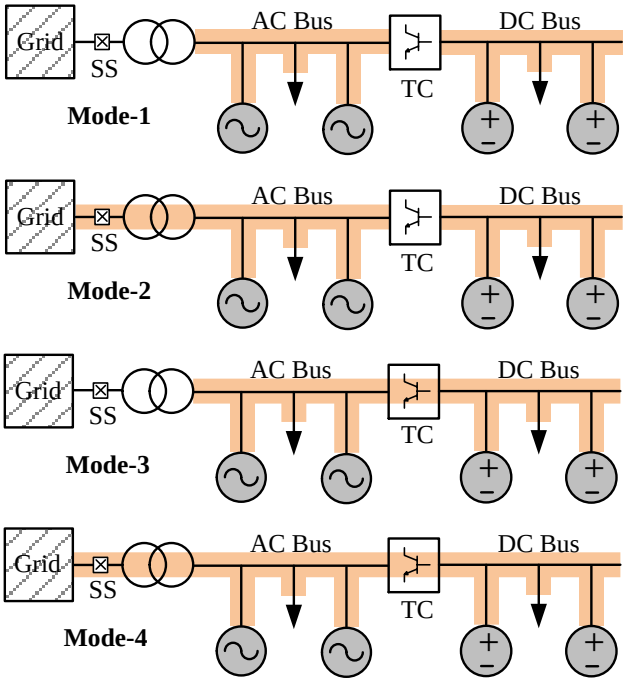

Fig. 6.1 Hybrid ac-dc microgrid system in different modes of operation.

The ac microgrid concept and control is discussed in Chapter 2 The dc microgrid is formed by a group of dc DERs and loads, connected to the same dc bus. Each DER is connected to the dc bus through a dc-dc converter. For an energy storage-based DER, a bidirectional converter is required to provide bidirectional power flow between the storage and the dc bus. For other dc DERs, a unidirectional dc-dc converter can be employed. In this study, boost converters are used for connecting the DERs to the dc bus (Fig. 6.2). The inductor and capacitor are designed to reduce the current and voltage ripples. It is to be noted that the state of charge of the batteries are not considered in this research. It has been assumed that the batteries are charged and available when needed. They are fully charged during the off-peak hours.

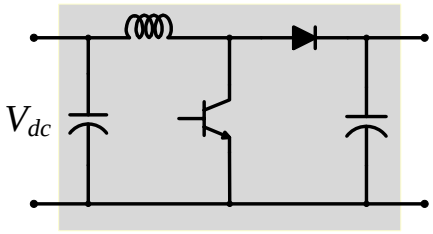

Fig. 6.2 Power electronic interface for DERs connected to dc buses.

6.2 Operation and control of the dc microgrid

The dc microgrid control consists of several modules, namely TC conduction status monitoring, Output power control and Converter switching control modules, as described below.

6.2.1 TC conduction status monitoring module

In this study, the dc microgrid islanding detection is based on monitoring the status of the TC and the assumption of the communication infrastructure availability, to transfer this information to the dc DERs. Note that no resynchronization is required for connecting the DERs to the dc bus.

6.2.2 Output power control module

Depending on the status of the TC, the DERs in the dc bus operate in two different modes:

- If the TC is on (i.e. conducting), the DERs are controlled in constant P mode and hence, the dc bus voltage is regulated by controlling the bidirectional power flow over the TC.
- If the TC is off (i.e. non-conducting), the DERs are operated in voltage control mode, based on droop. In this case, the voltage of each DER converter is varied based on the droop control, and pre-defined droop coefficients (m'), to regulate the dc bus voltage within the acceptable limits, while sharing the loads of the dc bus with the specified ratio. Hence, the output power of a converter (P) is measured and used to derive the reference for converter output voltage as [70]

$$V_{dc} = V_{dc,rated} - m'\left(P_{dc,rated} - P_{dc}\right) \tag{6.1}$$

where the suffix *dc* shows droop among DERs in the dc bus.

The block diagram of the control system for the converters of the DERs, connected to the dc bus, is shown in Fig. 6.3.

Note that the TC conduction status monitoring module issues a command to the reference selection block to select the proper reference.

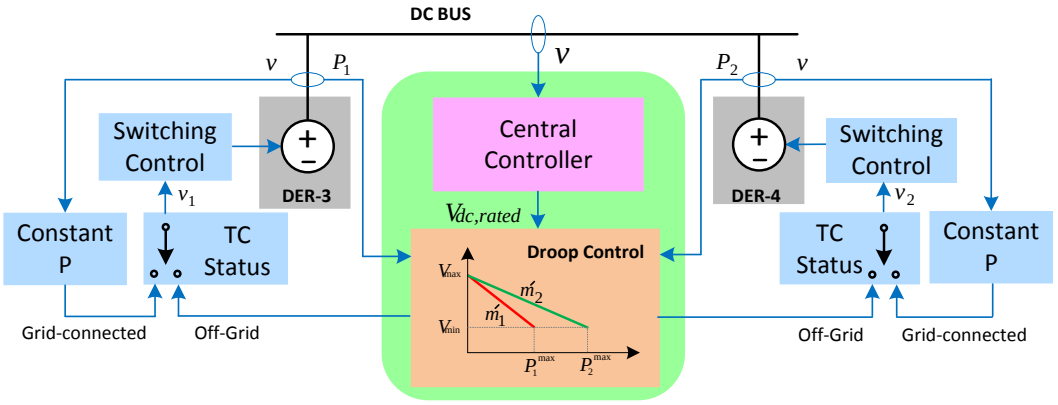

Fig. 6.3 Primary and secondary control levels of the considered dc microgrid system.

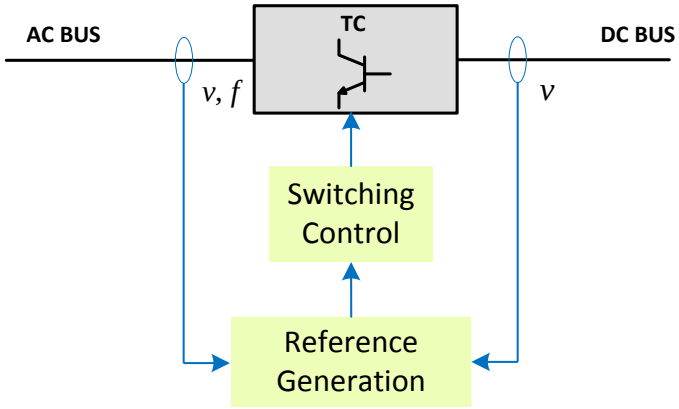

Fig. 6.4 Control schematic of the TC between the ac and dc buses in ac-dc hybrid microgrid system.

6.2.3 Converter switching control module

Converter switching control module is responsible for proper turn on and off of the IGBT in the boost converter, such that the desired reference voltage is generated across the dc capacitor. In this study, a closed-loop PI based pulse width modulation (PWM) technique is used to generate the IGBT switching function, u. Assuming a bipolar switching for the IGBTs, u_{dc} takes ±1 which will subsequently turn on and off the IGBT in the boost converter.

The switching function for the IGBT in the boost converter, u_{dc}, is generated by the help of PWM technique and using a feedback over the converter output voltage and current [104]. The block diagram of the closed-loop switching control system is shown in Fig. 6.5.

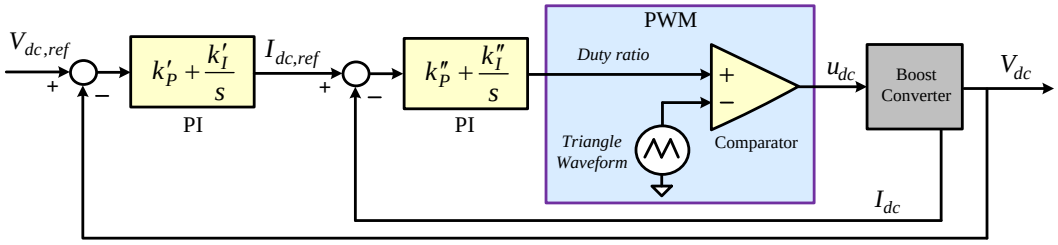

Fig. 6.5 Closed-loop switching control block diagram for dc DER converters.

6.3 Dynamic operation results of ac-dc microgrid

In order to investigate the performance of the proposed hybrid ac-dc microgrid, with the developed control strategies, the operation modes 1-4 are studied. The parameters of network, DER converters and filters, loads, TC and droop and controller coefficients are given in Table 6.1.

Table 6.1 Parameters of network, DER converters, filters and TC. controller coefficients for Fig. 6.1

MV Network	11 kVrms L-L, 50 Hz
MV Line Impedance	R = 0.2 Ω, L =10 mH
Transformer	30 kVA, 11 / 0.4 kV, Dyn1, 50 Hz, Z_I = 5%
AC Bus	400 Vrms L-L
DC Bus	350 V
VSCs and Filters for DERs and TC	R_f = 0.1 Ω, L_f = 0.36 mH, C_f = 50 μF, V_{dc} = 350 V, a = 3, h = 10^{-4}, Ts = 10^{-6} s, k_1 = 2.4613, k_2 = 2.9606, k_P = 1 , k_I = 100

Table 6.2 DER converter droop controller coefficients for Fig. 6.1

DER	Bus	Rating [kW]	L_T [mH]	m [rad/kW]	n [V/kVAr]	$ṁ$ [V/kW]
DER-1	AC	2	2.72	3.1416	18	–
DER-2	AC	4	1.36	1.5708	9	–
DER-3	DC	1	–	–	–	35
DER-4	DC	2	–	–	–	17.5

6.3.1 Mode-1

The TC is assumed to be in non-conducting status; hence, the ac and dc bus are isolated while the ac bus is assumed to be isolated from the grid, too. Under such conditions, the DERs in each bus share the load of the relevant bus and the central controller regulates the ac and dc bus voltages in ± 10% range and the frequency of ac bus in ± 0.5 Hz range.

It is assumed that the network is initially in steady-state condition, with a total load demand of approximately 5 kW in the ac bus. At t = 1 s, this load is increased by 3 kW (i.e. 60%) and at t = 2 s, the network load is decreased by 4 kW (i.e. 50%). The output active and reactive power ratio among DER-1 and 2, connected to the ac bus, is maintained as 1:2, as assigned (Fig. 6.6a-b) for all load changes (Fig. 6.6c). The frequency variations in the ac bus are within the acceptable limits of ± 0.5 Hz (Fig. 6.6d). The ac bus rms voltage drops below the minimum acceptable limit of –10% after the load increase at t = 1 s (Fig. 6.6e). Assuming that the central controller has discrete time steps, as discussed in section 2.2, it applies an adjustment in the droop curve characteristic of the DERs at t = 1.5 s (i.e. the first monitoring time step of the central controller after t = 1 s). Hence, the rated voltage of the DERs is increased from 240 to 258 V (Fig. 6.6f); thereby, the ac bus voltage is restored to approximately 240 V. After load reduction at t = 2 s, the ac bus voltage rises but does not exceed the maximum limit; hence central controller does not take any further action.

Similarly, the DERs in the dc bus share the loads in this bus. It is assumed that the network is initially in steady-state condition, with a total load demand of 3 kW in the dc bus. At t = 1 s, this load is increased by another 3 kW (i.e. 100%) and at t = 2 s, the network load is decreased by 1 kW (i.e. 17%). The output active power ratio among DER-3 and 4, connected to the dc bus, is maintained as 1:2, as assigned (Fig. 6.7a) for all load changes (Fig. 6.7b). The dc bus voltage is kept within the acceptable ± 10% limit (Fig. 6.7c); hence no action is taken by the central controller.

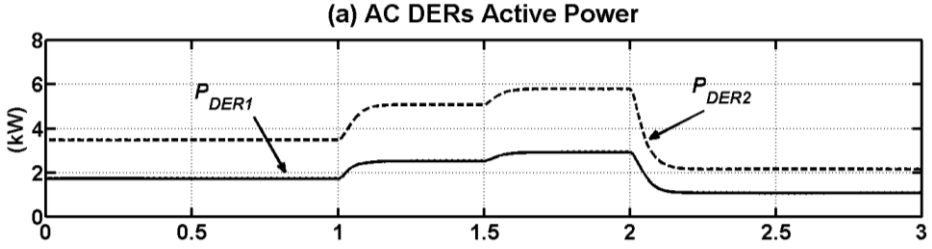

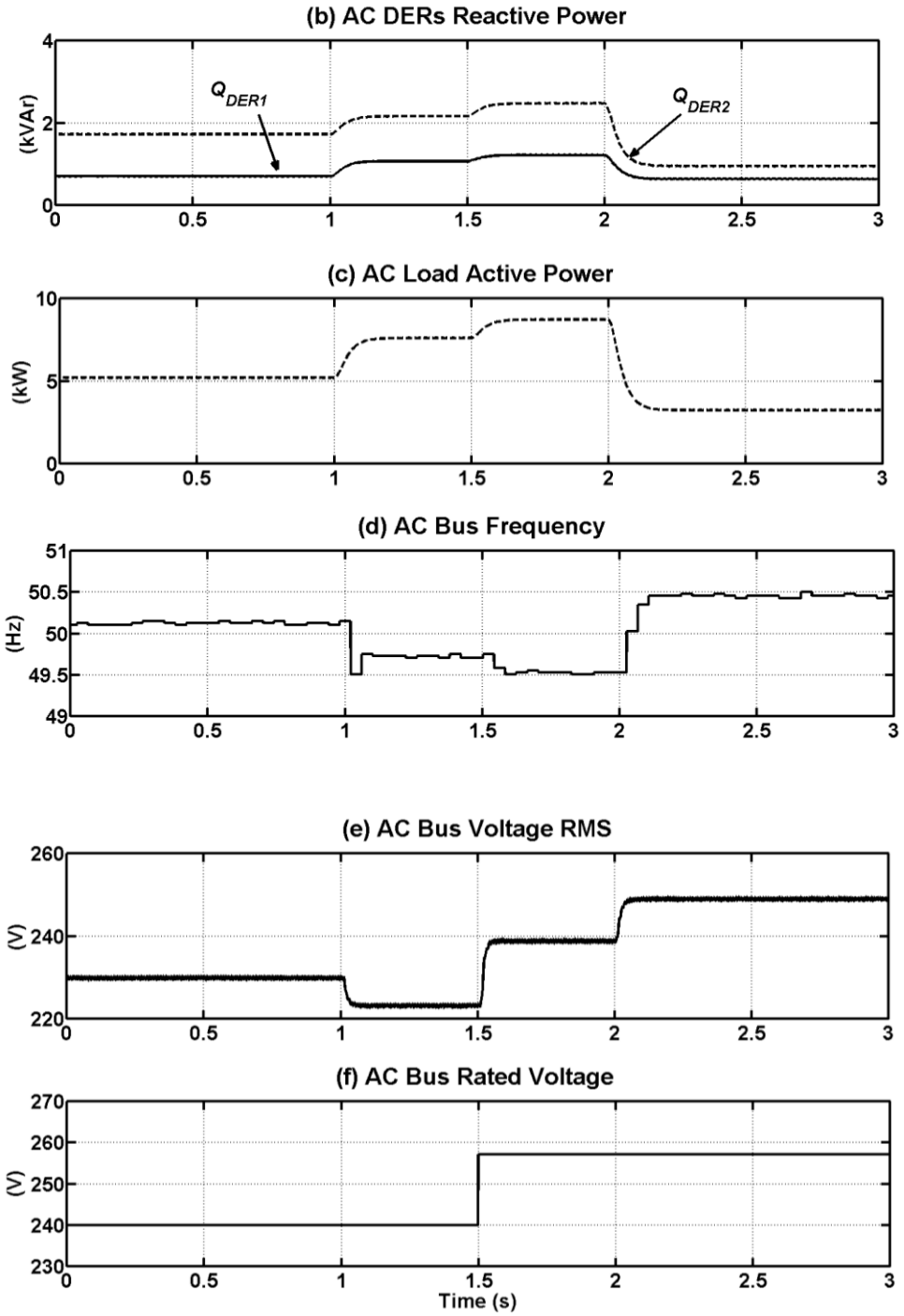

Fig. 6.6 Simulation results for the ac bus in Mode-1:

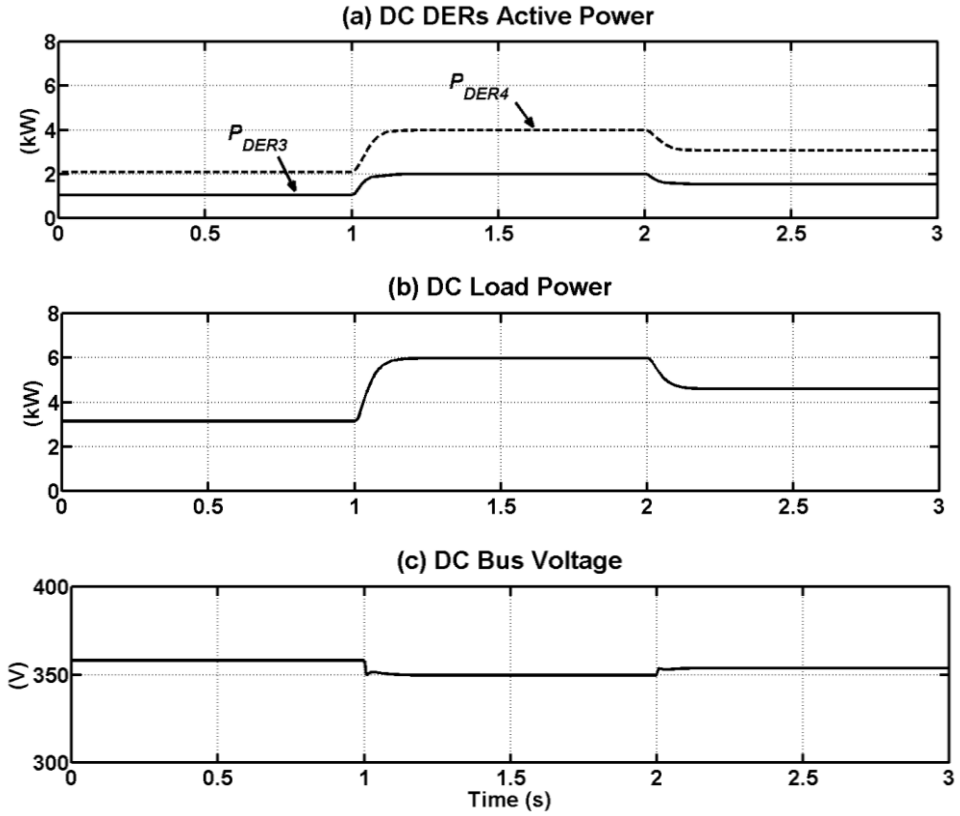

Fig. 6.7 Simulation results for the dc bus in Mode-1:

6.3.2 Mode-2

The TC is assumed to be in non-conducting status; hence the ac and dc bus are isolated while the ac bus is assumed to be connected to the grid. Under such conditions, the DERs in the ac bus operate in constant power mode, in their rated conditions, while the DERs in the dc bus operate in voltage control, based on droop, and the central controller regulates only the dc bus voltage.

It is assumed that the network is initially in steady-state condition, with a load demand of approximately 7 kW in the ac bus. At t = 1 s, this load is increased by 2 kW (i.e. 29%) and at t = 2 s, decreased by 6 kW (i.e. 66%). The output active and reactive power of DER-1 and 2, connected to the ac bus, is remained at the rated values, all the time (Fig. 6.8a-b). For t < 2 s, the grid supplies a portion of the load demand in the ac bus; however for t > 2 s, the ac bus exports power to the grid (Fig. 6.8a-b), depending on the variations of the load in the ac bus (Fig. 6.8c). The frequency of the ac bus is 50 Hz (Fig. 6.8d) and the ac bus rms voltage is remained unaffected (Fig. 6.8e). The performance of DERs in the dc bus is similar to the results shown in Fig. 6.7 and is not repeated here.

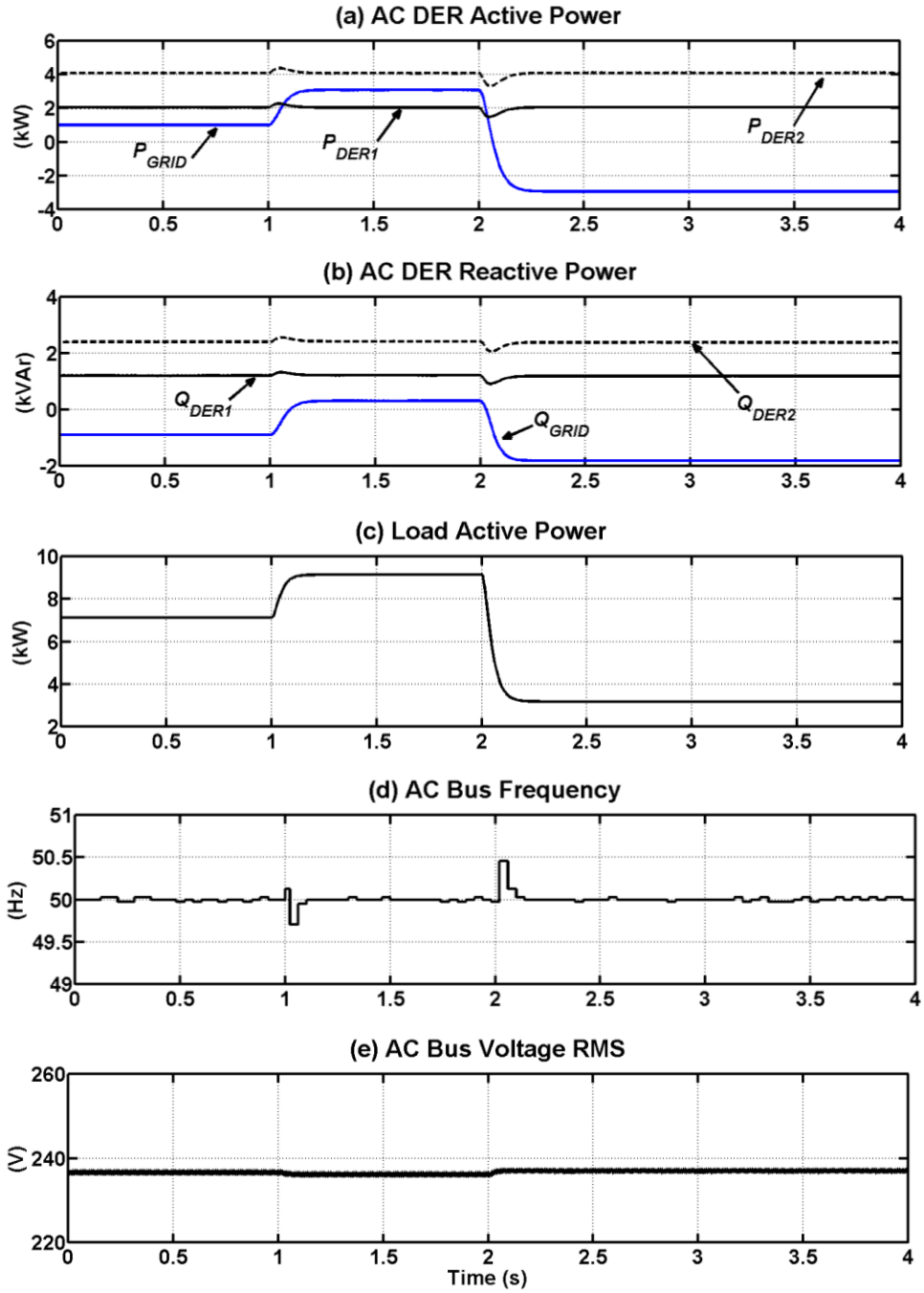

Fig. 6.8 Simulation results for the ac bus in Mode-2:

6.3.3 Mode-3

The TC is assumed to be in conducting status; hence the ac and dc bus are interconnected while the ac bus is assumed to be isolated from the grid. Under such conditions, the DERs in each bus share the load of the relevant bus and the TC regulates the voltage in both of the buses. In this case, the central controller operates as backup for the TC. The results are investigated for different scenarios, as below:

6.3.3.1 Load change in the ac bus

It is assumed that the network is initially in steady-state condition, with a load demand of approximately 6 kW in the ac bus. At t = 1 s, this load is increased by 2 kW (i.e. 33%) while the load connected to the dc bus is remained as before. The load change is contributed by DER-1 and 2, connected to the ac bus and the output active power ratio among them is maintained as 1:2 (Fig. 6.9a). DER-3 and DER-4, connected to the dc bus, do not contribute to the load change (Fig. 6.9b). For the ac bus load variation (Fig. 6.9c), the frequency and voltage variations in ac bus are within acceptable limits (Fig. 6.9d-e) and dc bus voltage is remained unaffected (Fig. 6.9f).

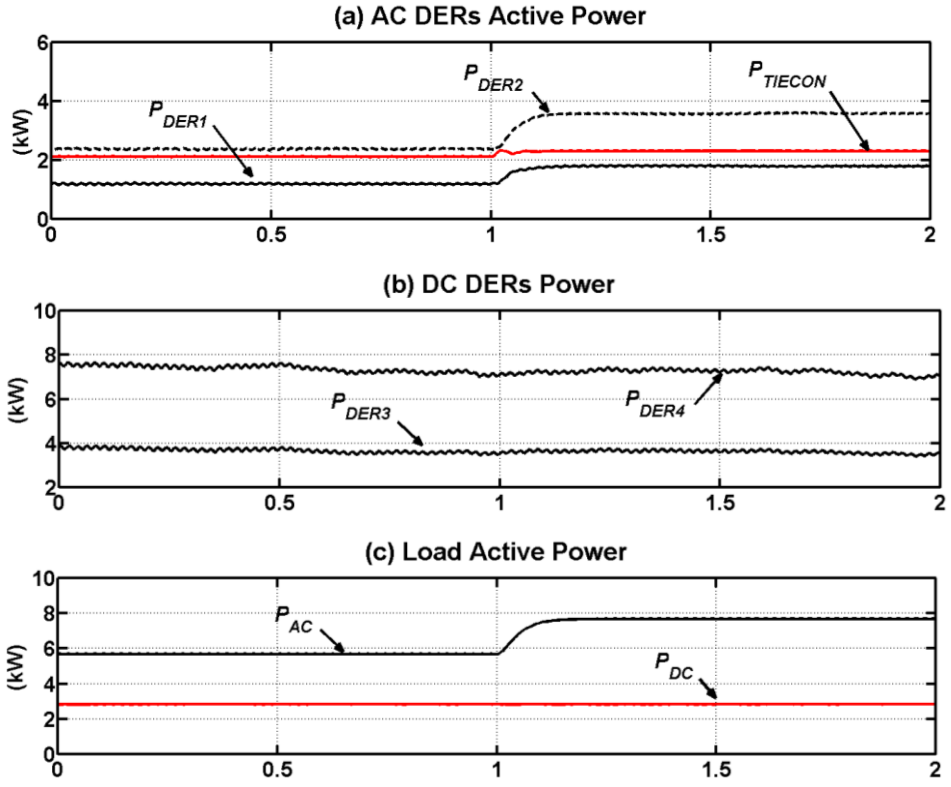

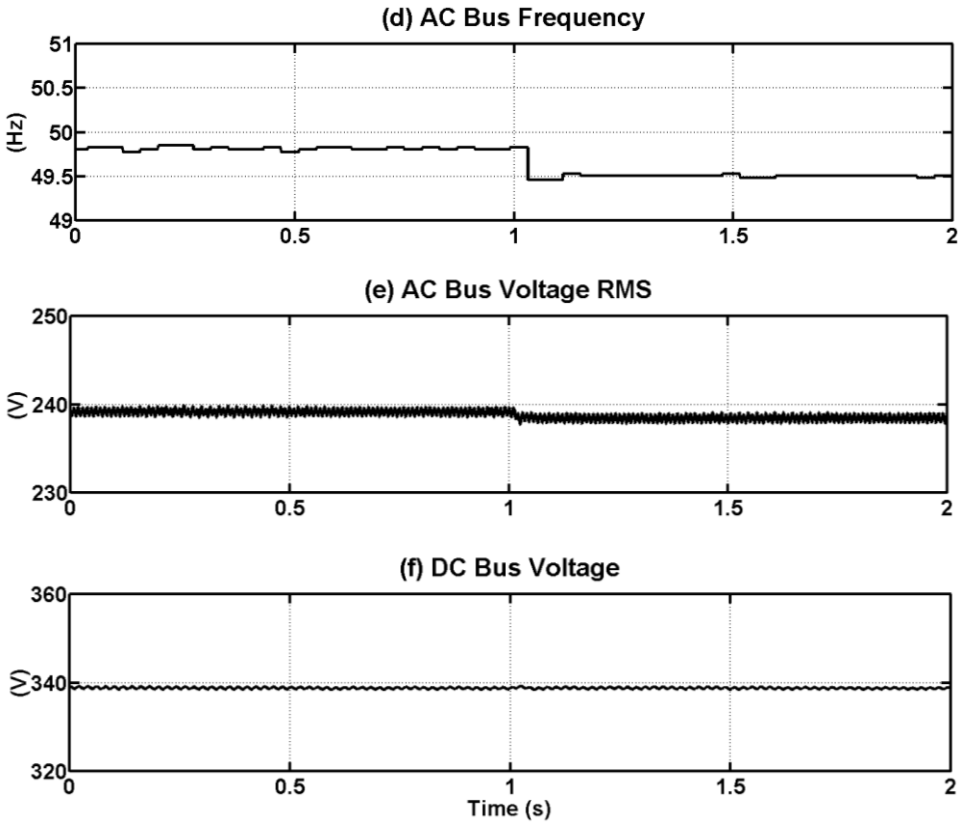

Fig. 6.9 Simulation results for the ac and dc bus in Mode-3, case 6.3.3.1:

6.3.3.2 Load change in the dc bus

The network of case 6.3.3.1 is considered, with a load demand of 3 kW in the dc bus. At t = 1 s, this load is increased by 3 kW (i.e. 100%). As the load change is in the dc bus, the output power of DER-1 and 2 is not affected (Fig. 6.10a); hence, the ac bus voltage and frequency will not be affected, too. DER-3 and DER-4, connected to the dc bus, contribute to the load change and the output active power ratio among them is maintained as 1:2 (Fig. 6.10b) for the load changes in the network (Fig. 6.10c).

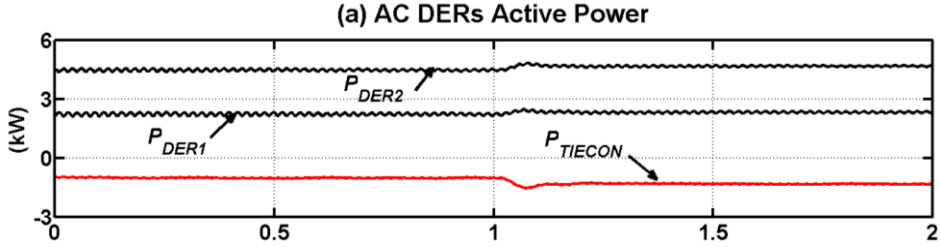

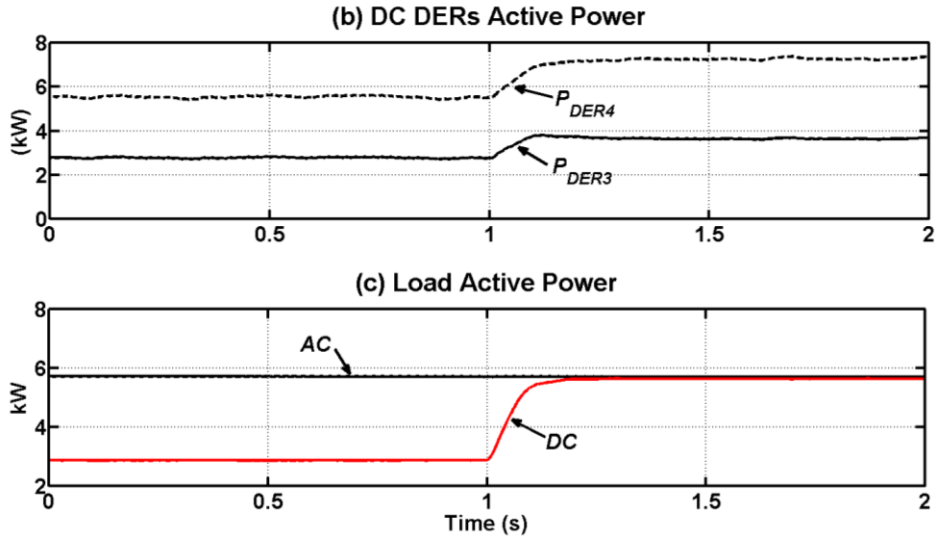

Fig. 6.10 Simulation results for the ac and dc bus in Mode-3, case 6.3.3.2:

6.3.3.3 AC bus DERs operating in maximum ratings

The network of case 6.3.3.1 is considered, where the DERs connected to the ac bus are assumed to be operating in their maximum ratings. In this condition, the ac bus load is approximately 6 kW where its 2 kW (33%) is supplied by the TC. At t = 1 s, the load in the ac bus is increased by another 2 kW (30%). The output active power of the DERs, connected to the ac bus, is remained unaffected (Fig. 6.11a). Hence, the DERs in the dc bus contribute to this extra load and the power transfer over the TC is increased by 2 kW (Fig. 6.11a). The output active power ratio among the DERs, connected to the dc bus, is maintained as 1:2 (Fig. 6.11b) to contribute to the load variations in the ac bus (Fig. 6.11c).

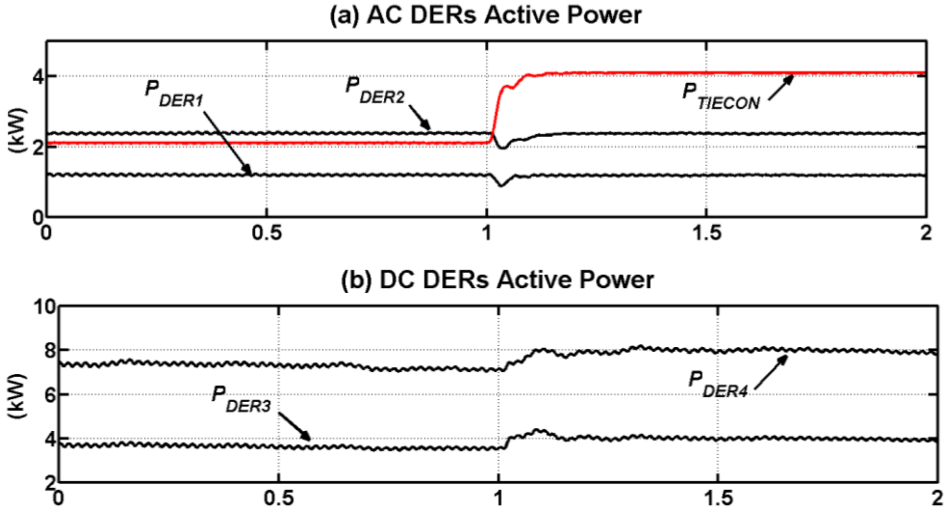

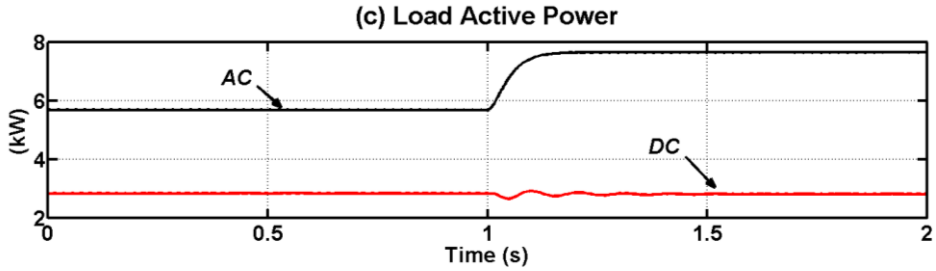

Fig. 6.11 Simulation results for the ac and dc bus in Mode-3, case 6.3.3.3:

6.3.3.4 DC bus DERs operating in maximum ratings

The network of case 6.3.3.2 is considered, where the DERs connected to the dc bus are assumed to be operating in their maximum ratings. In this condition, the dc bus load is 3 kW while the DERs, connected to this bus, are generating 6 kW. Therefore, the rest of the generated power is taken by the TC. However, only 1 kW is delivered to the ac bus (Fig. 6.12a), due to the power losses in the TC, which is approximately 5 kW. At t = 1 s, the load in the dc bus is increased by another 3 kW (i.e. 100%). Hence, the DERs in the ac bus contribute to this extra load and the power transfer over the tie-converter is increased by 3 kW (Fig. 6.12a). The output active power ratio among the DERs, connected to the ac bus, is maintained as 1:2 (Fig. 6.12a) while the output active power of the DERs, connected to the dc bus, is remained same as before (Fig. 6.12b) for the load variations in the network (Fig. 6.12c).

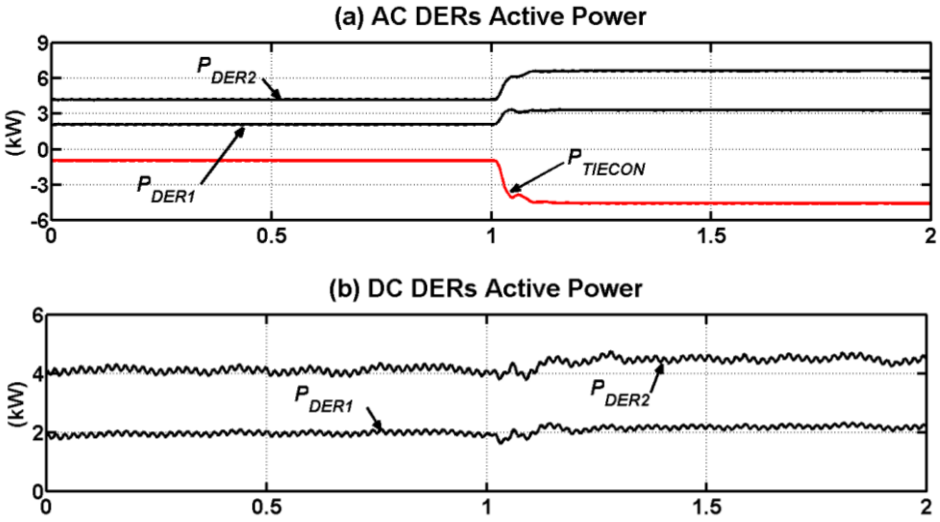

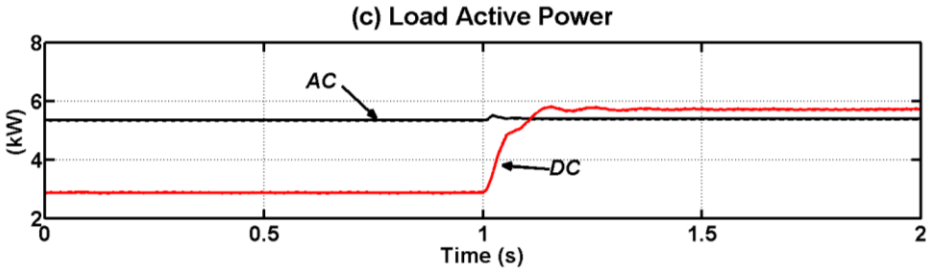

Fig. 6.12 Simulation results for the ac and dc bus in Mode-3, case 6.3.3.4:

6.3.4 Mode-4

The TC is assumed to be in conducting status; hence, the ac and dc buses are interconnected while the ac bus is assumed to be connected to the grid. Under such conditions, the DERs in the ac bus operate in constant power mode and the DERs in the dc bus operate in constant P mode. The extra power required by the loads or the surplus of the generated power by the DERs is exchanged by the grid.

It is assumed that the network is initially in steady-state condition, with a load demand of 4 kW in the ac bus and 1 kW in the dc bus. At t = 1 s, a load increase of 6 kW (i.e. 150%) is applied in the ac bus and at t = 2 s, a load increase of 5 kW (i.e. 500%) is applied in the dc bus. The load changes are very high to result in power flow reversing over the TC. The output power of all the DERs, in both buses, is maintained, as desired (Fig. 6.13a-b). For t < 1 s, the surplus of the power generated by dc DERs, minus the TC losses, is delivered to the ac bus and 6 kW surplus in ac bus is flowing to grid (Fig. 6.13c). As the load in the ac bus is increased at t = 1 s, the power flow over the TC is remained unaffected. In this case, since the power generation and demand in the AC bus are equal, the power exchange between the microgrid and grid is zero (Fig. 6.13c). At t = 2 s, as the load in dc bus increases, the power flow over the TC is reversed and the TC takes approximately 2 kW from the ac bus. Hence, bidirectional power flow between the two ac and dc microgrids as well as the microgrid and grid are validated.

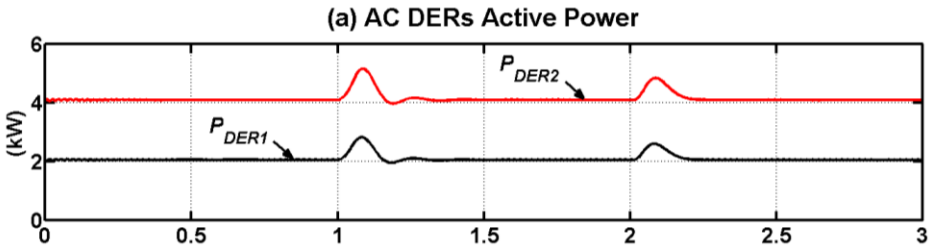

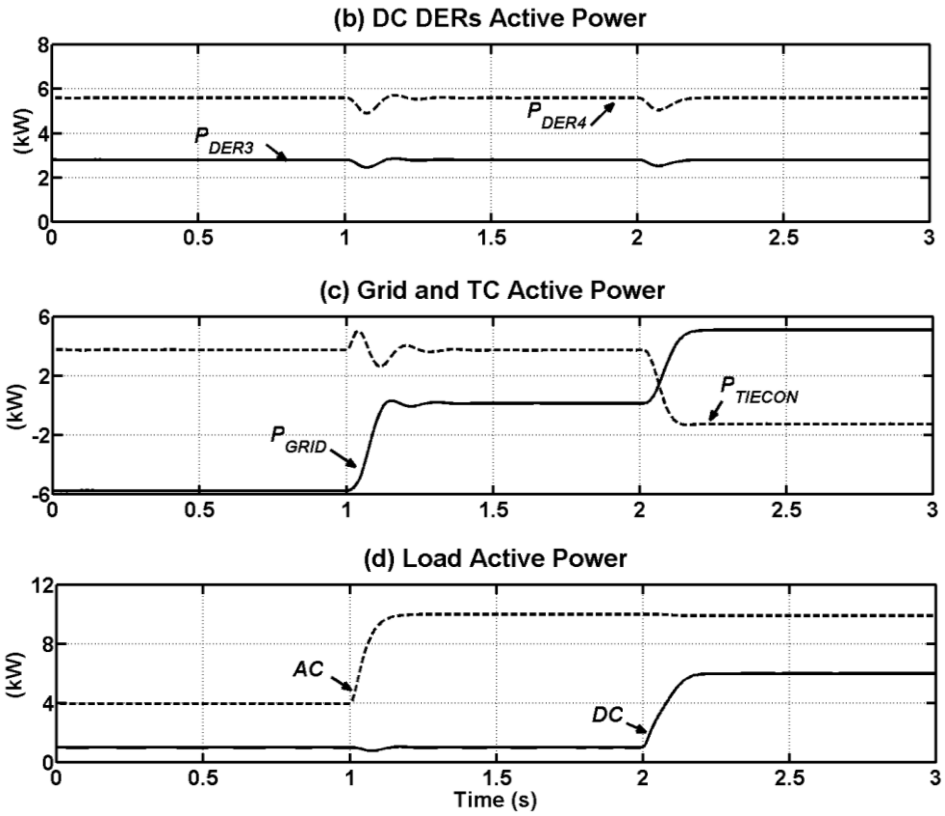

Fig. 6.13 Simulation results for the ac bus in case 6.3.4:

6.4 Summary

In this chapter, a hierarchical control system is proposed for the dynamic operation and control of the DERs connected to the ac and dc bus of a hybrid ac-dc microgrid. A secondary controller successfully regulates the dc bus voltage, ac bus voltage and ac bus frequency. However, when the two buses are interconnected, these parameters are effectively controlled by the active power flow and reactive power exchange by the TC. Four different modes of operation are identified for the hybrid microgrid and through the simulation results, it is shown that the microgrid with the proposed control system can successfully operate in all these four modes.

Chapter 7 Conclusions and Recommendations

In this chapter, the general conclusions of the thesis and recommendations for future research are presented.

7.1 Conclusions

The general conclusions of the thesis are:

(1) Several converter-interfaced DERs can be properly controlled to operate in their rated or MPPT conditions when the microgrid is operating in grid-connected mode. In off-grid mode, they can operate in reactive power-voltage and active power-frequency (or angle) droop to share the required active and reactive demand of the loads.

(2) Voltage-controlled DERs can effectively supply different types of loads of the microgrid such as balanced, unbalanced and harmonic loads. Compared to current-controlled DERs which need relatively complicated negative and zeros sequence extraction and harmonic component extraction, the voltage-controlled DERs do not need such computational complexity.

(3) For proper operation and control of the DERs in a microgrid, a hierarchical control system is required. The DERs performance and reference tracking is achieved by the help of the primary (lowest) level control. The microgrid central controller acts as the secondary control system and adjusts the set points for the primary controller to regulate the network voltage and frequency, if they are violated. It also sheds the non-critical loads if the primary control setting adjustments are not sufficient for keeping the voltage magnitude and frequency within the acceptable limits.

(4) Two or more neighboring microgrids can be interconnected to form a bigger microgrid in smart grid networks with self-healing capability. Interconnection of the neighboring microgrids can prevent load shedding in a

microgrid with deficiency of power, if the neighboring microgrids have enough generation capacity.

(5) A microgrid can be composed of single-phase DERs with different capacities, arbitrarily distributed among the three phases of the microgrid. In such a case, the single-phase DERs of the microgrid can operate in droop during the off-grid mode of operation. The excess power generated in a phase with higher number of single-phase DERs can be circulated to the other phase(s) through a distribution transformer with delta/wye configuration. Alternatively, a DSTATCOM can be utilized in the low voltage or medium voltage feeder to circulate the power among the phases.

(6) A microgrid can be composed of two buses –ac bus and dc bus, forming a hybrid ac-dc microgrid. Each bus has several DERs and loads and they are interlinked through an interlinking converter. This can be a viable network configuration for the future community houses. Depending on the presence of the grid or the conduction status of interlinking converter, different modes of operation can be considered. The DERs in each bus can supply its local loads whereas the DERs connected to the other bus can effectively supply the loads through the interlinking converter in case there is a deficiency in the local generation.

7.2 Thesis contribution to the knowledge

In this thesis, a three level hierarchical control system comprising primary, secondary and tertiary controllers was proposed for the proper operation and control of the DERs in a microgrid. The proposed primary controller is based on the converter voltage control and consists of two control loops; inner loop control and outer loop control. Outer loop controller generates the reference based on the operating condition of the microgrid which is fed to the inner loop controller where the switching signal are generated. An optimal robust feedback control system is utilized in order to produce the estimated voltage at the converter output. The proposed secondary controller adjusts the set points for the primary controller to ensure the voltage and frequency of the system are kept within the acceptable limits. It also dynamically adjusts the power sharing ratio among the DERs in the microgrid and sheds the loads to prevent voltage and frequency collapse in the system in the

event of DERs over loading. The numerical simulation carried out on PACAD ensures that the DERs with the developed control scheme can successfully supply different types of loads in a microgrid. Both three phase and single phase DERs were considered. In case of single-phase DERs with different ratings, unequally distributed among the three phases of a microgrid, two alternative methods were proposed to circulate the power from the phase with excess generation to the other phase(s) with lack of generation. In addition, the possibility of interconnecting two or more neighboring off-grid microgrids has been studied to reduce the load shedding possibility in a microgrid with deficiency of power, if the neighboring microgrids have sufficient generation capacity. Finally, a dc microgrid system was also proposed and its interconnection with an ac microgrid through an interlinking converter was discussed. Proper control and management methods were proposed to ensure the proper operation of the interlinked ac-dc hybrid microgrid for different operating modes. Several scenarios and case studies were considered and the proposed concepts were validated by extensive computer-based simulation studies in PSCAD/EMTDC.

7.3 Recommendations for future research

The scope for future research is as given below.

7.3.1 Simultaneous active and reactive power ratio adjustment

In this research, only the dynamic adjustment of the active power among parallel converter-interfaced DERs was investigated. The proposed method does not regulate the reactive power share among the DERs. A new dynamic power ratio adjustment method can be proposed in which the active and reactive power ratios are adjusted simultaneously for the DERs. In addition, the decision making algorithm embedded within the network tertiary controller can be developed to define the desired power ratio among different DERs of a microgrid. This can be a topic for future research.

7.3.2 Different interconnection topologies and decision making

In this research, the concept of interconnecting two or more neighboring microgrids was proposed and the primary level control of the DERs was investigated.

The decision making process before interconnection of the microgrids which is the functionality of the network tertiary controller was not considered in this research. The different mechanisms of interconnection of two or more neighboring microgrids as well as the decision making algorithm embedded in the network tertiary controller can be a topic for future research.

7.3.3 Control of state of charge of storage units in microgrids

The batteries considered as DERs in this research were assumed as sources of active power in the microgrid. However, they need to be charged as well. Therefore, the charging and discharging operation of the batteries can be further studied and the effect of the state of charge of the batteries on the microgrid operation can be analyzed further. This can be a topic for a future research.

7.3.4 Communication network and data transfer delay effect

In this research, it was assumed that the data transfer in the network (among the DERs and the microgrid central controller) is carried out immediately. However, depending on the communication network type and the number of DERs in the microgrid, the data transferring process may experience large delays and/or data packet loss may be observed. The proper communication network for the microgrid, data coding characteristics and the effect of the data transfer delay and data packet loss can be another topic for a future research.

References

[1] B. Kroposki, C. Pink, R. DeBlasio, H. Thomas, M. Simões, and P. K. Sen, "Benefits of power electronic interfaces for distributed energy systems," *IEEE Transactions on Energy Conversion*, vol. 25, no. 3, pp. 901–908, 2010.

[2] T. Senjyu, T. Nakaji, K. Uezato, and T. Funabashi, "A hybrid power system using alternative energy facilities in isolated island," *IEEE Transactions on Energy Conversion*, vol. 20, no. 2, pp. 406–414, 2005.

[3] R. H. Lasseter, "MicroGrids," in *IEEE Power Engineering Society Winter Meeting*, 2002, vol. 1, pp. 305–308 vol.1.

[4] N. Hatziargyriou, H. Asano, R. Iravani, and C. Marnay, "Microgrids," *IEEE Power and Energy Magazine*, vol. 5, no. 4, pp. 78–94, 2007.

[5] J. A. P. Lopes, C. L. Moreira, and A. G. Madureira, "Defining control strategies for MicroGrids islanded operation," *IEEE Transactions on Power Systems*, vol. 21, no. 2, pp. 916–924, 2006.

[6] M. C. Chandorkar, D. M. Divan, and R. Adapa, "Control of parallel connected inverters in standalone AC supply systems," *IEEE Transactions on Industry Applications*, vol. 29, no. 1, pp. 136–143, 1993.

[7] R. Majumder, A. Ghosh, G. Ledwich, and F. Zare, "Angle droop versus frequency droop in a voltage source converter based autonomous microgrid," *IEEE Power & Energy Society General Meeting*, pp. 1–8, 2009.

[8] R. Majumder, F. Shahnia, A. Ghosh, G. Ledwich, M. Wishart, and F. Zare, "Operation and control of a microgrid containing inertial and non-inertial micro sources," *IEEE Region 10 Conference (TENCON)*, pp. 1–6, 2009.

[9] C. N. Rowe, T. J. Summers, R. E. Betz, D. J. Cornforth, and T. G. Moore, "Arctan Power–Frequency Droop for Improved Microgrid Stability," *IEEE Transactions on Power Electronics*, vol. 28, no. 8, pp. 3747–3759, Aug. 2013.

[10] J. C. Vasquez, J. M. Guerrero, A. Luna, P. Rodriguez, and R. Teodorescu, "Adaptive Droop Control Applied to Voltage-Source Inverters Operating in Grid-Connected and Islanded Modes," *IEEE Transactions on Industrial Electronics*, vol. 56, no. 10, pp. 4088–4096, Oct. 2009.

[11] H. Bevrani and S. Shokoohi, “An Intelligent Droop Control for Simultaneous Voltage and Frequency Regulation in Islanded Microgrids,” *IEEE Transactions on Smart Grid*, vol. 4, no. 3, pp. 1505–1513, Sep. 2013.

[12] M. J. Sanjari and G. B. Gharehpetian, “Small signal stability based fuzzy potential function proposal for secondary frequency and voltage control of islanded microgrid,” *Electric Power Component Systems*, vol. 4, no. 5, pp. 1505–1513, 2013.

[13] B. Johnson, A. Davoudi, P. Chapman, and P. Sauer, “A unified dynamic characterization framework for microgrid systems,” *Electric Power Components and Systems*, vol. 40, no. 1, pp. 93–111, 2011.

[14] C. X. Dou, D. L. Liu, X. B. Jia, and F. Zhao, “Management and Control for Smart Microgrid Based on Hybrid Control Theory,” *Electric Power Components and Systems*, vol. 39, no. 8, pp. 813–832, 2011.

[15] R. Majumder, “Some Aspects of Stability in Microgrids,” *IEEE Transactions on Power Systems*, vol. 28, no. 3, pp. 3243–3252, Aug. 2013.

[16] R. Majumder, B. Chaudhuri, A. Ghosh, R. Majumder, G. Ledwich, and F. Zare, “Improvement of stability and load sharing in an autonomous microgrid using supplementary droop control loop,” *IEEE Power and Energy Society General Meeting*, vol. 25, no. 2, pp. 796–808, 2010.

[17] H. Nian and R. Zeng, “Improved control strategy for stand-alone distributed generation system under unbalanced and non-linear loads,” *IET Renewable Power Generation*, vol. 5, no. 5, pp. 323–331, Sep. 2011.

[18] F. Katiraei and M. R. Iravani, “Power Management Strategies for a Microgrid With Multiple Distributed Generation Units,” *IEEE Transactions on Power Systems*, vol. 21, no. 4, pp. 1821–1831, 2006.

[19] A. Yazdani and R. Iravani, “A unified dynamic model and control for the voltage-sourced converter under unbalanced grid conditions,” *IEEE Transactions on Power Delivery*, vol. 21, no. 3, pp. 1620–1629, 2006.

[20] W. Huang, M. Lu, and L. Zhang, “Survey on Microgrid Control Strategies,” *Energy Procedia*, vol. 12, pp. 206–212, 2011.

[21] Ying-Yi Hong, Ming-Chun Hsiao, Yung-Ruei Chang, Yih-Der Lee, and Hui-Chun Huang, “Multiscenario Underfrequency Load Shedding in a Microgrid Consisting of Intermittent Renewables,” *IEEE Transactions on Power Delivery*, vol. 28, no. 3, pp. 1610–1617, Jul. 2013.

[22] K. Seethalekshmi, S. N. Singh, and S. C. Srivastava, “A Synchrophasor Assisted Frequency and Voltage Stability Based Load Shedding Scheme for Self-Healing of Power System,” *IEEE Transactions on Smart Grid*, vol. 2, no. 2, pp. 221–230, Jun. 2011.

[23] A. Ghosh and G. Ledwich, *Power quality enhancement using custom power devices*. Kluwer Academic Publishers, 2002.

[24] R. Teodorescu, M. Liserre, and P. Rodriguez, *Grid converters for photovoltaic and wind power systems*. Wiley, 2011.

[25] F. Blaabjerg, R. Teodorescu, M. Liserre, and A. V. Timbus, “Overview of Control and Grid Synchronization for Distributed Power Generation Systems,” *IEEE Transactions on Industrial Electronics*, vol. 53, no. 5, pp. 1398–1409, Oct. 2006.

[26] J. Rocabert, G. Azevedo, I. Candela, R. Teoderescu, P. Rodriguez, and I. Etxebarria-Otadui, “Microgrid connection management based on an intelligent connection agent,” *IEEE 36th Annual Conference on Industrial Electronics (IECON)*, pp. 3028–3033, Nov. 2010.

[27] R. Majumder, A. Ghosh, G. Ledwich, and F. Zare, “Control of parallel converters for load sharing with seamless transfer between grid connected and islanded modes,” in *IEEE Power and Energy Society General Meeting*, 2008, pp. 1–7.

[28] T. L. Vandoorn, B. Meersman, J. D. M. De Kooning, and L. Vandevelde, “Transition From Islanded to Grid-Connected Mode of Microgrids With Voltage-Based Droop Control,” *IEEE Transactions on Power Systems*, vol. 28, no. 3, pp. 2545–2553, Aug. 2013.

[29] Il-Yop Chung, Wenxin Liu, D. A. Cartes, E. G. Collins, and Seung-Il Moon, “Control Methods of Inverter-Interfaced Distributed Generators in a Microgrid System,” *IEEE Transactions on Industry Applications*, vol. 46, no. 3, pp. 1078–1088, 2010.

[30] C. K. Sao and P. W. Lehn, “Control and Power Management of Converter Fed Microgrids,” *IEEE Transactions on Power Systems*, vol. 23, no. 3, pp. 1088–1098, 2008.

[31] F. Shahnia, R. P. S. Chandrasena, S. Rajakaruna, and A. Ghosh, “Primary control level of parallel distributed energy resources converters in system of multiple interconnected autonomous microgrids within self-healing networks,” *IET Generation, Transmission & Distribution*, vol. 8, no. 2, pp. 203–222, Feb. 2014.

[32] S. J. Ahn, I. Y. Park, I. Y. Chung, S. I. Moon, and et.al, “Power-Sharing Method of Multiple Distributed Generators Considering Control Modes and Configurations of a

Microgrid," *IEEE Transactions on Power Delivery*, vol. 25, no. 3, pp. 2007–2016, 2010.

[33] H. Karimi, H. Nikkhajoei, and R. Iravani, "Control of an Electronically-Coupled Distributed Resource Unit Subsequent to an Islanding Event," *IEEE Transactions on Power Delivery*, vol. 23, no. 1, pp. 493–501, 2008.

[34] R. Majumder, G. Ledwich, A. Ghosh, S. Chakrabarti, and F. Zare, "Droop Control of Converter-Interfaced Microsources in Rural Distributed Generation," *IEEE Transactions on Power Delivery*, vol. 25, no. 4, pp. 2768–2778, 2010.

[35] J. M. Guerrero, L. Garcia de Vicuna, J. Matas, M. Castilla, and J. Miret, "Output Impedance Design of Parallel-Connected UPS Inverters With Wireless Load-Sharing Control," *IEEE Transactions on Industrial Electronics*, vol. 52, no. 4, pp. 1126–1135, Aug. 2005.

[36] F. Shahnia, R. Majumder, A. Ghosh, G. Ledwich, and F. Zare, "Voltage imbalance analysis in residential low voltage distribution networks with rooftop PVs," *Electric Power Systems Research*, vol. 81, no. 9, pp. 1805–1814, 2011.

[37] F. Shahnia, R. Majumder, A. Ghosh, G. Ledwich, and F. Zare, "Operation and Control of a Hybrid Microgrid Containing Unbalanced and Nonlinear Loads," *Electric Power Systems Research*, vol. 80, no. 8, pp. 954–965, 2010.

[38] D. De and V. Ramanarayanan, "Decentralized Parallel Operation of Inverters Sharing Unbalanced and Nonlinear Loads," *IEEE Transactions on Power Electronics*, vol. 25, no. 12, pp. 3015–3025, Dec. 2010.

[39] U. Borup, F. Blaabjerg, and P. N. Enjeti, "Sharing of nonlinear load in parallel-connected three-phase converters," *IEEE Transactions on Industry Applications*, vol. 37, no. 6, pp. 1817–1823, Dec. 2001.

[40] M. Hamzeh, H. Karimi, and H. Mokhtari, "A New Control Strategy for a Multi-Bus MV Microgrid Under Unbalanced Conditions," *IEEE Transactions on Power Systems*, vol. 27, no. 4, pp. 2225–2232, Nov. 2012.

[41] T. Vandoorn, B. Meersman, J. De Kooning, and L. Vandevelde, "Controllable Harmonic Current Sharing in Islanded Microgrids: DG Units With Programmable Resistive Behavior Toward Harmonics," *IEEE Transactions on Power Delivery*, vol. 27, no. 2, pp. 831–841, Apr. 2012.

[42] C. Sao and P. W. Lehn, "Voltage balancing of converter fed microgrids with single phase loads," *IEEE Power and Energy Society General Meeting*, pp. 1–7, Jul. 2008.

[43] K. Moslehi and R. Kumar, “A Reliability Perspective of the Smart Grid,” *IEEE Transactions on Smart Grid*, vol. 1, no. 1, pp. 57–64, Jun. 2010.

[44] X. Fang, S. Misra, G. Xue, and D. Yang, “Smart Grid — The New and Improved Power Grid: A Survey,” *IEEE Communications Surveys & Tutorials*, vol. 14, no. 4, pp. 944–980, Fourth Quarter 2012.

[45] Haoming Liu, Xingying Chen, Kun Yu, and Yunhe Hou, “The Control and Analysis of Self-Healing Urban Power Grid,” *IEEE Transactions on Smart Grid*, vol. 3, no. 3, pp. 1119–1129, Sep. 2012.

[46] M. Kezunovic, “Smart Fault Location for Smart Grids,” *IEEE Transactions on Smart Grid*, vol. 2, no. 1, pp. 11–22, Mar. 2011.

[47] K. Moslehi, A. B. R. Kumar, and P. Hirsch, “Feasibility of a self-healing grid - part II benefit models and analysis,” *IEEE Power Engineering Society General Meeting*, p. 8 pp., 2006.

[48] A. Zidan and E. F. El-Saadany, “A Cooperative Multiagent Framework for Self-Healing Mechanisms in Distribution Systems,” *IEEE Transactions on Smart Grid*, vol. 3, no. 3, pp. 1525–1539, Sep. 2012.

[49] S. A. Arefifar, Y. A. I. Mohamed, and T. H. M. El-Fouly, “Supply-Adequacy-Based Optimal Construction of Microgrids in Smart Distribution Systems,” *IEEE Transactions on Smart Grid*, vol. 3, no. 3, pp. 1491–1502, Sep. 2012.

[50] A. Košťálová and P. M. S. Carvalho, “Towards self-healing in distribution networks operation: Bipartite graph modelling for automated switching,” *Electric Power Systems Research*, vol. 81, no. 1, pp. 51–56, Jan. 2011.

[51] R. J. Yinger, “Self-healing circuits at Southern California Edison,” *IEEE Transmission and Distribution Conference and Exposition (T&D), 2012*, pp. 1–3, 7.

[52] R. H. Lasseter, “Smart Distribution: Coupled Microgrids,” *IEEE Proceedings of the DOI - 10.1109/JPROC.2011.2114630*, vol. 99, no. 6, pp. 1074–1082, 2011.

[53] S. Rahman, M. Pipattanasomporn, and Y. Teklu, “Intelligent Distributed Autonomous Power Systems (IDAPS),” *IEEE Power Engineering Society General Meeting*, pp. 1–8, Jun. 2007.

[54] A. G. Madureira and J. A. Pecas Lopes, “Coordinated voltage support in distribution networks with distributed generation and microgrids,” *IET Renewable Power Generation*, vol. 3, no. 4, pp. 439–454, 2009.

[55] K. Pandiaraj, P. Taylor, N. Jenkins, and C. Robb, “Distributed load control of autonomous renewable energy systems,” *IEEE Transactions on Energy Conversion*, vol. 16, no. 1, pp. 14–19, 2001.

[56] R. Majumder, A. Ghosh, G. Ledwich, and F. Zare, “Operation and control of single phase micro-sources in a utility connected grid,” *IEEE Power & Energy Society General Meeting*, pp. 1–7, 2009.

[57] R. Majumder, “Reactive Power Compensation in Single-Phase Operation of Microgrid,” *IEEE Transactions on Industrial Electronics*, vol. 60, no. 4, pp. 1403–1416, Apr. 2013.

[58] J. Bryan, R. Duke, and S. Round, “Decentralized generator scheduling in a nanogrid using DC bus signaling,” *IEEE Power Engineering Society General Meeting*, pp. 977–982 Vol.1, Jun. 2004.

[59] A. Sannino, G. Postiglione, and M. H. J. Bollen, “Feasibility of a DC network for commercial facilities,” *IEEE Transactions on Industry Applications*, vol. 39, no. 5, pp. 1499–1507, Oct. 2003.

[60] A. Goikoetxea, J. M. Canales, R. Sanchez, and P. Zumeta, “DC versus AC in residential buildings: Efficiency comparison,” *IEEE EUROCON, 2013*, pp. 1–5, Jul. 2013.

[61] Y. Hayashi, “High power density rectifier for highly efficient future DC distribution system,” *Electrical Engineering Research*, vol. 1, no. 3, pp. 49–59, 2013.

[62] H. Kakigano, Y. Miura, and T. Ise, “Low-Voltage Bipolar-Type DC Microgrid for Super High Quality Distribution,” *IEEE Transactions on Power Electronics*, vol. 25, no. 12, pp. 3066–3075, Dec. 2010.

[63] H. Kakigano, Y. Miura, and T. Ise, “Distribution Voltage Control for DC Microgrids Using Fuzzy Control and Gain-Scheduling Technique,” *IEEE Transactions on Power Electronics*, vol. 28, no. 5, pp. 2246–2258, May 2013.

[64] I. Cvetkovic, Dong Dong, Wei Zhang, Li Jiang, D. Boroyevich, F. C. Lee, and P. Mattavelli, “A testbed for experimental validation of a low-voltage DC nanogrid for buildings,” *15th International Power Electronics and Motion Control Conference (EPE/PEMC), 2012*, pp. LS7c.5–1, Sep. 2012.

[65] A. Suzdalenko, M. Vorobyov, and I. Galkin, “Development of distributed energy management system for intelligent household electricity distribution grid,” *IEEE EUROCON, 2013*, pp. 1474–1478, Jul. 2013.

[66] Jaehong Kim, J. M. Guerrero, P. Rodriguez, R. Teodorescu, and Kwanghee Nam, "Mode Adaptive Droop Control With Virtual Output Impedances for an Inverter-Based Flexible AC Microgrid," *Power Electronics, IEEE Transactions on*, vol. 26, no. 3, pp. 689–701, Mar. 2011.

[67] M. Savaghebi, A. Jalilian, J. C. Vasquez, and J. M. Guerrero, "Secondary Control Scheme for Voltage Unbalance Compensation in an Islanded Droop-Controlled Microgrid," *IEEE Transactions on Smart Grid*, vol. 3, no. 2, pp. 797–807, Jun. 2012.

[68] A. Mehrizi-Sani and R. Iravani, "Online Set Point Modulation to Enhance Microgrid Dynamic Response: Theoretical Foundation," *IEEE Transactions on Power Systems*, vol. 27, no. 4, pp. 2167–2174, Nov. 2012.

[69] M. B. Delghavi and A. Yazdani, "Islanded-Mode Control of Electronically Coupled Distributed-Resource Units Under Unbalanced and Nonlinear Load Conditions," *IEEE Transactions on Power Delivery*, vol. 26, no. 2, pp. 661–673, Apr. 2011.

[70] Xiaonan Lu, J. M. Guerrero, Kai Sun, and J. C. Vasquez, "An Improved Droop Control Method for DC Microgrids Based on Low Bandwidth Communication With DC Bus Voltage Restoration and Enhanced Current Sharing Accuracy," *IEEE Transactions on Power Electronics*, vol. 29, no. 4, pp. 1800–1812, Apr. 2014.

[71] T. Dragicevic, J. M. Guerrero, J. C. Vasquez, and D. Skrlec, "Supervisory Control of an Adaptive-Droop Regulated DC Microgrid With Battery Management Capability," *IEEE Transactions on Power Electronics*, vol. 29, no. 2, pp. 695–706, Feb. 2014.

[72] Y. Ito, Y. Zhongqing, and H. Akagi, "DC microgrid based distribution power generation system," *The 4th International Power Electronics and Motion Control Conference(IPEMC), 2004*, vol. 3, pp. 1740–1745 Vol.3, Aug. 2004.

[73] Lie Xu and Dong Chen, "Control and Operation of a DC Microgrid With Variable Generation and Energy Storage," *IEEE Transactions on Power Delivery*, vol. 26, no. 4, pp. 2513–2522, Oct. 2011.

[74] P. Thounthong, B. Davat, S. Raël, and P. Sethakul, "Fuel cell high-power applications," *IEEE Industrial Electronics Magazine*, vol. 3, no. 1, pp. 32–46, Mar. 2009.

[75] Hou Yongping, Gang Wan, Jiang Wei, and Zhuang Mingxi, "Steady State Performance Modeling of a Fuel Cell Engine," *IEEE International Conference on Vehicular Electronics and Safety, 2006. ICVES 2006.*, pp. 424–427, Dec. 2006.

[76] S. Yerramalla, “Modeling and simulation of the dynamic behavior of a polymer electrolyte membrane fuel cell,” *Journal of Power Sources*, vol. 124, pp. 104–113, 2003.

[77] S. Busquet, “A new approach to empirical electrical modelling of a fuel cell, an electrolyser or a regenerative fuel cell,” *Journal of Power Sources*, vol. 134, pp. 41–48, 2004.

[78] D. Yu and S. Yuvarajan, “Electronic circuit model for proton exchange membrane fuel cells,” *Journal of Power Sources*, vol. 142, pp. 238–242, 2005.

[79] Ke Jin, Xinbo Ruan, Mengxiong Yang, and Min Xu, “Power Management for Fuel-Cell Power System Cold Start,” *IEEE Transactions on Power Electronics*, vol. 24, no. 10, pp. 2391–2395, Oct. 2009.

[80] I. H. Altas and A. M. Sharaf, “A novel on-line MPP search algorithm for PV arrays,” *IEEE Transactions on Energy Conversion*, vol. 11, no. 4, pp. 748–754, Dec. 1996.

[81] R. Gules, J. De Pellegrin Pacheco, H. L. Hey, and J. Imhoff, “A Maximum Power Point Tracking System With Parallel Connection for PV Stand-Alone Applications,” *IEEE Transactions on Industrial Electronics*, vol. 55, no. 7, pp. 2674–2683, Jul. 2008.

[82] V. Spitsa, X. Ran, R. Salcedo, J. F. Martinez, R. E. Uosef, F. de Leon, D. Czarkowski, and Z. Zabar, “On the transient behavior of large-scale distribution networks during automatic feeder reconfiguration,” *IEEE Transactions on Smart Grid*, vol. 3, no. 2, pp. 887–896, Jun. 2012.

[83] J. J. Justo, F. Mwasilu, J. Lee, and J. W. Jung, “AC–microgrids versus DC–microgrids with distributed energy resources: A review,” *Renewable Sustainable Energy Reviews*, vol. 24, pp. 387–405, 2013.

[84] J. M. Guerrero, J. C. Vasquez, and R. Teodorescu, “Hierarchical control of droop-controlled DC and AC microgrids — a general approach towards standardization,” *35th IEEE Annual Conference of Industrial Electronics, 2009. IECON ’09.*, pp. 4305–4310, Nov. 2009.

[85] F. Katiraei, R. Iravani, N. Hatziargyriou, and A. Dimeas, “Microgrids management,” *IEEE Power and Energy Magazine*, vol. 6, no. 3, pp. 54–65, Jun. 2008.

[86] J. C. Vasquez, R. A. Mastromauro, J. M. Guerrero, and M. Liserre, “Voltage Support Provided by a Droop-Controlled Multifunctional Inverter,” *IEEE Transactions on Industrial Electronics*, vol. 56, no. 11, pp. 4510–4519, Nov. 2009.

[87] Robert H. Lasseter, “Control and Design of Microgrid Components.” University of Wisconsin-Madison.

[88] A. M. Salamah, S. J. Finney, and B. W. Williams, “Autonomous controller for improved dynamic performance of AC grid, parallel-connected, single-phase inverters,” *IET Generation, Transmission & Distribution*, vol. 2, no. 2, pp. 209–218, Mar. 2008.

[89] A. Ghosh and G. Ledwich, “High bandwidth voltage and current control design for voltage source converters,” *20th Australasian Universities Power Engineering Conference (AUPEC), 2010*, pp. 1–6, Dec. 2010.

[90] A. Tewari, *Modern Control Design with Matlab and Simulink*. Wiley, 2002.

[91] A. Ghosh and G. Ledwich, “Load compensating DSTATCOM in weak AC systems,” *IEEE Transactions on Power Delivery*, vol. 18, no. 4, pp. 1302–1309, Oct. 2003.

[92] H. Bevrani, *Robust Power System Frequency Control*. Springer, 2009.

[93] B. Pal and B. Chaudhuri, *Robust Control in Power Systems*. Springer, 2005.

[94] “Western Power Distribution Construction Standards Handbook, 2007 (Available at http://www.westernpower.com.au/networkcontractors/Distribution_Construction_Standards_Handbook.html).”

[95] W. Enright, O. B. Nayak, G. D. Irwin, and J. Arrillaga, “An electromagnetic transients model of multi-limb transformers using normalized core concept,” in *International Conference on Power Systems Transients (IPST)*, 1997, pp. 93–98.

[96] F. Shahnia, A. Ghosh, G. Ledwich, and F. Zare, “Voltage unbalance improvement in low voltage residential feeders with rooftop PVs using custom power devices,” *International Journal of Electrical Power & Energy Systems*, vol. 55, no. 9, pp. 362–377, 2014.

[97] Sreenivasarao, Agarwal, and Das, “A T-connected transformer based hybrid DSTATCOM for three-phase, four-wire systems,” *International Journal of Electrical Power & Energy Systems*, vol. 44, no. 1, pp. 964– 970, 2013.

[98] S. Mazumder, A. Ghosh, F. Shahnia, F. Zare, and G. Ledwich, “Excess power circulation in distribution networks containing distributed energy resources,” *IEEE Power and Energy Society General Meeting*, pp. 1–8, Jul. 2012.

[99] F. Shahnia, A. Ghosh, G. Ledwich, and F. Zare, “An approach for current balancing in distribution networks with rooftop PVs,” in *IEEE Power and Energy Society General Meeting (PES)*, San Diego, USA, 2012, pp. 1– 6.

[100] B. Han, B. Bae, S. Baek, and G. Jang, "New configuration of UPQC for medium-voltage application," *IEEE Transactions on Power Delivery*, vol. 21, no. 3, pp. 1438–1444, Jul. 2006.

[101] A. Ghosh and A. Joshi, "A new approach to load balancing and power factor correction in power distribution system," *IEEE Transactions on Power Delivery*, vol. 15, no. 1, pp. 417–422, Jan. 2000.

[102] A. Ghosh, A. K. Jindal, and A. Joshi, "Inverter control using output feedback for power compensating devices," *Conference on Convergent Technologies for the Asia-Pacific Region (TENCON),2003*, vol. 1, pp. 48–52 Vol.1, Oct. 2003.

[103] G. Ramakrishna and O. P. Malik, "Radial basis function identifier and pole-shifting controller for power system stabilizer application," *IEEE Transactions on Energy Conversion*, vol. 19, no. 4, pp. 663–670, Dec. 2004.

[104] M. Akbari, S. M. M. Tafreshi, and M. A. Golkar, "Voltage control of a hybrid ac/dc microgrid in stand-alone operation mode," *IEEE Innovative Smart Grid Technologies - India (ISGT India), 2011*, pp. 363–367, Dec. 2011.

Publications arising from the thesis

Book Chapters

(1) F. Shahnia, **R.P.S. Chandrasensa**, S. Rajakaruna, and A. Ghosh, "Interconnected off-grid microgrids in smart grids with self-healing capability." in *Renewable Energy Integration, Challenges and Solutions*, edited by Hossain, Jahangir, Mahmud, Apel, pp. 347-381, Springer, 2014.

Journal papers (Published)

(2) F. Shahnia, **R.P.S. Chandrasena**, S. Rajakaruna and A. Ghosh, "Application of DSTATCOM for Surplus Power Circulation in MV and LV Distribution Networks with Single-phase Distributed Energy Resources," *Electric Power Systems Research*, Vol. 117, pp. 104-114, Dec. 2014.

(3) F. Shahnia, **R.P.S. Chandrasena**, S. Rajakaruna and A. Ghosh, "Primary control level of parallel distributed energy resources converters in system of multiple interconnected off-grid microgrids within self-healing networks," *IET Generation, Transmission and Distribution*, Vol. 8, Issue 2, pp. 203–222, 2014.

(4) **R.P.S. Chandrasena**, F. Shahnia, S. Rajakaruna and A. Ghosh, "Dynamic Operation and Control of a Hybrid Nanogrid System for Future Community Houses," Accepted to published in *IET Generation, Transmission and Distribution* future publication.

Journal papers (Under Review/Revision)

(5) **R.P.S. Chandrasena**, F. Shahnia, S. Rajakaruna and A. Ghosh, "Power Management, Operation and Control of Unequally Distributed Single-Phase DERs among the Three Phases of a Microgrid," Provincially accepted to be published in *Electric Power Components and Systems* future publication.

Conference papers (Published)

(6) **R.P.S. Chandrasena**, F. Shahnia and S. Rajakaruna, "Energy storage options for microgrid applications: A review," IEEE 9th International

Conference on Industrial and Information Systems (ICIIS), Gwalior, India, Dec. 2014.

(7) **R.P.S. Chandrasena**, F. Shahnia, A. Ghosh and S. Rajakaruna, "Operation and control of a hybrid ac-dc nanogrid for future community houses," 24th Australasian Universities Power Engineering Conference (AUPEC), Perth, Australia, Sep/Oct. 2014.

(8) **R.P.S. Chandrasena**, F. Barbieri, F. Shahnia, A. Ghosh and S. Rajakaruna, "Developing the guidelines for fabrication of laboratory prototype voltage source converters," 24th Australasian Universities Power Engineering Conference (AUPEC), Perth, Australia, Sep/Oct. 2014.

(9) **R.P.S. Chandrasena**, F. Shahnia, A. Ghosh and S. Rajakaruna, "Secondary control in microgrids for dynamic power sharing and voltage/frequency adjustment," 24th Australasian Universities Power Engineering Conference (AUPEC), Perth, Australia, Sep/Oct. 2014.

(10) F. Barbieri, **R.P.S. Chandrasena**, F. Shahnia, S. Rajakaruna and A. Ghosh," Application notes and recommendations on using TMS320F28335 digital signal processor to control voltage source converters," 24th Australasian Universities Power Engineering Conference (AUPEC), Perth, Australia, Sep/Oct. 2014.

(11) F. Shahnia, **R.P.S. Chandrasena**, A. Ghosh and S. Rajakaruna, "Application of DSTATCOM for surplus power circulation in MV and LV distribution networks with single-phase distributed energy resources," IEEE Power and Energy Society General Meeting (PES), Washington DC, USA, July 2014.

(12) **R.P.S. Chandrasena**, F. Shahnia, S. Rajakaruna and A. Ghosh, "Operation and control of three phase microgrids consisting of single-phase DERs," IEEE 8th International Conference on Industrial and Information Systems (ICIIS), Kandy, Sri Lanka, Dec. 2013.

(13) **R.P.S. Chandrasena**, Farhad Shahnia, S. Rajakaruna and A. Ghosh, "Control, operation and power sharing among parallel converter-interfaced DERs in a microgrid in the presence of unbalanced and harmonic loads," 23rd Australasian Universities Power Engineering Conference (AUPEC), Hobart, Australia, Sep. 2013.

(14) Farhad Shahnia, **R.P.S. Chandrasena**, S. Rajakaruna and A. Ghosh, "Off-grid operation of multiple interconnected microgrids with self-healing capability," IEEE Power and Energy Society General Meeting (PES), pp. 1-5, Vancouver, Canada, July 2013.

(15) M.S. Alotibe, **R.P.S. Chandrasena** and S. Rajakaruna, "Simplified voltage and frequency controller based on droop control for the dynamic analysis of a Microgrid," 22nd Australasian Universities Power Engineering Conference (AUPEC), pp. 1-8, Bali, Indonesia, Sep. 2012.

Appendix

Technical data and parameters

Table A. 1 PV, Boost Chopper, Converter and Controller

No. of PV cells in series	2
No. of PV cells in parallel	3
Output voltage of PV cell	0.1 V dc
Rated output power	3.06 kW
Radiation level	1100
Ambient Temperature	30^{o} C
Output voltage of Chopper	250 V dc
Boost Chopper Parameters	L =10 mH, C = 5 mF
Boost Chopper Controller	Hysteresis Voltage Control, k_p =0.0001, Hys.$_{bandwidth}$ =0.0002
Converter Structure	3 single-phase H-bridge converter
Converter Loss	R =0.1 Ω per phase
Transformer	0.25/0.415 kV, 0.5 MVA, Lr = 4.4 mH
LC Filter	L_f =49.8 mH, C_f =50 μF
Hysteresis Constant	10^{-5}

Table A. 2 Battery, Converter and Controller

No. of battery units in series	10
No. of battery units in parallel	2
output voltage of battery unit	12 V DC
Rated output power	2 kW, 226 A.hr
Converter Structure	3 single-phase H-bridge converter
Converter Loss	R=0.1 Ω per phase
Transformer	0.12/0.415 kV, 0.5 MVA, Lr = 4.4 mH
LC Filter	L_f =76.2 mH, C_f =50 μF
Hysteresis Constant	10^{-5}

Table A. 3 Fuel Cell, Boost Chopper, Converter and Controller

Fuel cell rated power	4 kW
Boost Chopper Parameters	L =1 mH, C =1 mF, f_{sw} =10 kHz
Boost Chopper Controller	Open loop control, Switch duty cycle=10%
Converter Structure	3 single-phase H-bridge converter
Converter Loss	R =1.5 Ω per phase
Transformer	0.4/0.415 kV, 0.25 MVA, Lr = 0.54 mH
LC Filter	L_f =38.1 mH, C_f =50 μF
Hysteresis Constant	10^{-5}